

RHEOLOGIC EVOLUTION OF CARBONATES AND SHALE

ALONG THRUST FAULTS

A Dissertation

by

RACHEL KRISTEN WELLS

Submitted to the Office of Graduate and Professional Studies of
Texas A&M University
in partial fulfillment of the requirements for the degree of

DOCTOR OF PHILOSOPHY

Chair of Committee,	Julie Newman
Committee Members,	Andreas Kronenberg
	William Lamb
	Ibrahim Karaman
	Steven Wojtal (Special appointment)
Head of Department,	Michael Pope

August 2017

Major Subject: Geology

Copyright 2017 Rachel Kristen Wells

ABSTRACT

Carbonates and shales are an integral component of fold-and-thrust belts. Deformation processes that control the rheology of these faults are influenced by internal and external conditions. To understand how these processes influence fault zone morphology, I examine 1) the evolution of a fault zone with evidence of variable slip rates, 2) the processes that contribute to the formation of a crystallographic fabric in fine-grained dolomite, and 3) the variables that influence the location of, and displacement along, carbonate-shale thrusts.

Evidence for variable slip rates is preserved along the Copper Creek thrust, as well as overprinting relationships suggesting episodic instability. Nanograins, vesicular calcite, and coated clasts indicate unstable slip and overprint calcite grains with interpenetrating grain boundaries and four-grain junctions suggesting aseismic creep. Based on cross-cutting relationships, we propose a sequence of deformation events consistent with episodic unstable slip.

While a crystallographic fabric in carbonates has been commonly attributed to dislocation creep, a weak fabric is common in fine-grained dolomites that deformed under conditions consistent with diffusion creep. I examine the mechanisms that contribute to the development of a fabric in experimentally and naturally deformed dolomites. Fine-grains that exhibit a weak fabric, four-grain junctions, and subgrains indicate dislocation and diffusion creep. Fine-grains that exhibit a stronger crystallographic fabric and subgrains indicate dislocation creep.

Several thrust sheets within the foreland of the Southern Appalachians contain dolomite along the base of the sheet. The locations of the Copper Creek and Town Knobs thrusts correlate with fracturing of the base at the dolomite that allowed infiltration of fluids and precipitation of veins. The Copper Creek thrust contains calcite veins that deformed by a combination of plasticity-induced fracturing and diffusion creep, resulting in a large displacement along a weak shear zone. In contrast, the Town Knobs thrust contains a dolomite, calcite, and silt shear zone that exhibits evidence for diffusion creep, dislocation creep, and cataclasis. These deformation mechanisms in these minerals did not accommodate as large a displacement along this fault, suggesting that increasing stress at a constant strain rate, or increasing strain rate at constant stress conditions, may have resulted in less displacement.

DEDICATION

I would like to dedicate my dissertation to my loving father Gregory Warren Wells (1953-2014). I would also like to thank my mom and sister for their continued encouragement and motivation. Thank you for your love and inspiration. I would especially like to thank my friends and colleagues for their enthusiasm, wit, and support throughout my program.

CONTRIBUTORS AND FUNDING SOURCES

This work was supervised by a dissertation committee consisting of Professor Julie Newman [advisor] and Andreas Kronenberg and William Lamb of the Department of Geology and Geophysics, and Professor Ibrahim Karaman of the Department of Material Science and Engineering. This work was also supervised by Professor Steven Wojtal of the Geology Department at Oberlin College. Transmission electron microscopy was done by Caleb Holyoke. Ray Guillemette provided assistance on the electron microprobe. Field assistance and data collection was partially supported by Sara Donnelly, Scott Leaseburg, and Katherine Tilghman as undergraduate research projects.

This research was supported by NSF grant EAR-0911586 to J. Newman, C. Holyoke, and A. Kronenberg. Additional support was also made by the American Association of Petroleum Geologists, Sigma Xi, and Texas A&M Graduate Enhancement Fund. The FE-SEM acquisition was supported by the National Science Foundation grant DBI-0116835, the Vice President for Research Office, and the Texas Engineering Experimental Station. Graduate study was also supported by the 2014-2015 Texas A&M University dissertation fellowship.

TABLE OF CONTENTS

	Page
ABSTRACT	ii
DEDICATION	iv
CONTRIBUTORS AND FUNDING SOURCES.....	v
TABLE OF CONTENTS	vi
LIST OF FIGURES.....	viii
1. INTRODUCTION.....	1
2. CYCLIC STABLE-UNSTABLE SLIP PRESERVED ALONG AN APPALACHIAN FAULT.....	4
2.1 Introduction	4
2.2 Copper Creek Thrust	5
2.3 Microstructures Consistent with Unstable Slip.....	6
2.4 Microstructures Consistent with Grain Growth	9
2.5 Model for an Unstable-Stable Cycle	11
2.6 Conclusions	14
3. LATTICE-PREFERRED ORIENTATION DEVELOPMENT IN FINE-GRAINED DOLOMITE SHEAR ZONES.....	16
3.1 Introduction	16
3.2 Materials and Methods	18
3.2.1 Experimental Samples.....	19
3.2.2 Natural Samples	21
3.2.3 Methods.....	22
3.3 Dolomite Microstructures and Textures.....	23
3.3.1 Experimental Deformed Dolomite	23
3.3.1.1 Polycrystalline Dolomite	23
3.3.1.2 Sheared Dolomite	28
3.3.2 Natural Deformed Dolomite.....	29
3.3.2.1 Pioneer Landing Thrust	29
3.3.2.2 Town Knobs Thrust	32
3.4 LPO Fabric in Fine-Grained Dolomite.....	33

	Page
3.4.1 Following Grain Size Reduction	34
3.4.2 Independent of Grain Size Reduction	36
3.4.3 Comparison to Nature	38
3.5 Role of Mixed Mechanisms	40
3.6 Conclusions	45
4. CONTROLS ON THE LOCATION OF, AND DISPLACEMENT ALONG, THRUST FAULTS IN THE SOUTHERN APPALACHIANS	47
4.1 Introduction	47
4.2 Geologic Setting	49
4.3 Methods	52
4.4 Results	53
4.4.1 Copper Creek Thrust	53
4.4.1.1 Footwall	53
4.4.1.2 Hanging Wall	55
4.4.1.3 Shear Zone	59
4.4.2 Town Knobs Thrust	62
4.4.2.1 Footwall	62
4.4.2.2 Hanging Wall	65
4.4.2.3 Fault Zone	72
4.5 Fault Zones Evolution	78
4.5.1 Deformation along the Copper Creek Thrust	78
4.5.2 Deformation along the Town Knobs Thrust	80
4.5.3 Copper Creek and Town Knobs Thrusts Comparison	82
4.5.4 Conditions During Deformation	83
4.6 Conditions for Macroscopic Structures	86
4.6.1 Controls on the Location of Faulting	86
4.6.2 Controls on Fault Displacement	87
4.7 Conclusions	88
5. SUMMARY	90
REFERENCES	93
APPENDIX A	109

LIST OF FIGURES

FIGURE	Page
2.1 Coated clasts.....	8
2.2 Vesicular calcite and nanograins.....	10
2.3 Stable-unstable slip model	12
3.1 Overview of localized zones of fine-grained dolomite	20
3.2 Experimentally deformed dolomite.....	25
3.3 EBSD maps	26
3.4 Pole figures of fine-grained dolomite.....	27
3.5 Naturally deformed dolomite	31
3.6 Comparison between the Town Knobs and Pioneer Landing thrust faults	42
3.7 Dolomite comparison	44
4.1 Map of the fault traces in the Southern Appalachians	50
4.2 Cross-section	51
4.3 Images of the Copper Creek thrust.....	54
4.4 Hanging wall dolomite	56
4.5 Hanging wall dolomite adjacent to the Copper Creek shear zone	58
4.6 Copper Creek shear zone.....	60
4.7 Copper Creek shear zone continued.....	61
4.8 Images of the Town Knobs thrust	63
4.9 Footwall dolomite in the Town Knobs thrust.....	64

	Page
4.10 Hanging wall siltstone and shale in the Town Knobs thrust	66
4.11 Hanging wall dolomite along the Town Knobs thrust	68
4.12 Hanging wall dolomite along the Town Knobs thrust continued.....	69
4.13 Hanging wall dolomite zone along the Town Knobs thrust.....	71
4.14 Mesoscopic structures along the Town Knobs shear zone.....	73
4.15 Town Knobs shear zone	74
4.16 Town Knobs shear zone continued	76
4.17 ‘Vein-like’ structure along the Town Knobs shear zone.....	77
4.18 Comparison	84
A.1 Copper Creek shear zone schematic.....	109
A.2 Structure and grain size overview	110
A.3 Twin-twin intersections.....	111
A.4 Vesicular calcite	111
A.5 Shear zone nanograins.....	111
A.6 Ultrafine-grained calcite in shear zone matrix	112

1. INTRODUCTION

The development of thrust faults is a critical process in the formation of mountain belts as a mechanism to distribute the deformation across the region. The deformation mechanisms that occur along these faults contribute to the overall fault zone morphology (e.g., thickness, meso- and microstructures) and displacement. Depending on the external (e.g., temperature, stress, fluid flow) and internal (e.g., lithology) conditions, cataclasis, dislocation creep, and diffusion creep can lead to brittle failure or ductile flow. Determining the rheology of the deforming fault rocks aids our understanding of processes and mechanics involved in the formation of these belts.

Localization along a thrust sheet is often attributed to the weak behavior of shale (Wiltschko and Chapple, 1977; Thomas, 2001, Ikari et al., 2009, Cobbold et al., 2009). However, carbonates are also frequently found along thrust faults, particularly as vein fill associated with these faults. Understanding the rheology of carbonate minerals common in vein fill relative to host rock shale and limestone is therefore important to understanding the development of larger-scale structures along foreland thrust faults (Appalachians: Wojtal and Mitra, 1986; Canadian Rockies: Kennedy and Logan 1997; the Alps: Molli et al., 2000; Molli et al., 2010). This study examines external (e.g., slip rate, stress, temperature, fluid flow) and internal (e.g., calcite vs dolomite veins) factors influencing deformation in experimentally and naturally deformed carbonates in an effort to understand the mechanisms that contribute to fault zone formation. Three separate studies are presented in Sections 2, 3, and 4.

Evidence of a seismic-aseismic cycle is recognized primarily through examinations of seismically active regions (e.g., southern California) (Chester et al., 1993; Scholz, 1998) and experimental studies (Marone, 1998; Di Toro et al., 2004) conducted at seismic slip rates. While recent evidence of seismic slip has been observed in experimentally deformed rocks and along seismically active faults, including nanograins associated with vesicular calcite (Han et al., 2007; Niemeijer et al., 2012; Violay et al., 2013; Collettini et al., 2014; Spagnuolo et al., 2015) and coated clasts (Boutareaud et al., 2008; Fondriest et al., 2012; Rempe et al., 2014), the preservation of these structures along ancient faults is influenced by weathering and destruction by subsequent deformation. In Section 2, an analysis of the strain rates preserved along the Copper Creek thrust is presented based on the preservation of nano-scale structures within a 2 cm shear zone. Based on these structures and their cross-cutting relationships with structures that are evidence of aseismic creep, an unstable-stable cycle is formulated.

Dolomite deformation in naturally deformed rocks has been commonly attributed to fracturing and dislocation creep, depending on the temperature during deformation (House and Gray, 1982a; Newman and Mitra, 1994; Davis et al., 2008; Holyoke, et al., 2013; Holyoke et al., 2014). Many studies (Woodward et al 1988; Busch and van der Pluijm, 1995; Bestmann et al., 2000) of naturally deformed carbonate fault zones assume dolomite deforms primarily by fracturing at low temperatures. Recent experiments have documented n values indicative of diffusion creep at higher temperature conditions (>700 °C), and at the faster strain rates (approximately 10^{-5} s $^{-1}$) (Davis et al., 2008; Delle Piane et al., 2008; Holyoke et al., 2014) associated with experimental deformation. Based on these

experiments, grain size must be very fine ($<10\ \mu\text{m}$) to activate diffusion creep at low temperatures ($\sim 300\ ^\circ\text{C}$). In Section 3, I present evidence of a weak crystallographic fabric in fine-grained dolomite, along with evidence for concurrent diffusion and dislocation creep in experimentally and naturally deformed dolomite.

Shale is commonly thought to be a weak lithology that controls the location of, and displacement along these weak fault zone (Ibanez and Kronenberg, 1993; Kennedy and Logan, 1998; Cobbold et al., 2009; Tesei et al 2012). Although shale is often considered weak based on mesoscale observations (Wiltschko and Chapple, 1977; Thomas, 2001; Ikari et al., 2009; Cobbold et al., 2009), microstructural observations at the micron-scale suggested that a continuous layer of calcite controlled the rheology of the naturally deformed shear zone, and was thus weaker than shale at low temperature conditions (Wells et al., 2014). The presence of multiple phases that deformed concurrently allows us to learn about the relative rheologies of carbonates and shale under similar (natural) conditions (e.g. temperature, pressure, strain rate, fluids). Section 4 examines the role of different lithologies (dolomite, calcite, siltstone and shale) and vein fillings (calcite and dolomite), and evolving external conditions (e.g., stress) in the formation or, and displacement along, large thrust sheets.

2. CYCLIC STABLE-UNSTABLE SLIP PRESERVED ALONG AN APPALACHIAN FAULT

2.1 Introduction

Evidence of a seismic-aseismic cycle is recognized primarily through examinations of seismically active regions (Chester et al., 1993; Scholz, 1998) and experimental studies (Marone, 1998; Di Toro et al., 2004) conducted at seismic slip rates (1 m/s; Heaton, 1990). The cycle is characterized by increasing and decreasing stress (Scholz et al., 1969; Dieterich, 1972; Sibson, 1975; Sibson, 1992). Evidence of seismic slip in natural fault zones is largely based on microstructures produced during high-speed friction experiments and those documented along active, or historically active, fault zones (Rowe and Griffith, 2015 and references therein). However, demonstrating seismic activity occurred along ancient fault zones is dependent on preservation of these structures (Kirkpatrick and Rowe, 2013). Overprinting processes further complicates the microstructural record. While pseudotachylites are considered the most conclusive evidence for seismic slip (e.g., Sibson, 1975), over the past decade, several studies have presented new evidence of seismic slip, including nanograins associated with vesicular calcite (Han et al., 2007; Niemeijer et al., 2012; Violay et al., 2013; Collettini et al., 2014; Spagnuolo et al., 2015) and coated clasts (Boutareaud et al., 2008; Fondriest et al., 2012; Rempe et al., 2014).

We report newly recognized microstructures preserved along the inactive Copper Creek thrust fault that are similar to microstructures produced in high-speed friction experiments and along seismically active faults. While we cannot be certain the Copper

Creek fault experienced seismic slip, these microstructures suggest that the fault experienced faster deformation rates than indicated by previously described microstructures consistent with aseismic diffusion creep (Wells et al., 2014), and suggest unstable, possibly seismic, slip. Overprinting relations further indicate cyclic episodes of unstable slip. Spatial and temporal relations between the microstructures presented here and the previously documented evidence for aseismic creep form the basis for a model for the evolution of the stable-unstable cycle.

2.2 Copper Creek Thrust

The Copper Creek thrust has an estimated net slip of 15-20 km, with temperatures during deformation estimated at 100-180 °C at a depth of 4-6 km (Wojtal and Mitra, 1986). At the Diggs Gap exposure (Knoxville, TN), a ~2 cm thick fault zone (Appendix A) separates shales in regional hanging wall flat from footwall shales also in a regional flat. Microstructures in the fault zone indicate intense, localized shearing (Appendix A summarizes grain size classes and associated microstructures), so we call this layer the shear zone in all that follows. Slickensides decorate the contact between the shear zone and the hanging wall, while the contact between the shear zone and the footwall is defined by a 300 µm thick layer of calcite veins. Microstructures within calcite veins suggest multiple episodes of vein formation and cyclic brittle and ductile deformation (Wells et al., 2014). The development of a lattice-preferred orientation (LPO) suggests dislocation climb and glide; however, evidence for dislocation climb is limited (Wells et al., 2014). Dislocation pile-ups at twin-twin intersections (Appendix A) resulted in plasticity-induced fracturing

(Fredrich et al., 1989) in coarse-grained ($>20 \mu\text{m}$) calcite and reduced grain size to $< 1 \mu\text{m}$ forming the finer grained layers (Wells et al., 2014).

The shear zone is composed of aggregate clasts ($> 50 \mu\text{m}$) of shale and vein calcite, which are surrounded by ultrafine-grained calcite (340 nm) and shale matrix. The ultrafine-grained calcite formed a stress-supporting network around shale (Wells et al., 2014). Grain boundaries of the ultrafine-grained calcite are interpenetrating and form four-grain junctions and ultrafine-grained calcite (340 nm) exhibits no LPO, suggesting it deformed primarily by grain-size sensitive diffusion creep-accommodated grain boundary sliding (Wells et al., 2014). Below, we describe newly recognized microstructures along the Copper Creek thrust that are 1) consistent with unstable, possibly seismic, slip, and 2) exhibit cross-cutting relations with the microstructures consistent with aseismic slip.

2.3 Microstructures Consistent with Unstable Slip

Several distinctive microstructures within the Copper Creek shear zone, including coated clasts, nanograins, and vesicular calcite, are consistent with those formed during high-speed friction experiments and observed along seismically active fault zones. Angular aggregate clasts ($> 50 \mu\text{m}$) composed of calcite and/or shale are partially coated ($< 35 \mu\text{m}$ thick) by an optically dark, ultrafine-grained calcite matrix (Figure 2.1), and are located within a mixed shale and ultrafine-grained calcite matrix. The coated clasts resemble clay-cortex clasts and matrix-coated clasts along seismically active faults (Boullier et al., 2009; Smith et al., 2011; Fondriest et al., 2012; Rempe et al., 2014) and produced during high-speed friction experiments (Ferri et al., 2010; De Paola et al., 2011; Rempe et al., 2014), which are attributed to fluidization during seismic slip. However, Han and Hirose (2012)

produced similar coated clasts at slightly slower slip rates. While the coated clasts from the ancient Copper Creek thrust are not as well-preserved as those observed along active fault zones and produced during experiments, their presence indicates deformation occurred at faster slip rates than microstructures suggesting diffusion creep, described in Wells et al., (2014). These clasts likely experienced alteration during these overprinting creep stages, reducing the coatings symmetry (e.g., Rowe and Griffith, 2015).

The formation of vesicular calcite and nanograins strongly indicates deformation occurred at or near seismic slip rates along the Copper Creek thrust. Vesicular textures, along twin and grain boundaries, occur in calcite veins within 2 cm of the fault zone (Figure 2.2A). Within the shear zone, circular pores (Figure 2.2B; Appendix A) occur within ultrafine-grained calcite (340 nm) matrix. These pores likely result from thermal decomposition of the calcite grains (Niemeijer et al., 2012; Collettini et al., 2013; Collettini et al., 2014; Smeraglia et al., 2017) during seismic slip events. Immediately below the slickenside surface, nanometer-scale clasts (50-150 nm) are observed (Figure 2.2C; Appendix A). Selected area electron diffraction of the clasts suggests they are polycrystalline with an average grain size of 6.8 nm (nanograins). The nanograins are angular and contain straight grain boundaries (Figure 2.2C; Appendix A). Energy dispersive spectroscopy analyses indicate the nanograins are calcium. The morphology of the nanograins are similar to those observed in high-speed friction experiments in which thermal decomposition (Han et al., 2007; Niemeijer et al., 2012; Collettini et al., 2013; Ree et al., 2014; Spagnuolo et al., 2015) or milling (Siman-Tov et al., 2013) have occurred. Nanograins presented in these studies usually occur in association with vesicular calcite,

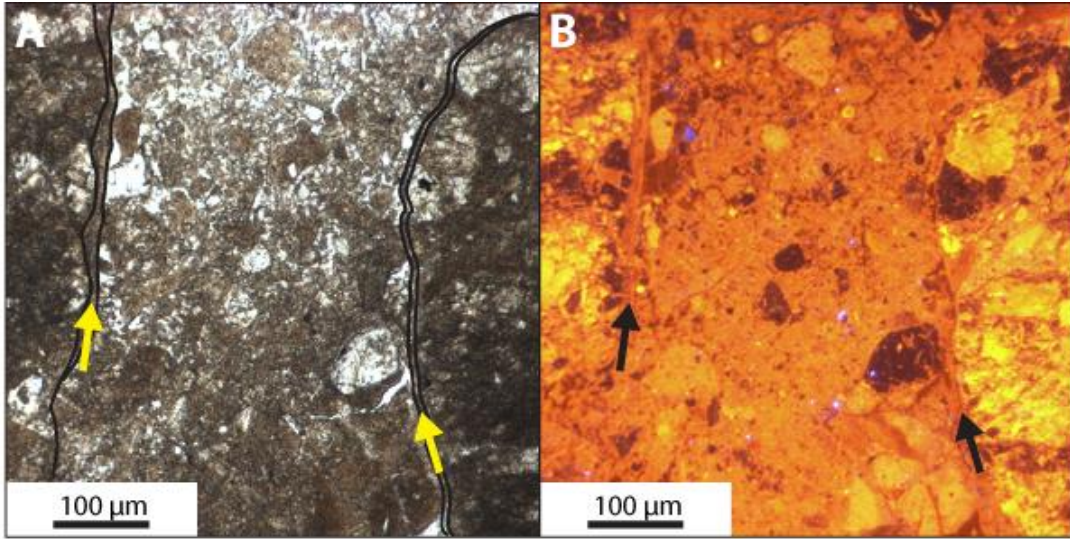


Figure 2.1. Coated clasts. (A-B) Optical photomicrographs of plane polarized light and corresponding CL image of large aggregate clasts partially coated by an ultrafine-grained calcite (outlined in black in A, yellow-black arrows). Overall shear zone image shown in Appendix A.

or are spatially distributed along cleavage planes.

Frictional heating during slip would result in the formation of lime, which would quickly form nanometer calcite grains (Han et al., 2007; Collettini et al., 2013; Violay et al., 2013). The occurrence of the nanoscale grains in conjunction with vesicular calcite suggest thermal decomposition, likely resulting from a seismic event. This evidence for thermal decomposition combined with evidence of fluidized flow within the Copper Creek fault rocks suggest that unstable slip, possibly seismic, occurred in addition to structures that formed during aseismic creep can be preserved along inactive fault zones.

2.4 Microstructures Consistent with Grain Growth

While the coated clasts, vesicular calcite, and nanograins (7 nm) are consistent with fast, possibly seismic, slip rates, equant ultrafine-grained calcite within the shear zone suggests grain growth and deformation at slower slip rates. Equant ultrafine-grained (310 nm) calcite grains ~1 mm below the slickenside surface exhibit a foam-like texture consisting of straight grain boundaries and triple junctions (Figure 2.2D). Clusters of angular nanograins (~30 nm) occur along the grain boundaries of the equant ultrafine-grained (310 nm) calcite (Figure 2.2D). Pores are not observed around the 310 nm calcite grains or 30 nm grains. The foam-like texture of equant ultrafine-grained (310 nm) calcite suggests static grain growth or growth during slower slip rates (Tullis and Yund, 1982; Barnhoorn et al., 2005). The 30 nm grains that occur along the grain boundaries of the coarser grains are an order of magnitude finer than the 310 nm grains, yet coarser than the 7 nm grains observed along the upper contact of the fault zone that likely formed as a porosity around the 30 nm grains, and the similar result of thermal decomposition. The location

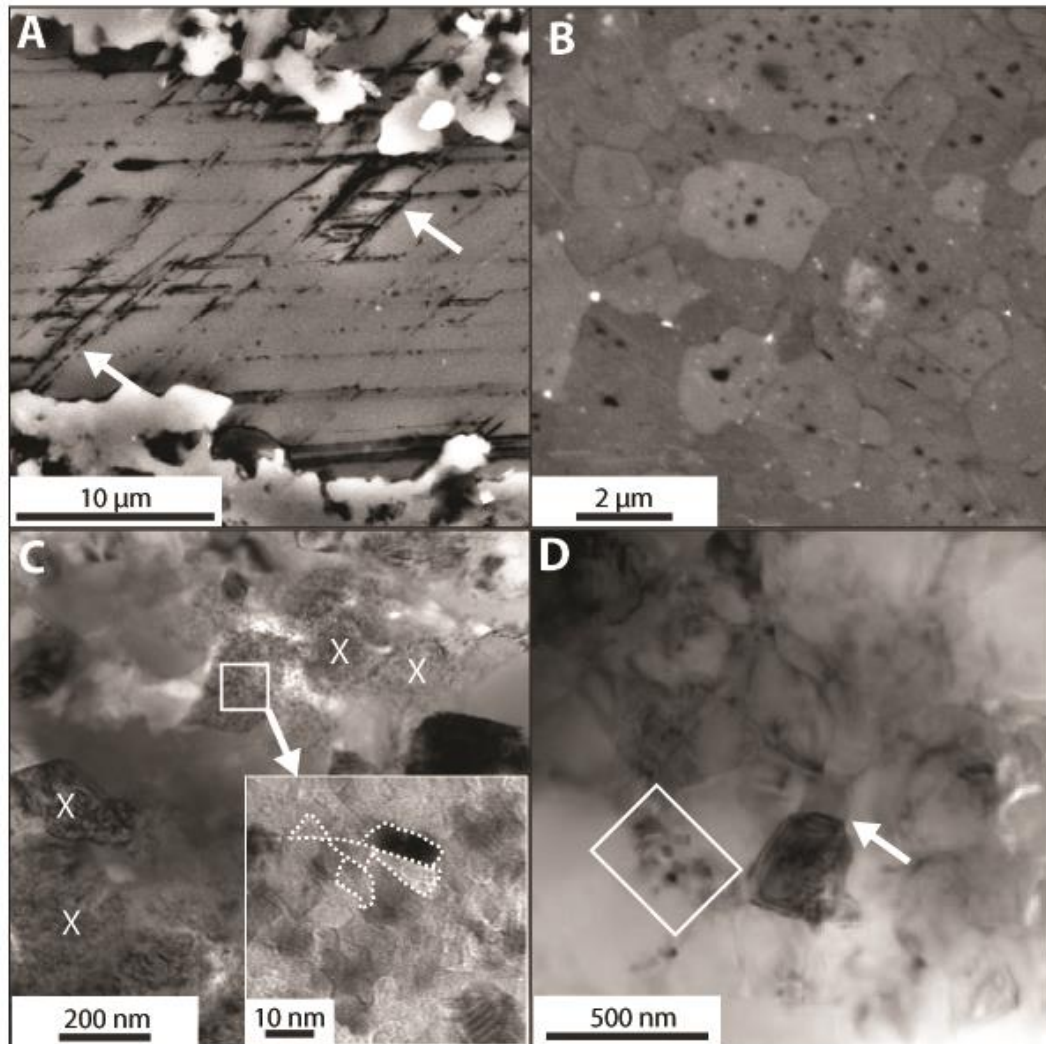


Figure 2.2. Vesicular calcite and nanograins. (A) Vesicular calcite (arrows) in veins within 2 cm of the fault zone. (B-D) are within the shear zone. (B) Vesicular structures (black) are observed in ultrafine-grained calcite matrix. (A-B) Backscatter electron images. (C) Nanometer aggregate clasts (X) are composed of 7 nm grains (dashed outlined) with straight grain boundaries. (D) Equant ultrafine-grained calcite with triple junctions (arrow), straight grain boundaries, and no porosity. A 200 μm cluster of 30 nm grains occurs along grain boundaries of the ultra-fine grained calcite (box). (C-D) Transmission electron images.

of the 30 nm nanograins with respect to the equant, ultrafine-grain calcite (310 nm), which exhibit evidence for grain growth, the lack of cluster morphology of the 7 nm grains suggest the 30 nm grains are the product of grain growth from the finer 7 nm grains. The 30 nm grains thus suggest an earlier episode of faster slip occurred prior to grain growth during aseismic creep. If grain growth had been the result of post-deformation annealing, it should have affected all nanometer grains similarly. The preservation of the 7 nm grains, therefore, suggests that the 30 nm grains resulted from grain growth during an earlier aseismic creep rather than post deformation. The preservation of 7 nm and 30 nm grains thus suggests the Copper Creek thrust experienced at least two unstable slip events, with the 7 nm grains representing the more recent slip event.

2.5 Model for an Unstable-Stable Cycle

The newly documented structures reported here coupled with those previously documented by Wells et al., (2014) indicate at least two cycles of unstable slip followed by aseismic creep along the Copper Creek thrust. We propose a sequence of deformation processes, recorded by microstructures in these fault rocks, that is consistent with cyclic episodes of unstable slip and aseismic creep (Figure 2.3A). To consider the changes in differential stress and strain rates during deformation, and the mechanics associated with unstable slip, we have constructed a deformation mechanism map for calcite at 180 °C based on flow laws for grain-size sensitive creep, grain-size sensitive plus grain size insensitive creep, and dislocation creep (Figure 2.3B). Our model focuses on calcite deformation, as calcite forms the stress-supporting framework of the fault zone (Wells et al., 2014). The

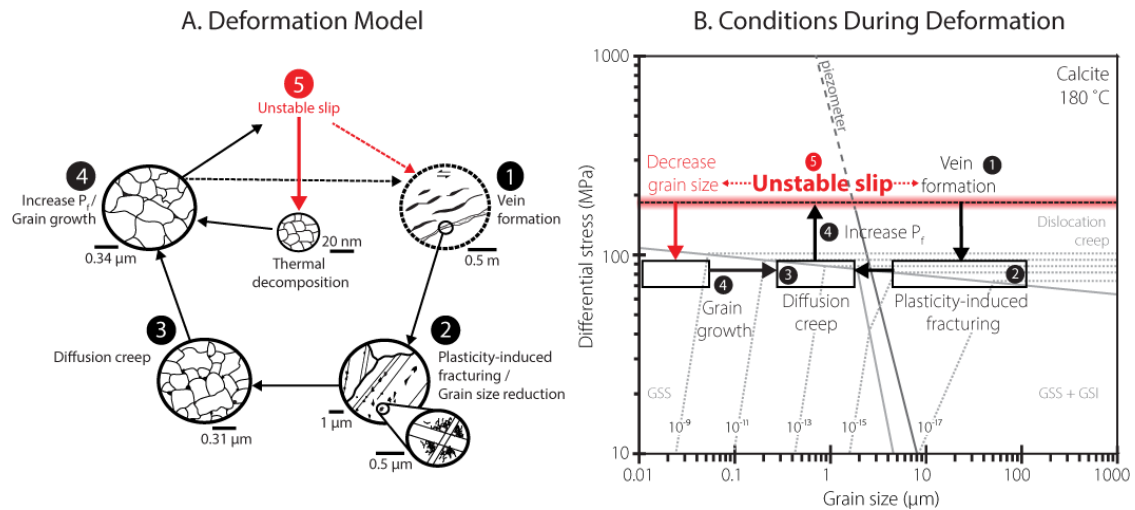


Figure 2.3. Stable-unstable slip model. (A) Model of the stable-unstable cycle. Stage 1: Fractures enable the formation of coarse-grained calcite veins. Stage 2: Vein calcite deforms by aseismic dislocation creep and twinning; plasticity-induced fracturing reduces grain size. Stage 3: Further aseismic deformation of ultrafine-grains by diffusion creep deformation. Stage 4: Aseismic grain growth and/or development of interpenetrating grain boundaries leads to an increase in pore fluid pressure and differential stresses. Stage 5: Increased stress may lead to localized fracturing (dashed arrows) or an unstable slip event (red), resulting in the formation of nanograins, vesicular calcite, and new fractures. (B) Deformation mechanism map constructed using calcite flow laws for grain-size sensitive creep (GSS; Herwegh et al., 2003), grain-size sensitive plus grain-size insensitive creep (GSS+GSI; Walker et al., 1990), and dislocation creep (de Bresser, 2002) at 180 °C. Byerlee's law at saturated conditions for continental crust is shown as a black dashed line (190 MPa). Calcite paleopiezometer is shown as a gray solid-dashed line (Barnhoorn et al., 2004).

shale beds contribute to these processes primarily through initial fracturing, likely the result of high pore fluid pressure (Hickmen et al., 1995), that enables fluid migration and allows the precipitation of coarse-grained calcite veins (Wells et al., 2014) (Stage 1).

During Stage 2, the newly formed coarse-grained calcite in veins develops twins and a LPO consistent with crystal plasticity. Crystal plasticity with only limited dislocation climb leads to stress concentrations and the formation of pores at twin-twin intersections, plasticity-induced fracturing, and a reduction in grain size (Wells et al., 2014) (Stage 2). Limited dislocation creep indicates the coarse-grained calcite plots near the dislocation creep - grain-size sensitive creep boundary, where strain rates are estimated between 10^{-11} - 10^{-13} s⁻¹ at stresses of 70-100 MPa (Stage 2) (Wells et al., 2014). Following grain size reduction, the ultrafine-grained calcite (340 nm) deforms by diffusion creep accommodated grain boundary sliding during aseismic creep, resulting in fault weakening or an increasing strain rate (Stage 3) (Wells et al., 2014).

Increased cohesion during the aseismic period is suggested by interpenetrating grain boundaries, as well as straight grain boundaries and triple junctions within the ultrafine-grained calcite grains (310 nm), indicating grain growth (Stage 4). As calcite grains grow, porosity decreases, resulting in rising pore fluid pressures (Sibson, 1977; Sibson, 1992; Hickman, et al., 1995). Stress increases along the fault zone, resulting in either localized brittle failure (e.g., fracturing followed by vein formation) or possibly seismic slip (Stage 1), resulting in fluidized structures, thermal decomposition of pre-existing calcite, and fracture formation (Stage 5). Brittle failure may occur at ~190 MPa, assuming Byerlee's Law at saturated conditions.

The nanometer calcite grains (7 nm), vesicular calcite, and coated clasts in the CC fault rocks suggest unstable slip (Stage 5). We propose that during slip, differential stress could have dropped by up to 50 MPa (Noda et al., 2009; Beeler et al., 2016) from an upper estimated stress of 190MPa to the lowest estimated stress during aseismic creep (Stage 5). Such a large stress drop estimate suggests a significant stress fluctuation occurs within this proposed cycle. Frictional heating during slip produces lime, quickly forming 7 nanometer calcite grains (Han et al., 2007; Collettini et al., 2013; Violay et al., 2013) with a relatively low coefficient of friction (Carpenter et al., 2015). Localized fluid flow results in coated clasts (Smith et al., 2008; Mitchell et al., 2015). Fractures are also likely to form during the unstable slip event, decreasing pore fluid pressure, effectively bringing the deformation back to the beginning of the cycle (Stage 1; vein formation). Subsequent cycles of deformation now contain nanometer grains within the fault zone, which will contribute to fault strengthening when grain growth, as evident by the preservation of the 30 nm grains, occurs during aseismic creep (Stage 4).

2.6 Conclusions

Nanograins, vesicular calcite, and coated clasts preserved along the Copper Creek thrust indicate slip at or near seismic rates. Coupled with evidence for grain-size sensitive diffusion creep in ultrafine-grained calcite, these microstructures record evidence for cyclic unstable -aseismic slip along an ancient thrust in the Southern Appalachians. Preservation of 7 nm grains adjacent to the slickenside surface as well as 30 nm grains within coarser calcite matrix that likely grew from ~7 nm during aseismic creep, suggest more than one episode of seismic deformation. Grain growth of the nanograins (7-310 nm) and diffusion creep of the

ultrafine-grained calcite (340 nm) increased cohesion of the fault zone during aseismic creep, resulting in fault strengthening and increased pore fluid pressure, perpetuating the stable-unstable cycle.

3. LATTICE-PREFERRED ORIENTATION DEVELOPMENT IN FINE-GRAINED DOLOMITE SHEAR ZONES

3.1 Introduction

Dolomite often deforms by localizing along narrow zones of finer ($< 20 \mu\text{m}$) grains. Whether in experiment studies (Davis et al., 2008; Delle Piane et al., 2008; Holyoke et al., 2013, 2014) or along natural systems (Woodward et al., 1988; Erickson, 1994; Hadizadeh, 1994; Newman and Mitra, 1994), similar localized zones develop and accommodate most of the deformation. These zones often form as a result of both brittle and ductile processes (Newman and Mitra, 1994; Holyoke et al., 2013). Many of these zones also contain a weak lattice preferred orientation (LPO). While these structures and fabric are common, the deformation processes that contribute to the formation of an LPO fabric are limited to a handful of studies.

Recent experimental work on dolomite (Davis et al., 2008; Delle Piane et al., 2008; Holyoke et al., 2013, 2014) indicates that the estimated deformation conditions for these zones might be consistent with being diffusion creep dominated. In these high temperature ($> 700 \text{ }^\circ\text{C}$) experiments, coarse-grained dolomite deformed by dislocation creep and dynamic recrystallization, which resulted in localized zones of fine-grained dolomite and a noticeable weakening from the peak stress (Holyoke et al., 2013, 2014). However, in experimentally deformed fine-grained dolomite with a stress exponent of ~ 1.3 , a weak LPO developed (Delle Piane et al., 2008). While the formation of a LPO might indicate dislocation creep, the development of a weak LPO combined with the conditions during

deformation suggest diffusion creep could have dominated. Extrapolation of these results (Davis et al., 2008; Delle Piane, 2008; Holyoke et al., 2013) to natural strain rates suggest that fine-grained dolomite may deform by diffusion creep at temperatures as low as approximately 300 °C at grain sizes less than 10 μm. However, it is not known if the microstructures and deformation mechanisms within the experimentally deformed localized zones, at high temperatures and fast strain rates, form by the same process as those observed in naturally deformed dolomites.

Current observations of naturally formed localized zones of fine-grained dolomite suggest multiple deformation mechanisms were active during deformation. Both brittle and ductile deformation mechanisms are common in naturally deformed dolomite over a range of temperatures. Localized zones in deformed dolomite are documented along the Lewis thrust in the Canadian Rockies (100-175 °C) (Erickson, 1994) as well as along the Saltville thrust (150-240 °C) (Hadizadeh, 1994) and the Pioneer Landing thrust in the Southern Appalachians (~300 °C) (Newman and Mitra, 1994). At lower temperatures (< 300 °C), deformation tends to be dominated by brittle processes (Woodward et al., 1988; Erickson, 1994; Hadizadeh, 1994). At higher temperatures (> 300 °C), a limited number of studies suggest that coarse-grained dolomite deforms by dislocation creep (White and White, 1980; Newman and Mitra, 1994), resulting in a c-axis lattice preferred orientation (LPO) oriented perpendicular to the foliation (Leiss and Barber, 1999). This LPO is similar to that formed in experimental studies (Delle Piane et al., 2008). The processes associated with either fine-grain dolomite or within fine-grained zones remain unclear.

The deformation mechanisms that dominate within these zones have important implications for the relative strengths of common crustal lithologies. In an effort to understand the deformation processes that control deformation within these localized zones, we examine microstructures present within experimentally deformed dolomite, and compare these structures with those observed along localized zones in naturally deformed dolomites. Our objective is to determine the deformation processes that influence the development of a weak LPO within fine-grained dolomite. Using optical and electron microscopy, and electron-backscattered analyses to determine LPOs, we evaluate the microstructures these zones, and to infer the dominant deformation mechanisms active at these conditions. In experimentally deformed dolomite, both dislocation and diffusion creep work to form a weak c-axis LPO. However, in naturally deformed dolomites, the conditions (e.g., temperature) can strongly influence the dominant processes and strength of the resulting LPO in fine-grained zones.

3.2 Materials and Methods

This study examined two experimentally deformed dolomite samples and two naturally deformed dolomite samples. The two experimentally deformed samples were previously examined in Holyoke et al., (2013, 2014). Naturally deformed samples originate from the Pioneer Landing thrust and the Town Knobs thrust in the Southern Appalachians. The Pioneer Landing thrust deformed at or near the estimated temperature for activation of diffusion creep in fine-grained dolomite, as estimated from Holyoke et al., (2014), while the Town Knobs thrust deformed at temperatures below the estimate.

3.2.1 *Experimental Samples*

This study examines two experimentally deformed dolomite samples with localized zones of fine-grained dolomite from Holyoke et al. (2013) (single polycrystalline core; experiment D-11) and Holyoke et al. (2014) (fine grain shear setup; experiment D-26) (Figure 3.1A, 3.1B). Both samples were deformed using a Griggs-type triaxial piston cylinder rock deformation apparatus at a temperature of 900 °C and at a strain rate of 10^{-4} s^{-1} . The estimated stress exponent (n) is ~1.3 for each sample (Holyoke et al., 2013, 2014). The observations made in this study are consistent with Holyoke et al., (2013, 2014), and adds an in-depth analysis of the finer grains.

The single polycrystalline sample deformed Madoc dolomite at 900 °C, and at a confining pressure of 1150 MPa with total strain 41% (Holyoke et al., 2013). Starting material is coarse-grained (240 μm) and contains straight grain boundaries, few twins, and a weak, pre-existing c-axis fabric (maximum point concentration: ~2) (Davis et al., 2008). Secondary phases are less than 1% of the total bulk compositions (Davis et al., 2008).

The fine-grained shear sample deformed a ~735 μm layer of synthetic dolomite (average grain diameter: 2.5 μm) between two coarse-grained Madoc dolomite pistons. The sample was deformed at a confining pressure of 1140 MPa to ~10% shortening (Holyoke et al., 2014). Synthetic dolomite was formed by hot isostatic pressing described in Davis et al. (2008). The undeformed synthetic dolomite contains no porosity and no secondary phases (Davis et al., 2008).

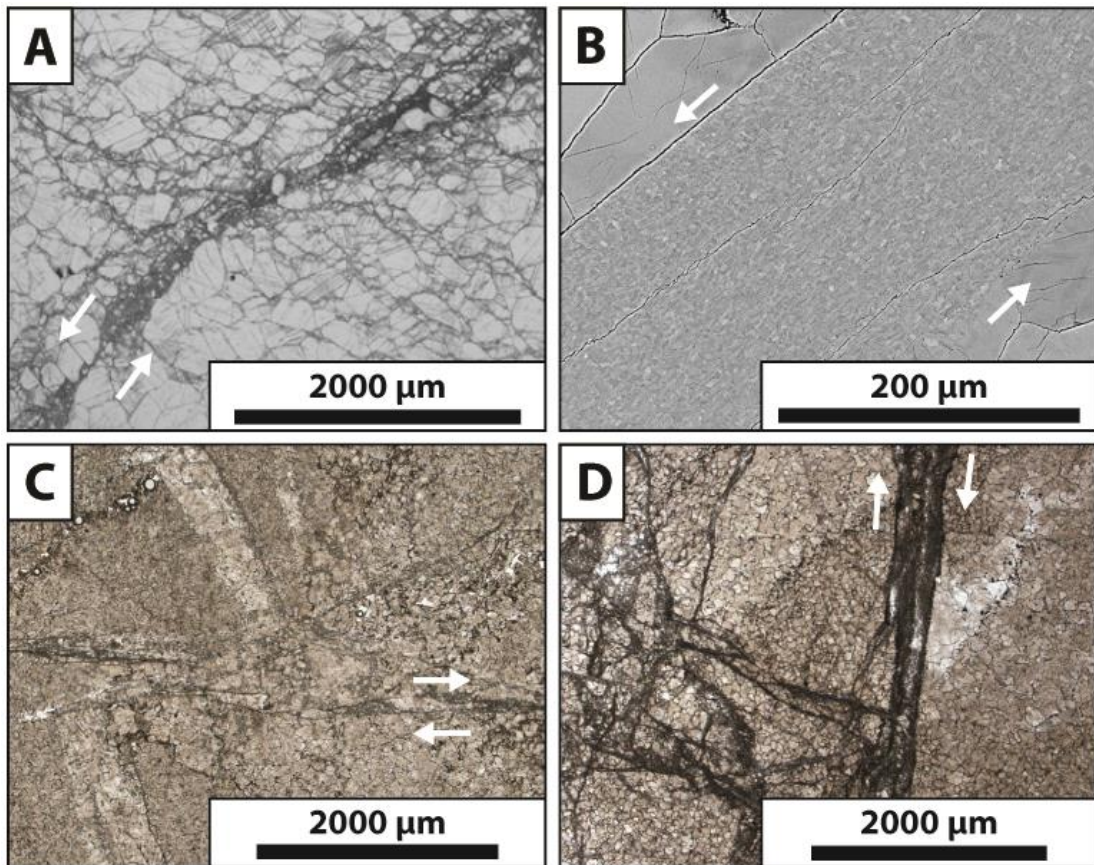


Figure 3.1. Overview of localized zones of fine-grained dolomite. BSE images of experimentally deformed (A) polycrystalline dolomite (modified from Holyoke et al., (2013)) and (B) fine-grained sheared dolomite. The maximum compress stress is oriented vertically for both images. Optical photomicrographs of naturally deformed dolomite from (C) the Pioneer Landing thrust and (D) the Town Knobs thrust. Fault displacement is oriented top to the left for both images. Localized zones of fine-grained dolomite (fgz) offset coarse-grained host dolomite, fine-grained host dolomite, stylolites (sty), dolomite veins (v), and another localized zone. Optical photomicrograph.

3.2.2 *Natural Samples*

We also examined two naturally deformed fine-grained shear zones from the exposures of the Pioneer Landing thrust and Town Knobs thrust, located in the foreland fold-and-thrust belt of the Southern Appalachians (King and Ferguson, 1960; Harris, 1976; Harris and Milici, 1977) (Figure 3.1C, 3.1D). Pioneer Landing thrust is located in the Mountain City tectonic window, which is transitional between the Blue Ridge Province and the Valley and Ridge Province in Eastern Tennessee. Temperatures during deformation are estimated to have been ~270 °C (burial depth of 9 km, 30 °C/km). The Pioneer Landing thrust is associated with a duplex structure that emplaces Cambrian Shady dolomite on top of Cambrian Shady dolomite, and has an estimated displacement of 100-320 m (King and Ferguson, 1960; Newman and Mitra, 1994). For this study, we examined dolomite collected from the hanging wall (Figure 3.1C). Newman and Mitra (1994) documented dolomite veins and stylolites in the coarse-grained host dolomite (average grain size: 36 μm). Observations made in this study are consistent with observations documented in Newman and Mitra (1994).

The Town Knobs thrust is located ~125 km to the west of the Pioneer Landing fault, and is the roof thrust of a duplex structure associated with the Saltville thrust (Figure 3.1D), which places the Cambrian Rome Formation on the Cambrian Conasauga Group (Haney, 1966; Woodward, 1985). The Town Knobs thrust is structurally located above the Saltville thrust (estimated burial depth of 5-8 km; House and Gray, 1982b) and structurally below the Copper Creek thrust (estimated burial depth of 4-6 km; Harris, 1976; Harris and Milici, 1977). Based on these estimates, we suggest a burial depth of 4-8 km for the Town Knobs

and, thus, estimate temperatures of deformation between 100-240 °C (burial depth 4-8 km, 30 °C/km). Displacement is estimated at ~275 m (Haney, 1966). Both the hanging wall and footwall at this exposure are dolomite units; however, the footwall dolomite is homogeneous while the hanging wall dolomite is silty (percentage of K-feldspar-rich silt varies throughout the bed) and is cross-cut by calcite veins. Samples described in this contribution were collected from the homogeneous footwall dolomite (Figure 3.1D). Dolomite veins and zones of fine-grained dolomite are observed within the coarse-grained host dolomite.

3.2.3 Methods

Standard (~30 μm) or ultrathin (~5 μm) sections were made for each localized zone for microstructural analysis. Sections are oriented parallel to the maximum compressive stress direction for experimental samples, and perpendicular to the foliation and parallel to lineation in the shear zone studied for natural samples. Analyses of the coarse-grained host dolomite and large-scale microscopic features were made using optical microscopy. Additional microstructural analyses within the fine-grained zones were made using a scanning electron microscopy (SEM: FEI Quanta 600 FE-SEM housed in the Microscopy and Imaging Center, Texas A&M University), including backscatter electron (BSE) imaging with orientation contrast. The lattice orientation of individual dolomite grains was collected using a SEM with electron backscatter diffraction (EBSD) capabilities. EBSD data was analyzed using texture analysis software MTEX in Matlab. Grain boundaries were set at a misorientation of greater than 20°, while subgrains were set at misorientations of less than 20°. Grain size was determined using image analysis software (ImageSXM).

3.3 Dolomite Microstructures and Textures

3.3.1 Experimentally Deformed Dolomite

3.3.1.1 Polycrystalline Dolomite

Following deformation, a localized zone of fine-grained dolomite (20-100 μm) oriented $\sim 45^\circ$ to the maximum compressive stress direction developed within the coarse-grained polycrystalline dolomite (Holyoke et al., 2013, 2014). We examined the finer grains within the 20-250 μm thick localized shear zone (Figure 3.1A; Figure 3.2A-C). The host grains contain twins, and fine grains along the grain and twin boundaries. Holyoke et al. (2013) discusses in detail the coarse-grain microstructures. Within the localized zone, the average grain size is 1.6 μm .

While most the grains within the zone are less than 5 μm , coarser grains are observed within the zone. The larger grains are usually irregular shaped (Figure 3.2C); however, there are slightly elongated in some sections of the shear zone (Figure 1A). Elongated grains with a shape preferred orientation (SPO) have an axial ratio of 1:2, which is oriented parallel to the shear zone. All coarser dolomite grains have irregular to interpenetrating grain boundaries and patch-gradational grayscale, which suggests distortions in the crystal lattice (Figure 3.1C). Some of the grayscale variation at the coarse-grain boundaries mimics subgrain-like structures. The subgrain-like structures are more common within the elongated grains than in the irregular-shaped grains (Figure 3.1A).

The finer grains that compose most of the localized shear zone vary in shape from equant to elongate. Equant grains with straight grain boundaries often form triple junctions with neighboring grains (Figure 3.2A). Coarser, elongated grains occur near the equant

grains. Grains with irregular grain shapes have interpenetrating grain boundaries. Several of these grains contain tapered edges, particularly along coarser dolomite grains. Four-grain junctions are common (Figure 3.2B, 3.2C). Some of the four-grain junctions involve fine grains with tapered edges along elongated grain boundaries. It is unclear if the grayscale distortion, which occurs at the four-grain junction, within the coarser grain is a grain or subgrain because the grain boundary is indiscernible (Figure 3.2B). The alignment of grain boundaries is also observed, whether the grains are equant or irregular shaped (Figure 3.2A, 3.2B).

The spatial distribution of similarly oriented grains and grain boundary characteristics were analyzed using EBSD (Figure 3.3). Within the polycrystalline shear zone, there are no continuous layers of similar oriented grains (Figure 3.3A). However, there are localized, discontinuous bands ($\sim 10\ \mu\text{m}$ in length) of similarly oriented grains oriented parallel to the shear zone. Coarser grains within the shear zone often have misorientation boundaries of less than 5° within the grain, which suggest that the grayscale variations (i.e., subgrain-like structures) observed in BSE images (Figure 3.2A-C) are subgrains. In some cases, the largest grains ($>10\ \mu\text{m}$) are filled with low angle boundaries except for a small portion of the grain ($\sim 2\ \mu\text{m}$) (Figure 3.3A). Grain boundary misorientations of less than 10° occur between finer grains, primarily on the end of elongated grains within the discontinuous bands (Figure 3.3A). The lattice orientation of individual dolomite grains are plotted on stereoplots for the c - $\{0001\}$, a - $\{112\bar{0}\}$, and r - $\{101\bar{4}\}$ (Figure 3.4). A weak c -axis LPO oriented perpendicular to the shear zone (Figure 3.4A), with a point maxima of 2.4, is observed in the localized shear zone

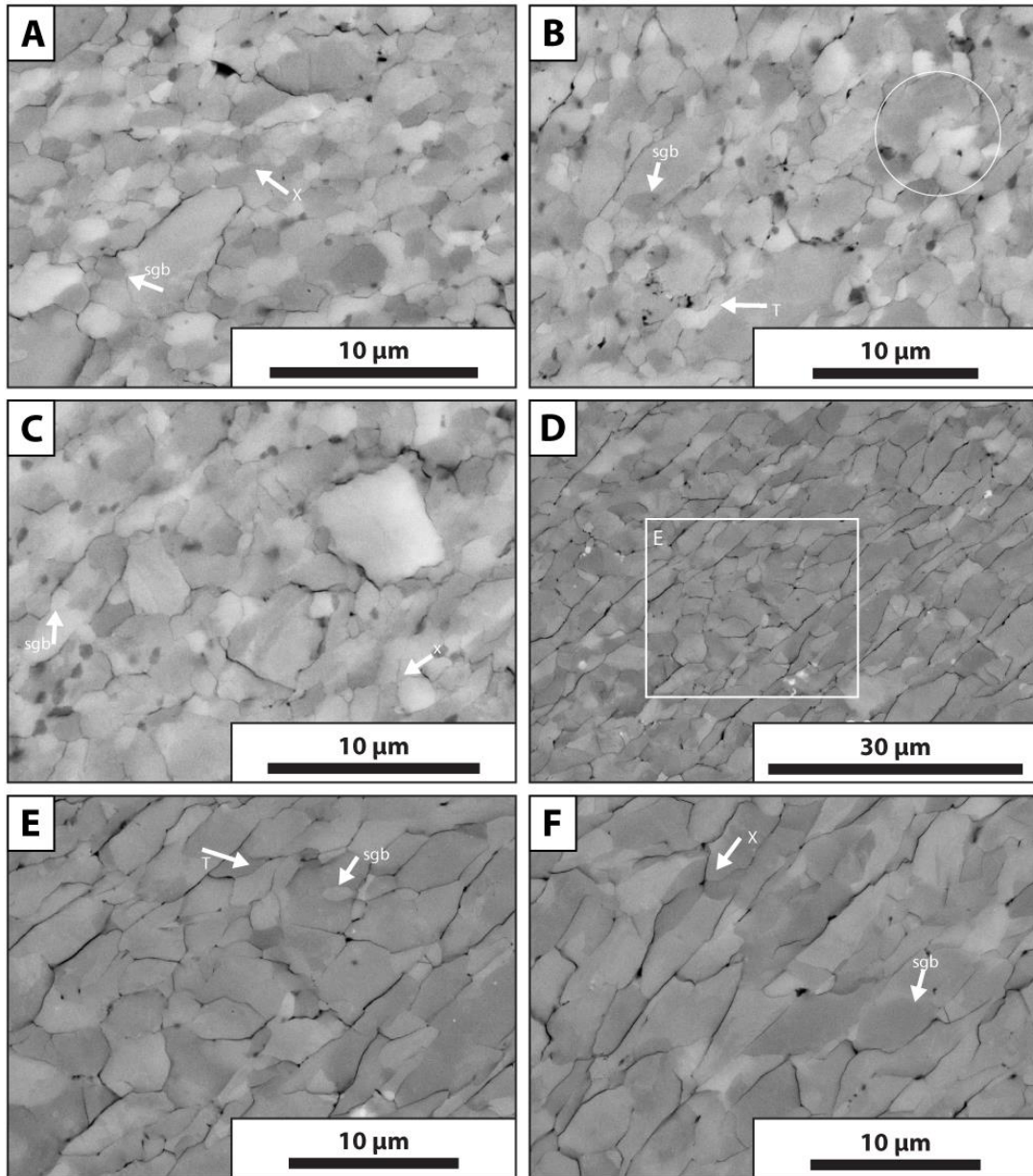


Figure 3.2. Experimentally deformed dolomite. BSE images of (A)-(C) polycrystalline dolomite and (D)-(F) sheared fine-grained dolomite. (A) Within the localized zone, subgrains (sgb), aligned grain boundaries (agb), and four-grain junctions (X) are common. (B) In the BSE image, larger grains are elongated and contain subgrains (sgb), while smaller grains have irregular to tapered grain boundaries. Subgrains form structures similar to four-grain junctions with neighboring grains (circle). (C) Larger grains contain subgrains (sgb) and irregular grain boundaries. Four-grain junctions are also observed (x). (D) Within the experimentally sheared fine-grained dolomite. Layers of irregular shaped grains are adjacent to layers of grains with a strong SPO parallel to the shear zone. (E) Elongated grains contain subgrains (sgb) and irregular grain boundaries. Some grains contain tapered edges (T) and form four-grain junctions (x). (F) Subgrains (sgb) within elongated grains form a four-grain junction with neighboring grains (circle). BSE images.

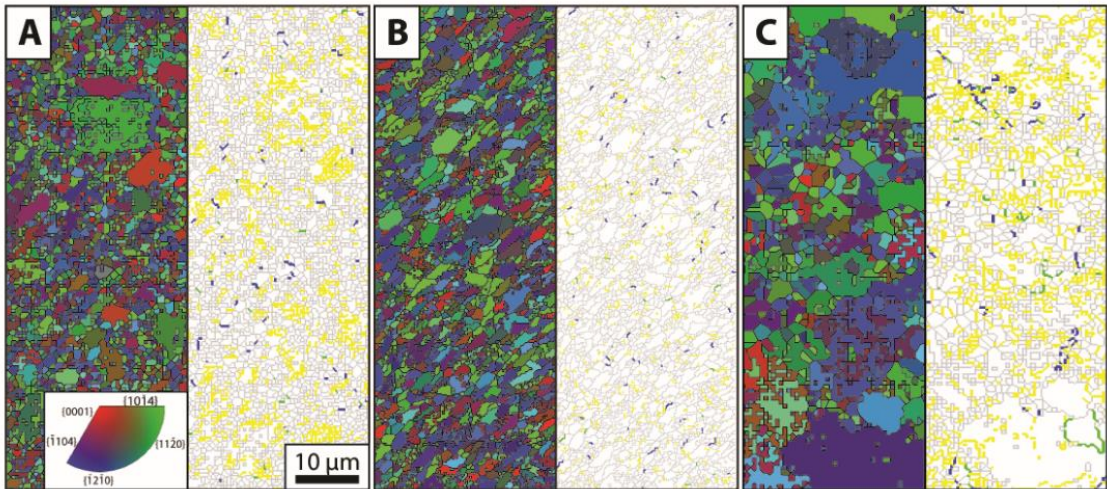


Figure 3.3. EBSD maps. Inverse pole figure map from an area within the localized zone and corresponding grain boundary maps for (A) experimentally deformed polycrystalline dolomite, (B) experimentally deformed fine-grained sheared dolomite, and (C) naturally deformed dolomite along the Pioneer Landing thrust. Arrows indicate direction of slip. Low angle boundaries are assigned less than 20 of misorientation. Grain boundaries of 1-5 (yellow), 5-10 (green), 10-20 (blue), and >20 (grey) are shown.

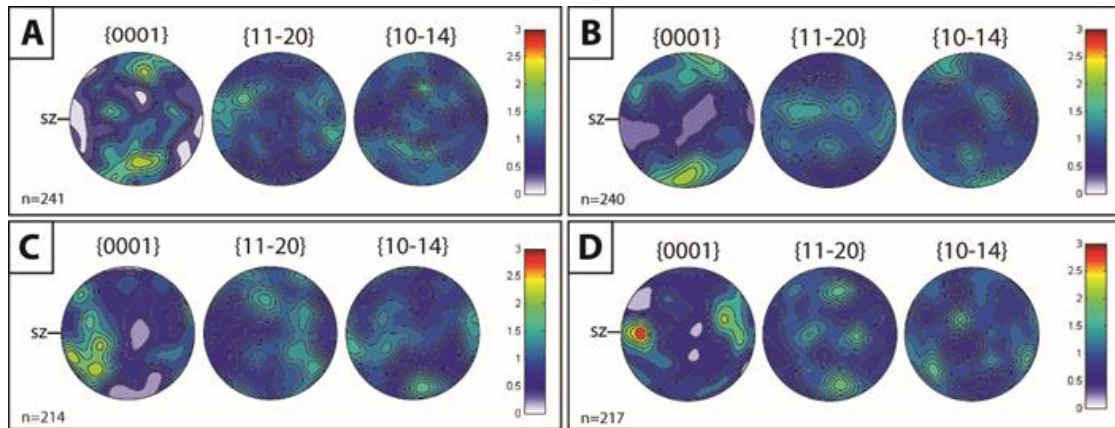


Figure 3.4. Pole figures of fine-grained dolomite. Contoured plots of c- $\{0001\}$, a- $\{11-20\}$, and r- $\{10-14\}$ axes for (A) experimentally deformed polycrystalline dolomite, (B) experimentally deformed fine-grained dolomite, (C) naturally deformed along the Pioneer Landing thrust, and (D) naturally deformed along the Town Knobs thrust. A weak c-axis LPO oriented perpendicular to the shear direction developed in both experimental samples, while a weak c-axis LPO oriented $\sim 30^\circ$ from horizontal to the shear zone developed along the Pioneer Landing thrust. The strongest c-axis LPO observed in this study developed along the Town Knobs thrust, and is oriented parallel to the shear zone.

3.3.1.2 Sheared Dolomite

The starting shear zone thickness of 735 μm is reduced to 230 μm during shear (Figure 3.1B). While Holyoke et al., (2014) observed an increase in grain size from 2.5 to 3.1 μm , we observe grains as large as 8.5 μm . Grain size and shape varies between bands of equant shape to bands of elongated grains within the shear zone (Figure 3.2D-F). Each band is less than 25 μm wide, and oriented parallel to the shear zone. The coarse-grained Madoc dolomite pistons remained undeformed.

Bands of fine, equant grains have an average grain size of 5 μm . Interpenetrating grain boundaries and tapered edges are common. Several grains form four-grain junctions with other grains, some with patchy grayscale and subgrains (Figure 3.2E). Voids are observed at the center of some of the junctions.

A strong SPO with an axial ratio of 1:4 occurs in other bands within the shear zone (Figure 3.2D, 3.2F). While all the grains within the shear zone are fine-grained, the elongated grains are slightly larger than the more equant dolomite grains. Elongated grains have aligned grain boundaries parallel to the shear zone, which is accentuated by fractures that formed during unloading of the sample (Figure 3.2F). These grains often contain interpenetrating grain boundaries and patchy grayscale. Subgrain and subgrain-like structures (i.e., indiscernible grain boundaries) are common, and seem to form four-grain junctions with neighboring grains (Figure 3.2F).

An EBSD map of the fine-grained dolomite in the center of the shear zone shows elongated grains oriented parallel to the shear zone, as well as bands of finer grains (Figure 3.3D). There are no continuous layers of similarly oriented grains; however, grains oriented

in the $(1\bar{1}04)$ and $(1\bar{2}1\bar{0})$ direction form short, discontinuous bands within the shear zone (Figure 3.3A). While low-angle boundaries ($< 5^\circ$) is common in the polycrystalline shear zone, similar grain boundaries with low misorientation are not as common within the fine-grained shear sample. Most of the low-angle boundaries occur within or immediately adjacent to coarser, elongated grains. A weak c-axis LPO formed within the shear zone, and is oriented perpendicular to the shear direction (Figure 4B). The point maximum is 2.3, which is similar to that observed within the polycrystalline shear zone.

3.3.2 Naturally Deformed Dolomite

3.3.2.1 Pioneer Landing Thrust

Microstructures near and within a localized zone of fine-grained dolomite were documented from a sample located within the Pioneer Landing fault hanging wall, approximately 1 m from the shear zone (Figure 3.5A-C). The host dolomite at this location is composed of coarse-grained dolomite (average grain size: 42 μm) and fine-grained dolomite (average grain size: 19 μm), which are separated across stylolites. Dolomite veins, offset by stylolites, and narrow zones of fine-grained dolomite (20-100 μm thick) that exhibit localized shear across them are common (Figure 3.1C). This study examined a localized zone of fine-grained dolomite that appears to be oriented parallel to the main fault zone; however, there could be some 3D orientation of the zone that we cannot account for because of the 2D nature of the thin section (Figure 4A-C). The host dolomite near this localized zone contains undulatory to patchy extinction and serrate grain boundaries (Figure 3.6B). Subgrains are common within the host grains, and discontinuous zones of fine-grained dolomite ($< 10 \mu\text{m}$) are common. Dolomite host grains are occasionally twinned, and some

of these twins have irregular boundaries. The host structures and discontinuous zones are documented throughout the hanging wall (Newman and Mitra, 1994).

A localized zone of fine-grained dolomite (1-20 μm) examined for this study is up to 60 μm thick and offsets stylolites, dolomite veins, and other localized zones (Figure 3.1C). The boundary between localized zones and the coarse-grained host dolomite is sharp, and stylolites oriented parallel to the local shear zone occur within the center of these zones (Figure 3.6A-C). While Newman and Mitra (1994) documented fine grains with a strong SPO in several localized zones, the zone we observe for this study does not contain a SPO. A few grains are elongated; however, they are not common (Figure 3.6C). Fine-grains within these localized zones contain interpenetrating to irregular grain boundaries (Figure 3.6C). Four-grain junctions are rare, and the few that are observed, due contain voids at the center of the junction (Figure 3.6C). Some of the larger grains ($> 3 \mu\text{m}$) contain subgrain-like structures, while patchy grayscale is rare (Figure 3.6C).

We do not observe any spatial relationships between similarly oriented grains within the shear zone or any discontinuous bands (Figure 3.3C). Coarse dolomite grains adjacent to the localized zone contain numerous subgrains with a misorientation less than 5° . Within the shear zone, these low-angle grain boundaries occur primarily within some of the larger grains ($> 3 \mu\text{m}$) (Figure 3.3C). The density of these low-angle boundaries is similar to what is observed in the experimentally deformed polycrystalline dolomite. Fine-grained dolomite within the localized zone contains a weak c-axis LPO, with a point maximum of 2.4, subparallel to the shear zone. The fine-grained dolomite LPO is similar in strength to those produced in the experimentally deformed fine-grained dolomite zones.

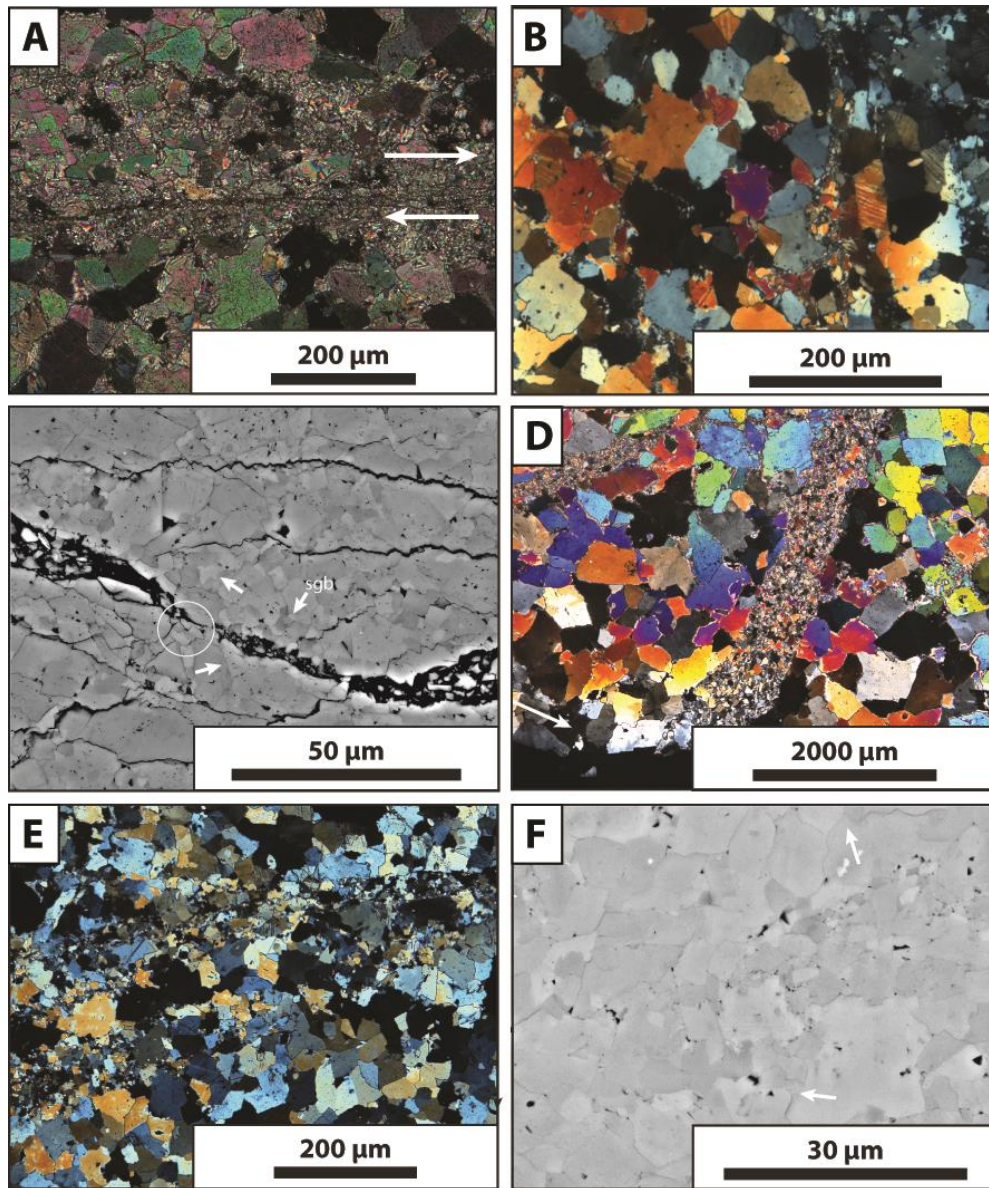


Figure 3.5. Naturally deformed dolomite. Microstructures along (A)-(C) the Pioneer Landing thrust and (D)-(E) the Town Knobs thrust. (A) An overview of a localized zone that contains fine-grained dolomite. Optical photomicrograph. (B) Discontinuous zones of fine-grain dolomite cross-cut coarse-grained host dolomite. Lobate grain and irregular grain boundaries (arrows), patchy extinction, subgrains (sgb) and twins occur in coarse-grained host dolomite. Optical photomicrograph. (C). Interpenetrating grain boundaries (arrows) and subgrains occur within the fine-grained dolomite. Within the circled area, grains appear to form a four-grain junction structure. BSE image. (D) A localized zone of fine-grained dolomite (~630 μm wide). Optical photomicrograph. (E) Coarse-grained dolomite contains lobate grain boundaries (arrows), patchy extinction, and deformation bands. Thin twins are rare (T). Fine-grained dolomite is observed around coarse-grained boundaries (fg). Optical photomicrograph. (F) Within the localized zone, fine-grained dolomite surrounds larger grains, which contain lobate grain boundaries, patchy extinction, and subgrains (sgb). Porosity (black) is ~1%. BSE image.

3.3.2.2 Town Knobs Thrust

We examined two samples located ~12 m and ~50 m into the footwall from the Town Knobs shear zone. In both samples, the host dolomite contains segregated sections of coarse- and fine-grained dolomite that range in grain size from 10-200 μm (average 45 μm), often separated by stylolites (Figure 3.1D-F). Patchy undulatory extinction, deformation bands, lobate to serrated grain boundaries, and inter- and intragranular fractures are common in the host dolomite (Figure 3.6D, 3.6E). Fine-grained dolomite ($< 10 \mu\text{m}$) is common along these microfractures. We also observe subgrains along host grain boundaries, as well as along deformation bands. Thin twins are rare within the coarse-grained dolomite (Figure 3.6E). Discontinuous zones of fine-grained dolomite ($< 20 \mu\text{m}$ thick) anastomose around coarser dolomite grains (Figure 3.6E).

The localized zones (~1 mm wide) of fine-grained dolomite offset stylolites and other localized zones (Figure 3.1D). The boundary between the fine-grained zone and the host dolomite is sharp, and coarse-grained dolomite veins are common within these zones (Figure 3.1D). Coarser grains ($> 20 \mu\text{m}$) within the localized zone have similar microstructures to those observed within the coarse-grained host dolomite including patchy to undulose extinction, subgrains, and lobate grain boundaries (Figure 3.6F). The fine-grained dolomite within the localized zones ranges from 1-60 μm (average grain size: 2.9 μm). The finer grains ($< 20 \mu\text{m}$) that surround the coarser grains contain irregular grain boundaries. Unlike the fine-grained dolomite within the experimentally deformed dolomite shear zones and along the Pioneer Landing thrust, the grains within the Town Knobs shear zone do not exhibit a strong variation in greyscale.

To determine if the fine-grains within the shear zone contain a LPO similar to those observed in other localized zones, lattice orientations were collected of individual fine grains. The fine-grained dolomite within localized zones does contain a c-axis LPO (point maximum: 3.1), which is oriented parallel to the main shear zone (Figure 3.5D). The c-axis LPO is stronger than the LPO observed within localized zones along the Pioneer Landing thrust and experimentally deformed dolomites. As a result of the different microstructures, grain size, and LPO present within the shear zone, this study did not analysis the spatial distribution of the lattice orientation.

3.4 LPO Fabric in Fine-Grained Dolomite

Localized zones are observed in both experimental and naturally deformed dolomites that formed over a range of conditions. These fine-grained zones exhibit some degree of LPO, mainly within the c-axis. There are several reasons for the occurrence of a LPO within fine-grained dolomite. The existence of a pre-existing LPO fabric or processes (e.g., dislocation creep) associated with grain size reduction may result in fine grains with a LPO. However, new processes active within the fine-grained zone could influence the strength of a pre-existing LPO or form a new LPO fabric. The processes that control grain size reduction are of particular importance as it may influence the microstructures and fabric within localized zones (e.g., Turner et al., 1956; Skrotski and Welch, 1983; Wenk and Christie, 1991; Wenk et al., 1997; de la Chapelle et al., 1998). All coarse-grained dolomite samples examined in this study experienced grain size reduction followed by strain localization along the newly formed fine grains. While there may be some debate over whether specific processes influenced the fabric observed along these zones, we also

examined experimentally deformed fine-grained dolomite that did not undergo grain size reduction. Our observations along this zone, helps us to understand the more complicated deformation history observed in our other samples.

3.4.1 Following Grain Size Reduction

All three scenarios are considered while examining the LPO fabric in the experimentally deformed polycrystalline dolomite. Madoc dolomite is the only sample examined in this study with a pre-existing weak LPO (Davis et al., 2008); therefore, we must consider if this fabric affected the LPO we observe in the fine-grained zones following strain localization. Earlier studies indicate static recrystallization may develop (Tommasi et al., 2008) or weaken and destroy (Humphreys and Hatherly, 1995; Wenk et al., 1997; Stöckhert and Duyster, 1999) a pre-existing LPO. The Madoc core was allowed to anneal within the Griggs apparatus before stress was applied. During this time, the annealing could have destroyed the pre-existing LPO fabric. Evidence of post-deformation annealing (e.g., foam structure, triple junctions) within the shear zone is limited, and several experimental studies (Ree and Park, 1997; Heilbronner and Tullis, 2002; Barnhoorn, et al., 2005) have documented little to no effect on a LPO fabric following deformation. Limited post-deformation annealing and similarities to the fine-grained sheared dolomite fabric, which did not contain a pre-existing fabric, indicate any pre-existing LPO observed in the Madoc dolomite did not affect the final LPO observed within the localized shear zone.

The formation of the localized zone within the coarse-grained dolomite is the result of grain size reduction during deformation (Holyoke et al., 2014), which could influence the fabric observed within the fine-grained zone. Undulatory extinction, twins, and fine-grains

along twin boundaries observed in coarse host grains (D-11; Holyoke et al., 2013, 2014) indicates dislocation creep processes. These structures indicate localization occurred by dislocation glide and bulge recrystallization, resulting in grain size reduction to $\sim 1.6 \mu\text{m}$ grains (Holyoke et al., 2013, 2014). Following grain size reduction by dislocation creep processes, fine-grains may contain a strong LPO fabric (Turner et al., 1956; Skrotzki and Welch, 1983; Wenk and Christie, 1991; Wenk et al., 1997; de la Chapelle et al., 1998). If dislocation creep continued to dominate within the localized zone, we would expect a strong LPO fabric. However, we observe a relatively weak LPO fabric in the localized zones. This observations suggest that deformation mechanisms other than dislocation creep could be responsible for the development or strength of the LPO (Schmid et al., 1987; Walker et al., 1990; Goldsby and Kohlstedt, 2001; Sundberg and Copper, 2008), or that other deformation mechanisms altered the LPO fabric following grain size reduction (e.g., dislocation creep transitions to diffusion creep or brittle fracture following grain size reduction) (Boullier and Gueguen, 1975; Wenk and Christie, 1991; Bestmann and Prior, 2003; Wells et al., 2014).

Experimental results for dolomite deformation, including the suite of experiments of which this was a part of (Holyoke et al., 2013), predict diffusion creep for this grain size ($\sim 7 \mu\text{m}$) at 900°C , with an estimated $n=1.3$ (Holyoke et al., 2014). Based on the microstructures observed in the localized zone (e.g., interpenetrating grain boundaries and dislocation-free grains (Holyoke et al., 2014)), the LPO in the experimentally deformed polycrystalline dolomite may also be the result of diffusion-accommodated grain boundary sliding. If deformation transitioned from dislocation creep dominated to diffusion creep dominated following grain size reduction, this could reduce the strength of the LPO fabric. Evidence of

dislocation creep is observed within the shear zone as subgrains. Subgrains primarily occur within the coarser grains, but these structures could be relics from earlier in the evolution when dislocation creep dominated. Alternatively, dislocation processes and diffusion processes may have contributed concurrently to the deformation (e.g., de Bresser et al., 2001). While coarser grains with irregular grain boundaries may be remnant, smaller elongated grains with subgrains may indicate active dislocation creep within the localized zone. The competing processes could then influence the strength of the LPO we observe within the fine-grain zone. However, we can eliminate remnant processes as a contributor to the formation of a weak LPO fabric.

3.4.2 Independent of Grain Size Reduction

The development of a LPO in the absence of grain size reduction enables us to examine the processes that contribute to the formations of a LPO without worrying about relic structures and transitioning processes. While the polycrystalline experiment experienced grain size reduction, the fine-grained dolomite within the shear experiment (D-26; Holyoke et al., 2014) did not. The weak LPO fabric observed in the fine-grained dolomite is not a relic of earlier deformation but formed during deformation.

Based on microstructural observations, fine-grained dolomite deformed by diffusion creep within the shear zone. Interpenetrating grain boundaries and four-grain junctions are common within the fine-grained dolomite, which suggest diffusional processes and grain boundary sliding. Further, the experimental results suggest stress exponent of $n=1.3$, consistent with diffusion creep. While dislocation creep is often attributed to the formation of a LPO, recent studies (Sundberg and Copper, 2008; Miyazaki et al., 2013) suggest

diffusion creep could contribute to a LPO in the absence of dislocation creep. Crystallographically controlled diffusion creep may lead to a weak LPO (Sundberg and Copper, 2008; Miyazaki et al., 2013). Grain growth in the shear experiment increased grain size from 2 μm to 8.5 μm , which also resulted in a SPO (Holyoke et al., 2014). These structures also consistent with diffusion creep, and may indicate crystallographically controlled diffusion creep occurred during deformation. However, we also observe evidence of dislocation creep, mainly in the formation of subgrains. These observations would indicate that diffusional processes alone did not contribute to the formation of a weak c-axis LPO in fine-grained dolomite.

The occurrence of subgrains indicates that some of the fine-grained dolomite deformed by dislocation creep. Dislocation creep could have occurred to accommodate grain boundary sliding (Gifkins, 1976; Pshenichnyuk et al., 1997). The formation of a weak LPO at low strains (Hansen et al., 2011; Michibayashi et al., 2013) and a strong LPO at high strains (Hansen et al., 2012) in experimentally deformed olivine is thought to be the result of dislocation-accommodated grain boundary sliding. The majority of the subgrains occur within the larger and elongated dolomite grains. The density of the structures is less than what is observed in the polycrystalline experiment. These observations indicate that in the absence of grain size reduction, dislocation creep is activated within the fine-grained dolomite and appears to contribute to the formation of a LPO.

Based on the evidence, the formation of a weak LPO in fine-grained dolomite seems to be the result of both diffusion- and dislocation-accommodated grain boundary sliding. Despite two processes contributing to a LPO, a weak LPO developed within the zone.

Hansen et al., (2011) suggested strains may influence the strength of the LPO when dislocation creep-accommodated grain boundary sliding occurs. It is possible that the shear experiment, which was strained 10%, was not sufficient to generate a stronger LPO. If diffusion creep is not contributing to the fabric, the weak LPO could be the result of competing dislocation-diffusion creep. As diffusional process accommodates the deformation, grain size increases. This may lead to a transition from diffusion creep to dislocation creep. However, this does not suggest dislocation creep now dominates, just that this process is influencing deformation. The competing processes could then result in a fairly weak LPO within the fine-grained shear zone.

3.4.3 Comparison to Nature

An extrapolation of the experimental conditions suggests that diffusion creep may be observed in naturally deformed dolomite at temperatures as low as 300 °C (Holyoke et al., 2014). Both natural samples documented in this study have an estimated temperature during deformation near this boundary. The naturally deformed samples also share some similar structures and fabrics to those observed in the experimentally deformed dolomites. Particularly within the coarse-grained dolomite, both the experimentally polycrystalline dolomite and host grains from each natural fault zone contain twins, undulatory extinction, lobate grain boundaries, and subgrains indicate crystal plastic and dislocation glide and grain boundary mobility, resulting in grain size reduction (Barber et al., 1981; Hirth and Tullis, 1992; Newman and Mitra, 1994). Deformation bands, which we only observe along the Town Knobs thrust, indicate dislocation mobility transitioning into subgrain development (Barber et al., 1981). Unlike the experimental studies, fractures are common,

indicating brittle processes also contributed to grain size reduction. However, extensive subgrain development suggests climb-accommodated subgrain rotation recrystallization dominated deformation in the host dolomite, resulting in grain size reduction (Barber et al., 1981; Hirth and Tullis, 1992; Newman and Mitra, 1994). The similarity between the experimentally deformed polycrystalline dolomite and natural deformed dolomites indicates the observed localized zones formed by relatively the same processes. Evidence for dislocation creep has previously been observed in naturally deformed dolomite but at higher estimated temperatures (600 °C: White and White, 1980; ~270 °C: Newman and Mitra, 1994). Barber et al., (1981) and Leiss and Barber (1999) attribute c-slip $((0001)\langle 21\bar{1}\bar{0}\rangle)$ as the primary domain for dislocation movement at low temperature conditions.

Within the experimentally and naturally formed localized zones, we observe two slightly different fabrics. The weak c-axis LPO observed within the localized zones of fine-grained dolomite along the Pioneer Landing thrust has is similar in strength to both experimentally deformed dolomite samples (Figure 3.4). However, the orientation of the point maxima is subparallel along the natural shear zone, as oppose to perpendicular. The difference in orientation may be a result of an unknown 3D orientation within the natural shear zone. Based on the fabric and conditions extrapolated from experimental studies (Holyoke et al., 2014), diffusion creep may have accommodated some of the displacement within the Pioneer Landing shear zone. An examination of the structures reveals fine grains with irregular grain boundaries, and four-grain junction structures, which suggest diffusion creep. However, there are also coarser grains with undulatory extinction and subgrains, which suggest some accommodation by dislocation creep. Whether both processes were

active during deformation is uncertain except that most of the structures observed within the fine-grained dolomite experiment, which did not experience grain size reduction, are observed within the Pioneer Landing shear zone. Based on the observations of both experimentally deformed dolomite, the activation of dislocation and diffusion creep within the fine-grained zone is possible.

While the weak c-axis LPO observed in the Pioneer Landing thrust closely resembles the fabric in the experimentally deformed dolomites, a stronger LPO observed within Town Knobs shear zone. At lower estimated temperatures, brittle and ductile processes resulted in grain size reduction. Localization along the newly formed fine-grained zones, however, seems to be dominated by dislocation creep. The grains within the zone are slightly coarser than those within the experimentally deformed fine-grained zones and along the Pioneer Landing thrust, and subgrains are more common within many of those grains along the Town Knobs thrust. These structures, in addition to a relatively stronger crystallographic fabric, suggest at slightly lower temperatures, the LPO development within fine-grained dolomite is controlled by dislocation creep rather than a mix of dislocation and diffusion creep.

3.5 Role of Mixed Mechanisms

While both natural fault zones deformed near comparable conditions, we observe one shear zone that deformed by diffusion and dislocation creep, and another that deformed by dislocation creep alone. To further understand the processes and conditions for grain size reduction and subsequent deformation of naturally deformed fine-grained dolomite, we constructed dolomite stress-grain size deformation mechanism maps using dolomite flow

laws (Davis et al., 2008; Delle Piane et al., 2008; Holyoke et al., 2013) to constrain the conditions during deformation of the naturally deformed dolomite. One mechanism map is generated at 240 °C, which is the highest estimated temperature for the Town Knobs thrust (Figure 6A), and another map is generated at 300 °C, which is the highest estimated temperature for the Pioneer Landing thrust (Figure 3.6B).

Although temperatures during deformation along the Town Knobs thrust are estimated to be lower than the along the Pioneer Landing thrust, we observe similar microstructures (e.g., lobate grain boundaries, subgrains) in the host dolomite along both fault zones. The activation of dislocation creep (e.g., subgrains) within the host dolomites indicate deformation occurred at stresses up to 450-500 MPa at strain rates of $\sim 10^{-11}$ - 10^{-15} s⁻¹. The formation of dolomite veins (i.e., evidence for brittle processes) indicate stresses reached ~ 240 MPa along the Town Knobs thrust (240 °C, maximum burial depth of 6 km) and ~ 300 MPa along the Pioneer Landing thrust (300 °C, maximum burial depth of 10 km), based on the frictional strength (Byrelee's law) of saturated crustal. The concurrent development of fractures and dislocation creep (e.g., veins formed within localized zones) may indicate strain rates of 10^{-11} - 10^{-13} s⁻¹ were more common.

While coarse-grained host dolomite deforms by similar processes over a range of temperatures, deformation of fine-grained dolomite along localized zones is strongly influenced, at least in part, by temperature. Following grain size reduction along the Town Knobs thrust, considerable weakening within the localized zones of fine-grained of diffusion creep in the fine-grained dolomite indicates stresses along these localized zones

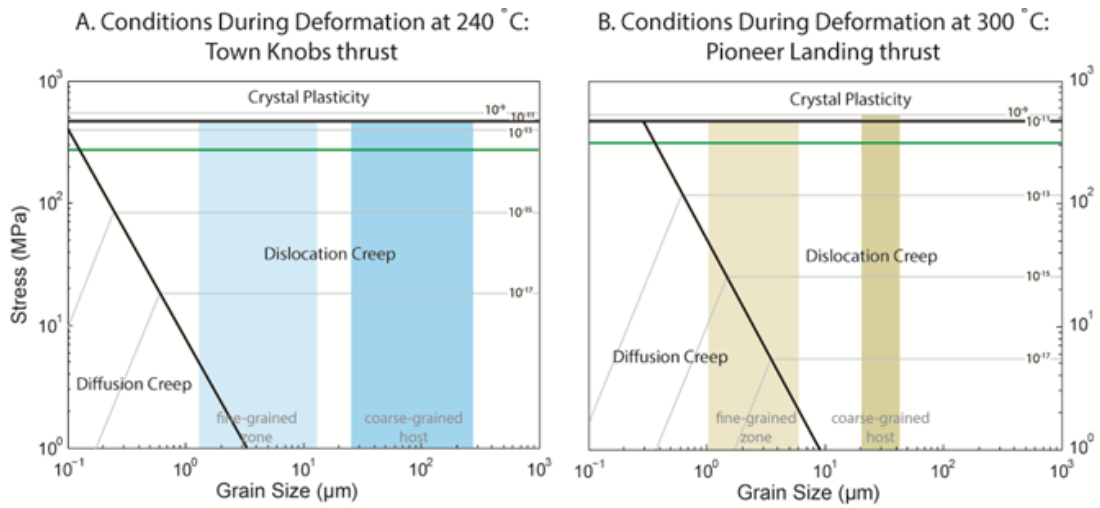


Figure 3.6. Comparison between the Town Knobs and Pioneer Landing thrust faults. A comparison of fine-grained dolomite in the experimentally and naturally deformed dolomites in this study to previously reported microstructures of naturally (Wenk and Shore, 1975; White and White, 1980) and experimentally (Wenk and Shore, 1975; Delle Piane et al., 2008) deformed fine-grained dolomite. Figure is adapted from Holyoke et al., (2013).

dropped below 30 MPa. We also compare the fine-grained dolomites examined in this study to other experimentally (Wenk and Shore, 1975; Delle Piane et al., 2008) and naturally (Wenk and Shore, 1975; White and White, 1980) deformed fine-grained dolomite (Figure 3.7). In dolomite would only have occurred with a decrease in strain rate. The development of dolomite veins within localized zones indicate stresses remained high along the fine-grained zones, resulting in brittle deformation. At slightly higher temperatures, evidence all of these examples, a weak LPO is observed. All fine-grained dolomite examples are mapped on a temperature vs. stress deformation mechanism map for dolomite at a known grain size. Experimentally deformed dolomite is at the boundary between dislocation creep and diffusion creep is marked for a 1, 10, 100, and 250 μm grain size, and strain rates are equal at the boundary. The fine-grained dolomite along the Town Knobs thrust, which contain a relatively strong LPO, is the only naturally deformed fine-grained dolomite that plots firmly within the dislocation creep regime (Figure 3.7).

Examples of naturally deformed fine-grained dolomite along the Pioneer Landing thrust and those presented in White and White (1980) and Wenk and Shore (1975) plot at the dislocation-diffusion creep boundary or well within the diffusion creep field (Figure 3.7). The location near the boundary indicates that dislocation creep and diffusion creep contribute, to some degree, equally to the deformation of fine-grained dolomite. Studies of olivine (Hirth and Kohlstedt, 1995) and calcite (Schmid et al., 1987; Rutter et al., 1995; de Bresser et al., 2001) suggested that while deformation transitions from the dislocation creep regime into the diffusion creep regime, dislocation creep process remain active, particularly near the boundary. This may explain the weak LPO observed in naturally deformed

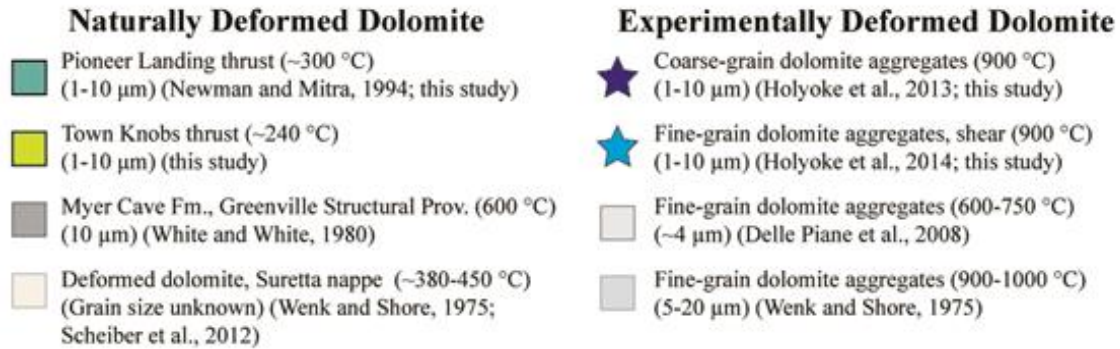
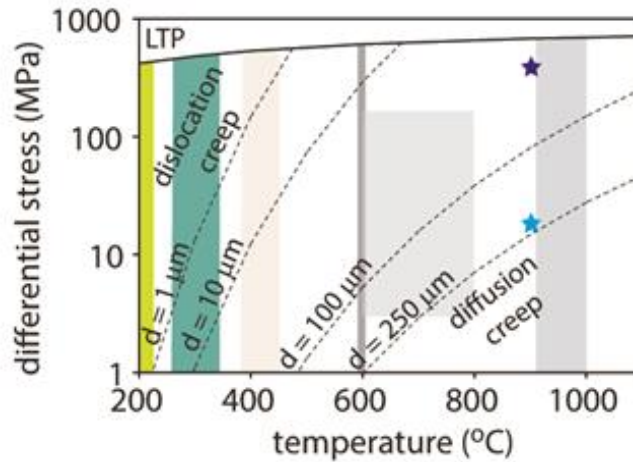


Figure 3.7. Dolomite comparison. Deformation mechanism map for dolomite crated using experimentally derived flow laws (Davis et al., 2008; Delle Piane et al., 2008; Holyoke et al., 2013). Byrelee’s law is marked in green for a saturated crustal rock at 6 km and 10 km depth. (A) Coarse-grained host dolomite and fine-grained dolomite, within localized zones, along the Town Knobs thrust are plotted at 240 °C. (B) Coarse-grained host dolomite and fine-grained dolomite, within localized zones, along the Pioneer Landing thrust are plotted at 300 °C.

dolomite in this study, and in Wenk and Shore (1975) and White and White (1980), which plots near the dislocation-diffusion creep boundary (Figure 3.7). Hirth and Kohlstedt (1995) hypothesis does not apply to our experimental samples and experimentally deformed dolomite presented in Delle Piane et al., (2008), which plot well within the diffusion creep regime (Figure 7). The development of a LPO in samples that are located within the diffusion creep regime, and not near the dislocation-diffusion creep boundary, suggest dislocation processes still contribute a significant amount to the overall deformation of the fine-grained dolomite. Alternatively, de Bresser et al., (2001) suggested that grain growth of calcite led to a balance between dislocation and diffusion creep. While their hypothesis was made for boundary conditions, evidence of grain growth in experimentally deformed shear dolomite indicates this process could be the reason for the development of concurrent dislocation-diffusion processes well into the diffusion creep regime.

3.6 Conclusions

A c-axis LPO formed in localized zones of fine-grained dolomite at experimentally conditions of 900 °C, and in natural conditions as low as ~240 °C. Microstructures indicate evidence for dislocation and diffusion creep in both experimentally deformed dolomites and in naturally deformed dolomite at temperatures of approximately 300 °C (Pioneer Landing thrust), suggesting that both processes accommodated displacement within the fine-grained shear zones and the formation of a weak c-axis LPO. The formation of four-grain junctions alongside evidence for dislocation and diffusion processes indicates displacement was accommodated by both diffusion creep- and dislocation creep accommodated grain boundary sliding. At lower temperatures (~240 °C; Town Knobs thrust), the development of

a stronger c-axis LPO, in addition to subgrains and irregular grain boundaries, suggest dislocation creep accommodated both grain size reduction and the formation of a relatively weak crystallographic fabric within fine-grained dolomite.

4. CONTROLS ON THE LOCATION OF, AND DISPLACEMENT ALONG, THRUST FAULTS IN THE SOUTHERN APPALACHIANS

4.1 Introduction

Foreland fold and thrust belts are dominated by low-angle thrust faults, many of which contain shale adjacent to the fault zone (Canadian Rockies – Erickson, 1994; Southern Appalachians – Rich, 1934; House and Gray, 1982a; Wojtal and Mitra, 1986). For example, the Chattanooga shale forms the footwall of the Cumberland thrust in the Southern Appalachians, which has an estimated displacement of ~11 km (Rich, 1934). Rich (1934) hypothesized that the location of, and displacement along, the Cumberland thrust was the result of weak behavior of the underlying shale unit, and that it was only when friction became too great that the fault would cut upward through a more competent layer. The shale-rich Rome Formation is common throughout the Southern Appalachians and is found along the trace of several major fault zones, including the Hunter Valley thrust, Copper Creek thrust, Clinchport thrust, and the Saltville thrust (Woodward, 1995).

While thrust faults are common within shale-rich formation, both within the hanging wall and footwall, thick dolomite units are also present along many faults in the Canadian Rockies (Erickson, 1994), and the Southern Appalachians (Wojtal and Mitra, 1986), primarily within the hanging wall. This is particularly noticeable in the Southern Appalachians, where a thick (3-7 m) dolomite unit, within the shale-rich Rome Formation, is found either adjacent to, or within meters of, the fault zone and can be traced along strike of several major thrust faults. This thick dolomite bed is also observed along minor faults

and smaller duplex structures, such as the Town Knobs thrust (Haney, 1966). The Copper Creek thrust is a relatively large displacement thrust fault. An exposure of the Copper Creek thrust north of Knoxville, TN contains a ~5 m thick dolomite unit within a few meters of its fault trace (Wojtal and Mitra, 1986). At a second exposure of the Copper Creek thrust, 40 km along strike northwest of Rogersville, TN, we observe a similar dolomite bed immediately adjacent to the fault zone.

At low-temperature conditions typical of foreland fold and thrust belts ($< 300\text{ }^{\circ}\text{C}$), dolomite is typically assumed to be stronger than the adjacent limestone and shale units (e.g., Handin and Hager, 1958; Erickson, 1994; Hadizadeh, 1994), and brittle deformation has been well documented within Rome Formation dolomite (Haney, 1966; Smith, 1968; House and Gray, 1982b; Hadizadeh, 1994). Within some of these fault zones, calcite and shale exhibit evidence for ductile processes (Hunter Valley thrust – Kennedy and Logan, 1998; Copper Creek thrust – Wells et al., 2014). Along the Copper Creek thrust, the shear zone contains numerous calcite veins that deformed by plasticity-induced fracturing and diffusion creep (Wells et al., 2014), while folded shale dominates the Hunter Valley shear zone (Wojtal and Mitra, 1986; Kennedy and Logan, 1998). Because these studies focus on the weakest deforming material, the role of dolomite in the overall development of the macro- and mesoscale structures is rarely addressed.

We hypothesize that the location of many of these low angle faults in the foreland of the Southern Appalachians faults is determined by the strength and behavior of the thick dolomite bed within the shale-rich Rome Formation. In this study, we present microstructural evidence across a large displacement fault (Copper Creek thrust) and a

smaller displacement fault (Town Knobs thrust) that contain dolomite immediately adjacent to the fault zone. Localization at the base of the dolomite bed, along each fault, is the result of dominantly brittle behavior of this strong lithology, which influenced the location of each fault zone. Based on our meso- and microscopic observations, adjacent shale beds remain relatively undeformed and only contribute a small portion to the overall displacement. Instead, evolving internal (e.g., host and vein material) and external (e.g., stress) controls the displacement along these faults.

4.2 Geologic Setting

The foreland fold-and-thrust belt of the Southern Appalachians is characterized by many large displacement low angle thrust faults (Figure 4.1) (Haney, 1966; Harris, 1976; Harris and Milici, 1977; Woodward, 1985). The Copper Creek thrust and Town Knobs thrust are two of several faults located in the Valley and Ridge province (Figure 4.2). The Rome Formation is in the hanging wall of each fault (Figure 4.2; Woodward, 1985; 1988). A thick dolomite bed within the Rome Formation can be observed within the hanging wall, immediately adjacent to the shear zone, of the Copper Creek and Town Knobs thrusts.

The Copper Creek thrust is a large displacement fault (15-20 km) (Harris, 1976; Harris and Milici, 1977; Woodward, 1985) and temperatures during deformation are estimated at 100-180 °C, based on burial depth (30 °C/km; Harris, 1976; Harris and Milici, 1977). The Rome Formation forms the hanging wall, while the shale-rich Moccasin Formation forms the footwall (Lemiski and Kohl, 2006). Along the Copper Creep thrust, displacement was accommodated primarily by deformation along calcite veins within a narrow shear zone (Wells et al., 2014).

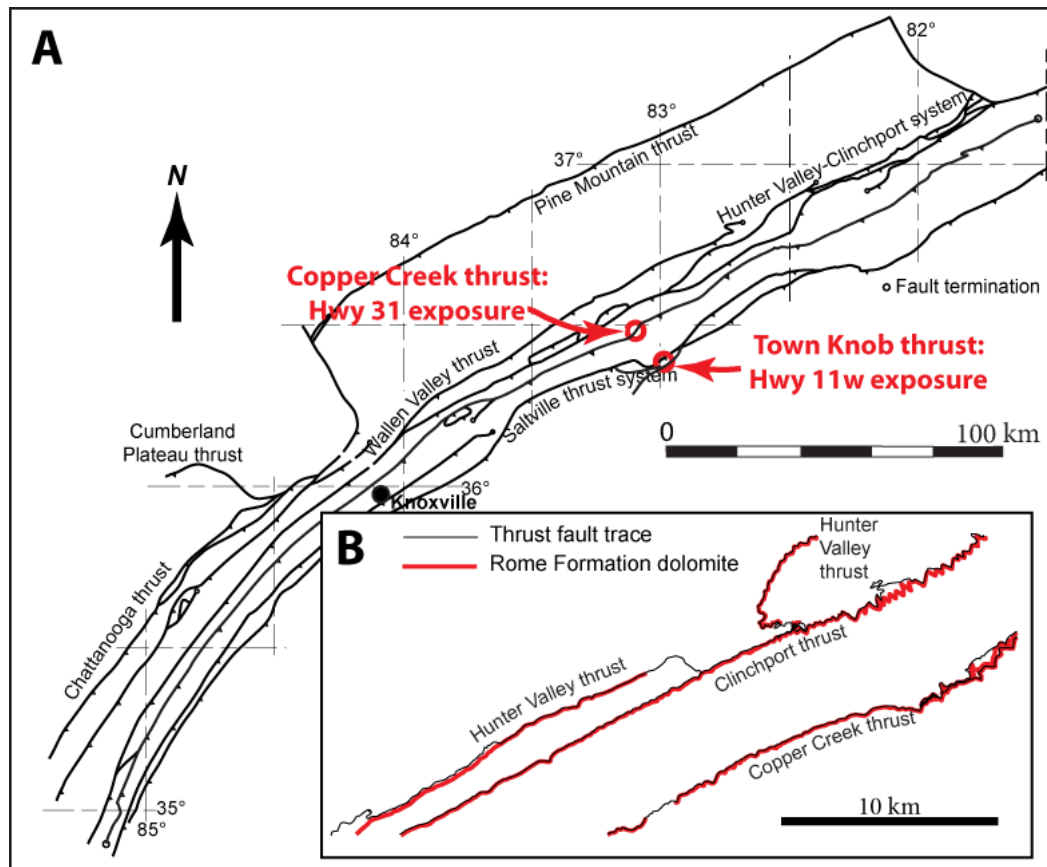


Figure 4.1. Map of fault traces in the Southern Appalachians. (A) Exposure of the Copper Creek thrust along Hwy 31 and an exposure of the Town Knobs thrust along Hwy 11w are marked. (B) Dolomite within the Rome Formation can be traced along strike of several major faults. Modified from Hatcher et al., 2007.

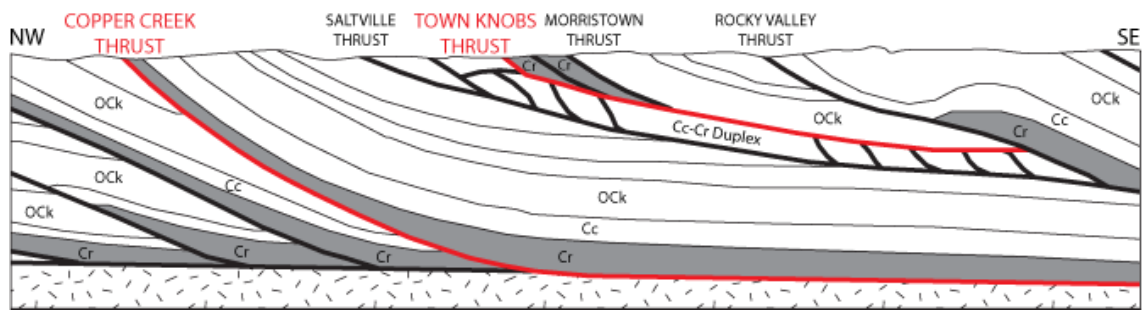


Figure 4.2. Cross-section. Several major thrust faults in the Southern Appalachians, including the Town Knobs thrust and the Copper Creek thrust, contain the Rome Formation within the hanging wall. Modified from Woodward et al., 1988.

The Town Knobs thrust is one of several duplex structures in the foreland of the southern Appalachians. The Town Knobs thrust is the roof thrust of a Conasauga Group-Rome Formation duplex, associated with the Saltville thrust (Smith, 1968; Woodward, 1985). Displacement is estimated to have been less than 275 m (Haney, 1966). While there are no specific burial depth estimations for the Town Knobs thrust, it forms the roof thrust of a duplex structure associated with the Saltville thrust (Woodward, 1985). The Saltville thrust has an estimated temperature during deformation of 150-240 °C, based on burial depth of 5-8 km (30 °C; House and Gray, 1982b). Based on the structural relationship with the Saltville thrust, we estimate that temperatures during formation of the Town Knobs thrust were similar (150-240 °C). At this exposure, the Rome formation forms the hanging wall and the Conasauga Group (limestone and dolostones) form the footwall. Localization along the Town Knobs thrust occurred between the dolomite bed within the Rome formation and dolomite units in the Conasauga Group.

4.3 Methods

Mesoscale observations were made along the Copper Creek thrust (along Tennessee 11w, ~18 km north of Mooresburg, TN) and Town Knobs thrust (along Hwy11, ~3 km west of Rogersville, TN) exposures. Samples were collected along transects from the footwall into the hanging wall across both faults. From these samples, we made ultrathin (< 5 µm thick) and standard thin-sections of each sample, oriented perpendicular to the foliation and parallel to the lineation of the thrust fault. Due to the variable grain sizes, we used optical and electron microscopy (SEM: FEI Quanta 600 FE-SEM housed in the Microscopy and Imaging Center, Texas A&M University) to document microstructures at different scales.

Long and short diameters were determined from grain traces from optical and BSE images using image analysis software (ImageSXM), and the average of the diameters are reported here as grain size. ImageSXM analyses were also used to determine porosity. Compositions of grains were determined using energy dispersive spectroscopy (EDS) and wavelength dispersive spectroscopy (WDS) on an electron microprobe. Cathodoluminescence (CL) revealed slight differences in composition between host rock and veins. X-ray diffraction (XRD) analyses were used to determine the composition of shale beds. Linear fracture density was determined using fracture count across specific linear lengths. The orientation and thickness of each fracture that crossed that line were also recorded.

4.4 Results

4.4.1 Copper Creek Thrust

4.4.1.1 Footwall

The footwall of the Copper Creek thrust contains shale with interbedded limestone and micrite (Figure 4.3, 4.3B). Limestone and micrite beds range in thickness from 1-30 cm. XRD analysis indicates shale units are composed of clay particles, mica, quartz, dolomite, and calcite. Fractures and stylolites are observed 5 m below the fault zone and shale layers contain rare folds. Randomly oriented zones of calcite (< 200 μm thick) are observed, rarely, in beds of micrite. The calcite zones contain fine- (< 20 μm) and coarse- (20-50 μm) grained vein calcite. There is little evidence for penetrative deformation in the footwall. Even within 35 cm of the fault zone, we observe sedimentary structures (e.g., shells, burrows) within micrite beds.



Figure 4.3. Images of the Copper Creek thrust. (A) Rome Formation is emplaced on top of the Moccasin Formation. Dolomite unit within the shale-rich Rome formation is adjacent to the fault zone. (B) Fractured shale and limestone beds. (C) Shale beds are folded ~5 m above the dolomite bed. (D) The shear zone contains dolomite clasts (outlined) within a grey, foliated matrix.

4.4.1.2 Hanging Wall

The hanging wall of the Copper Creek thrust is composed primarily of shale and siltstone beds with a thick (7 m) dolomite bed adjacent to the fault zone. The shale and siltstone layers above the dolomite bed are commonly folded. Asymmetrical chevron-type folds are observed in shale beds approximately ~0.5 km above the fault zone, resulting in a secondary foliation. More concentric-style, though asymmetric, folds are observed in shale units within 7 m above the shear zone, and immediately above the dolomite unit (Figure 4.3C). Minor fractures are observed within the thick dolomite bed.

Within the 7 m dolomite bed (Figure 4.3; Figure 4.4), at 4 m above the fault zone, optical microscopy of the dolomite reveals fractures and dispersed areas and localized zones (< 500 μm wide) of fine-grained dolomite (< 20 μm) within coarse-grained dolomite host (50-225 μm grain size) (Figure 4.4A-C). The linear fracture density at this location is 2 fractures/mm, which includes inter- and intragranular fractures. The offset along these fractures and localized zones is typically less than 1 mm. The coarse-grained host dolomite contains lobate to serrated grain boundaries, and patchy undulatory extinction (Figure 4.4B). Within some of the host grains, intragranular fractures parallel extinction boundaries. Fewer than 4% of coarse-grained host dolomite grains are twinned. Subgrains are common, particularly near zones of localized fine-grained dolomite (Figure 4.4B-C). The localized zones of fine-grained dolomite (< 20 μm) often occur between larger dolomite grains (Figure 4.4C). Fine-grained dolomite within these localized zones contain lobate grain boundaries and subgrains (Figure 4.4C).

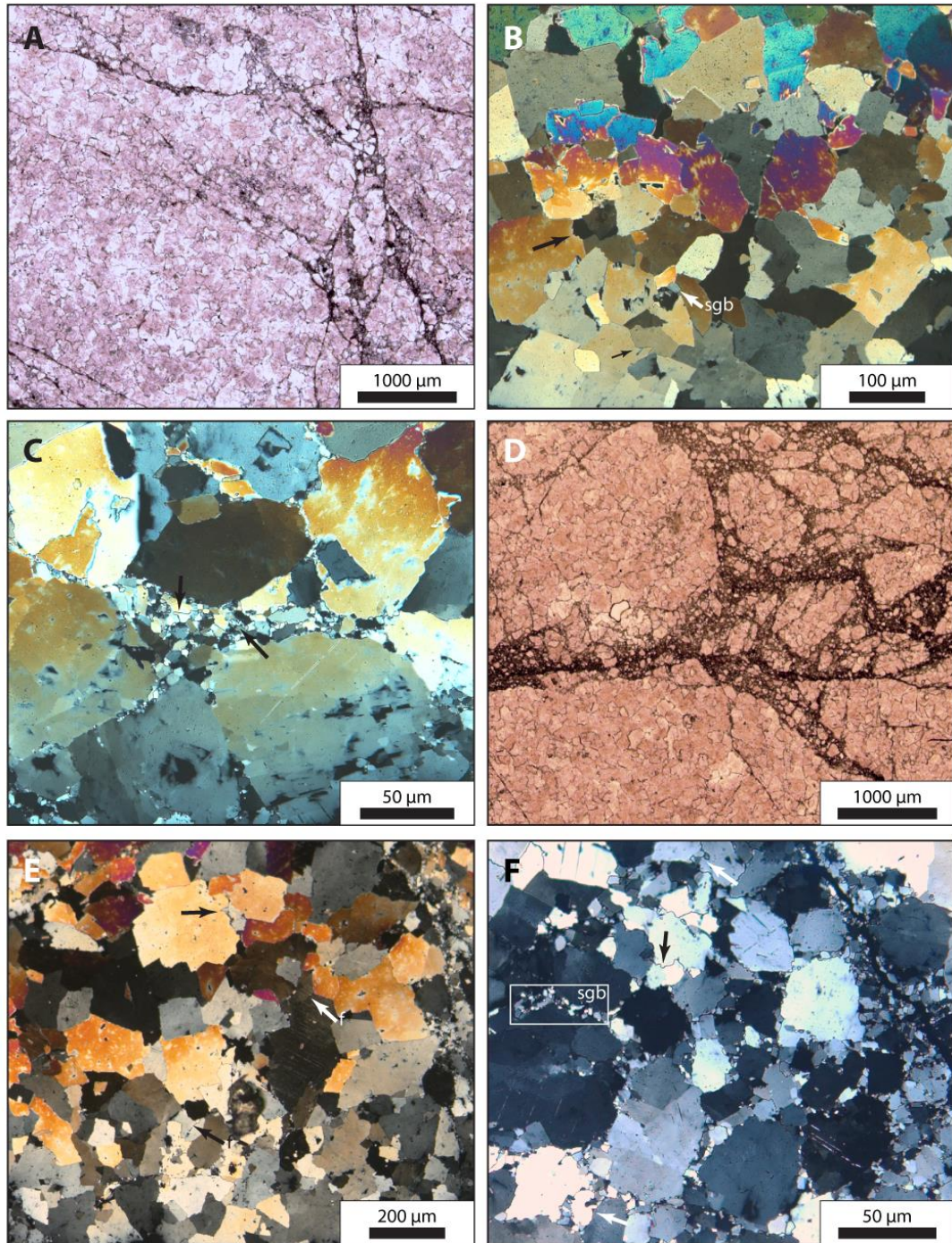


Figure 4.4. Hanging wall dolomite. (A) - (C) Dolomite ~4 m above the shear zone. (A) Host dolomite contains fractures and localized zones of fine-grained dolomite, as well as (B) patchy extinction, serrated grain boundaries (arrows), and subgrains (sgb). (C) Finer dolomite grains contain lobate grain boundaries (arrow) and patchy extinction. (D) - (F) Dolomite ~1.5 m above the shear zone. (D) Zones of fine-grained dolomite are more common. (E) Host dolomite contains serrated grain boundaries (arrows), undulatory extinction, twins, and intragranular fractures (f). (F) Subgrains are common at coarse grain boundaries. Optical photomicrographs.

1.5 m above the fault zone, also within the dolomite unit, the host dolomite contains more fractures and localized zones of fine-grained dolomite are more common (Figure 4.4D-F). The fracture density within the coarse-grained host dolomite increases to 3.7 fractures/mm (Figure 4.4D). The coarse-grained host dolomite contains undulatory extinction and serrated grain boundaries (Figure 4.4E). Thin twins are most abundant at this location, with 19% of coarse grains twinned. Zones of fine-grained dolomite are also common, and the zones have increased in thickness to 400 μm . Within the fine-grained dolomite zones, fine-grains contain patchy extinction and lobate grain boundaries (Figure 4.4F). Larger grains within these zones contain subgrains at grain boundaries (Figure 4.4F). Porosity within fine-grained zones, 1.5 m above the fault zone, is 14%.

The host dolomite immediately adjacent to the fault zone is defined by angular to sub-rounded dolomite aggregate clasts set in a poorly sorted fine-grained matrix (Figure 4.5A), rather than the distinct zones of fine-grained dolomite observed farther into the hanging wall dolomite. In general, there is also less coarse-grained dolomite ($> 50 \mu\text{m}$) compared to dolomite samples 1.5 m and 7 m above the fault zone. The fracture density immediately adjacent to the fault zone increases to 7 fractures/mm, and numerous calcite veins cross-cut both the fine-grained matrix and the dolomite clasts. Coarse-grained dolomite (50-150 μm) contains undulatory extinction, irregular grain boundaries, and subgrains (Figure 4.5B-C). Twins are rare as there are fewer coarse-grained dolomite grains. The fine-grained matrix that dominates the sample surrounds the coarser dolomite and consists of dolomite with an average grain size of 0.8 μm . Coarser dolomite grains within

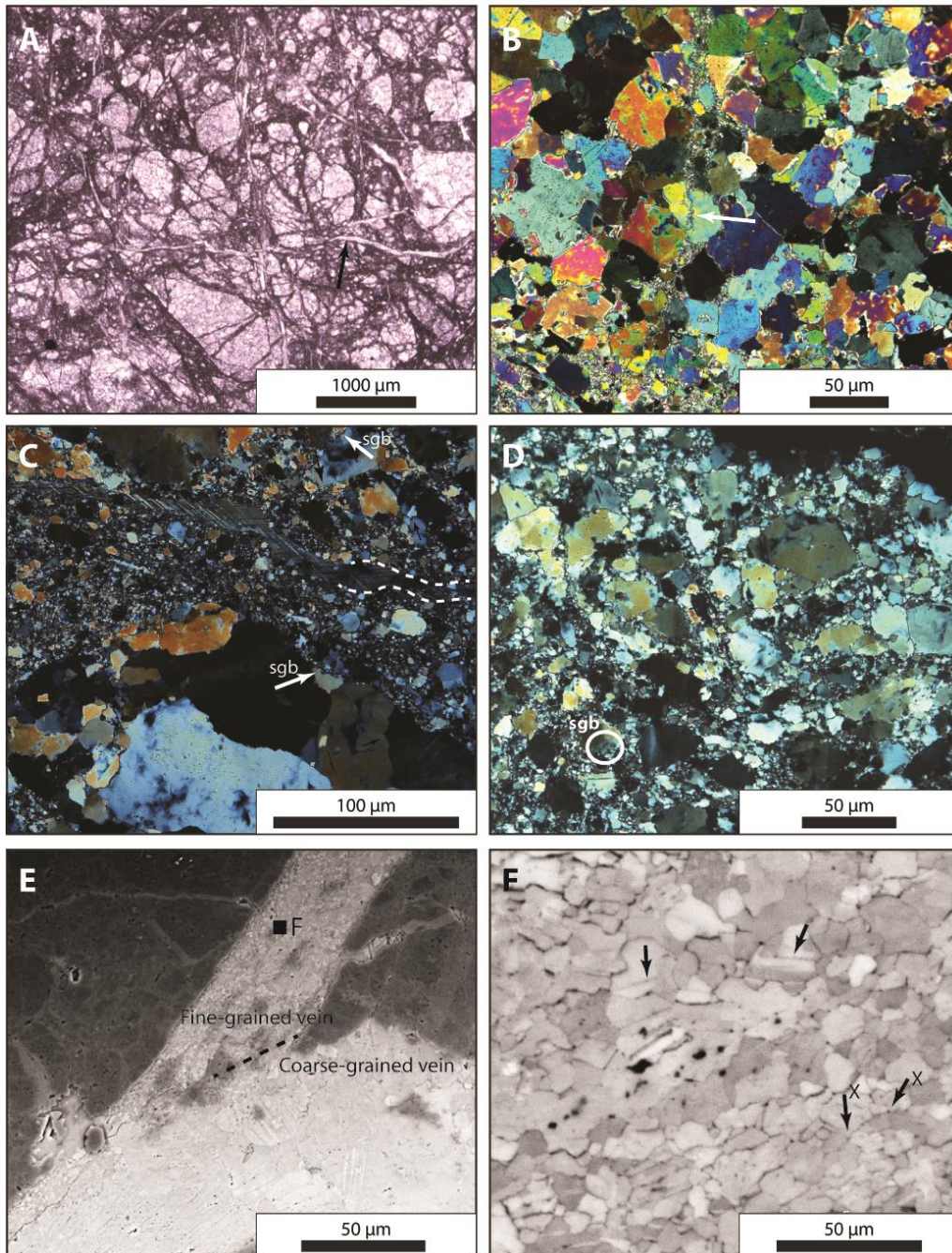


Figure 4.5. Hanging wall dolomite adjacent to the Copper Creek shear zone. (A) – (D) Optical photomicrographs. (A) Calcite veins cross-cut dolomite clasts and zones of fine-grained dolomite. (B) Host dolomite contains serrated grain boundaries, and zones of fine-grained dolomite (arrow). (C) Twinned calcite veins (dashed lines) cross-cuts fine-grained dolomite. Subgrains (sgb) are common in coarser dolomite grains. (D) In a localized fine-grained dolomite zone, coarser grains contain lobate grain boundaries, subgrains, and patchy extinction. (E) – (F) BSE images. (E) Coarse-grained calcite vein cross-cuts fine-grained calcite vein. (F) Fine-grained calcite contains twins (arrows), irregular grain boundaries, triple junctions, and four-grain junctions (X).

the matrix have lobate grain boundaries, patchy extinction, and subgrains (Figure 4.5D). Porosity within the fine-grained dolomite matrix is less than 4%.

While a few calcite veins are observed 1.5 m above the fault zone, most calcite veins within the hanging wall occur immediately adjacent to the fault zone. Coarse-grained calcite veins cross-cut fine-grained calcite veins within localized zones of fine-grained dolomite (Figure 4.5A, 4.5E). The average grain size within the coarse-grained calcite veins is 38 μm . However, the grain size of the coarser grains is strongly dependent on the thickness of the vein. Twins within the coarse-grained calcite are irregular and far more common than twins within the dolomite grains (Figure 4.5B). Subgrains ($\sim 2 \mu\text{m}$) are common at calcite grain boundaries and along twin boundaries (Figure 4.5B). Twinned calcite veins occur within zones of fine-grained dolomite (Figure 4.5C, 4.5E). Fine-grained calcite within veins (average grain size: 0.5 μm) contains irregular grain boundaries and are also twinned (Figure 4.5D-F). Finer calcite grains ($< 1 \mu\text{m}$) form four-grain junctions with neighboring grains (Figure 4.5F). Porosity within the fine-grained calcite veins is less than 1%.

4.4.1.3 Shear Zone

The Copper Creek fault zone is up to 30 cm thick, and is composed of a grey, foliated matrix that surrounds elongated dolomite clasts (Figure 4.3D; Figure 4.6; Figure 4.7). Within the dolomite clasts, we observe similar microstructures to those observed within the hanging wall dolomite immediately adjacent to the shear zone. These structures include coarse-grained dolomite in a fine-grained dolomite matrix, cross-cut by numerous calcite veins (Figure 4.6B). We also observe localized zones of clay-rich matrix, demarcated by calcite veins, within the dolomite clasts (Figure 4.7A-C).

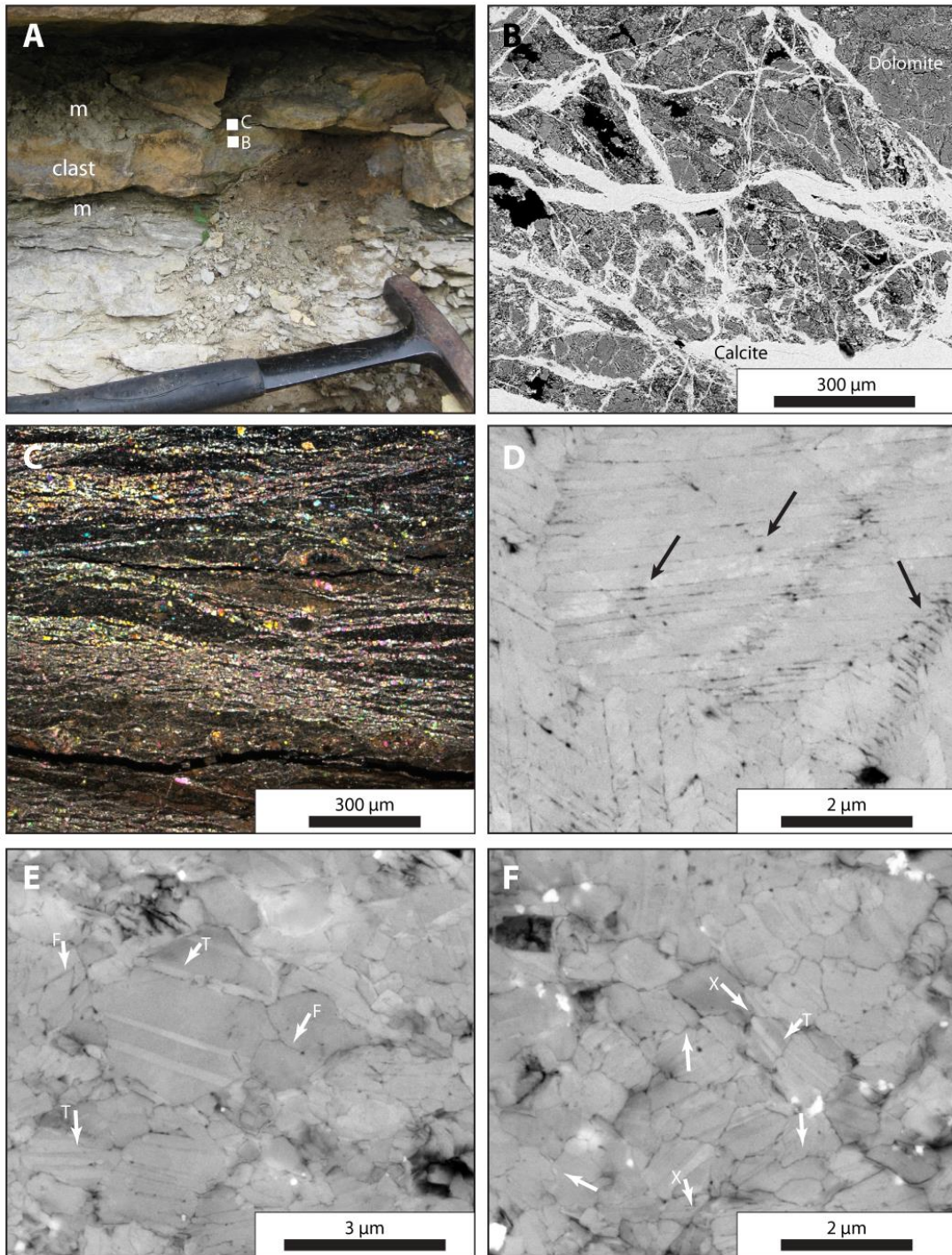


Figure 4.6. Copper Creek shear zone. (A) Dolomite clasts adjacent to grey, foliated matrix (m). (B) Dolomite clasts contain cross-cutting calcite veins. BSE Image. (C) Grey, foliated matrix is composed of fault parallel calcite veins. Optical photomicrograph. (D) Coarse-grained calcite veins contain voids (black) at twin-twin intersection (arrows). BSE image. (E) Finer calcite grains contain twins (T) and fractures (F). BSE image. (F) Fine-grained calcite contains twins, interpenetrating grain boundaries (arrows), and four-grain junctions (X). BSE image.

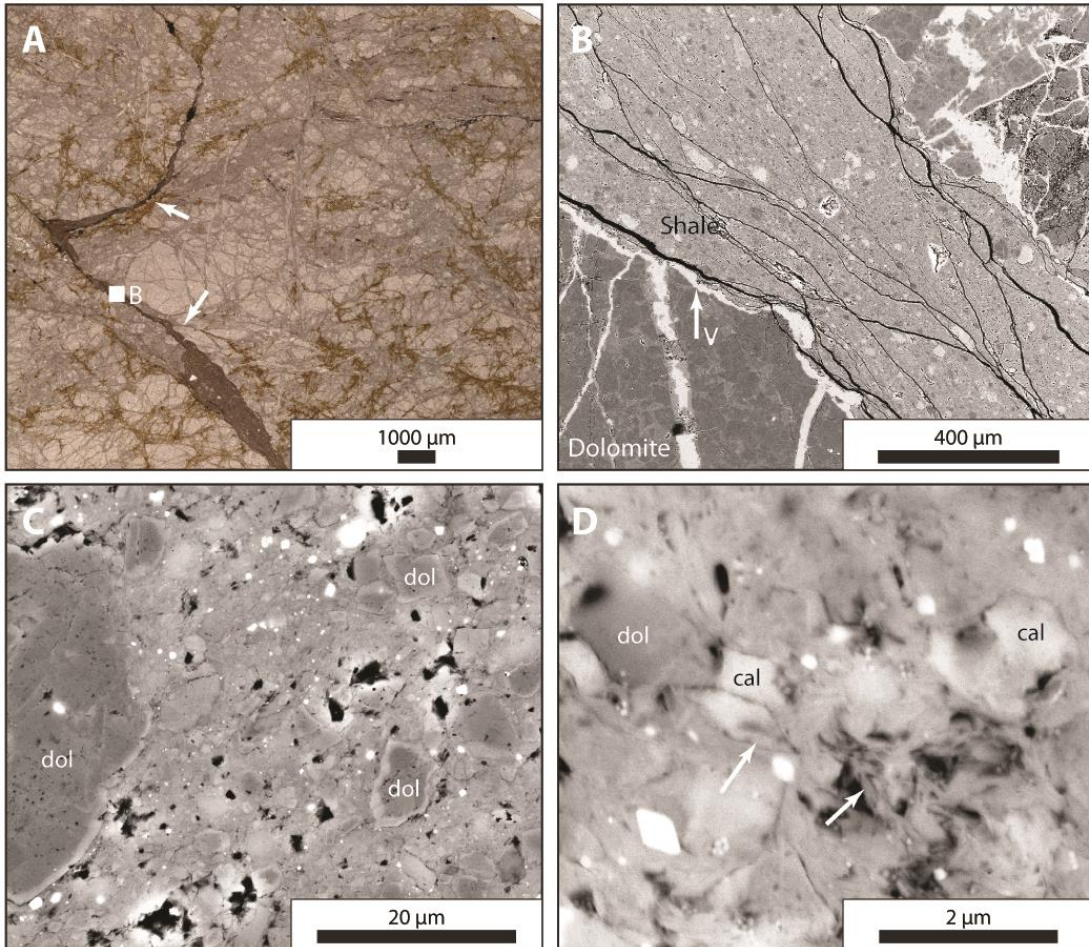


Figure 4.7. Copper Creek shear zone continued. (A) Shale-rich shear zone (arrows) are also observed in dolomite clasts. Optical photomicrograph. (B) – (D) BSE images. (B) Calcite veins (V) separate shale-rich shear zone from dolomite. (C) Shale matrix surrounds dolomite grains (dol). (D) Shale-rich matrix contains mica (arrows), and fine-grained dolomite and calcite grains.

The foliated matrix that surrounds dolomite clasts within the fault zone is composed of fault parallel calcite veins and shale (Figure 4.6C). However, calcite veins form an interconnected network (stress-supporting network) within the foliated matrix. Coarse-grained calcite veins are twinned and contain voids at twin-twin intersections and along twin boundaries (Figure 4.6D). Areas of intermediate-sized calcite grains (0.5-3 μm) contain twins and intragranular fractures, which often occur along twin boundaries (Figure 4.6E). Ultrafine-grained calcite grains ($< 1 \mu\text{m}$) contain irregular to interpenetrating grain boundaries, twins, intragranular fractures along twin boundaries, and four-grain junctions (Figure 4.6F). Pores are also common at grain boundaries. Shale is not observed within the areas of ultrafine-grained calcite.

4.4.2 Town Knobs Thrust

4.4.2.1 Footwall

The footwall of the Town Knobs thrust is dolomite of the Conasauga Group. Within the footwall dolomite, bedding parallel stylolites are common. The majority of mesoscopic stylolites are oriented 50-70° clockwise from the fault zone. Veins, ‘vein-like’ zones of fine-grained material, and minor faults are also commonly observed in the footwall dolomite (Figure 4.8A-B).

Most of the footwall dolomite is composed of coarse-grained dolomite (average grain size 45 μm), with serrated grain boundaries, deformation bands, and subgrains (Figure 4.9A-B). The coarse-grained dolomite is cross-cut by intergranular fractures and zones of fine-grained dolomite (Figure 4.9B-C). Twins are rare in the host dolomite. The mesoscopic ‘vein-like’ structures (Figure 4.8C), which are often 0.5-2 cm wide and occur throughout the

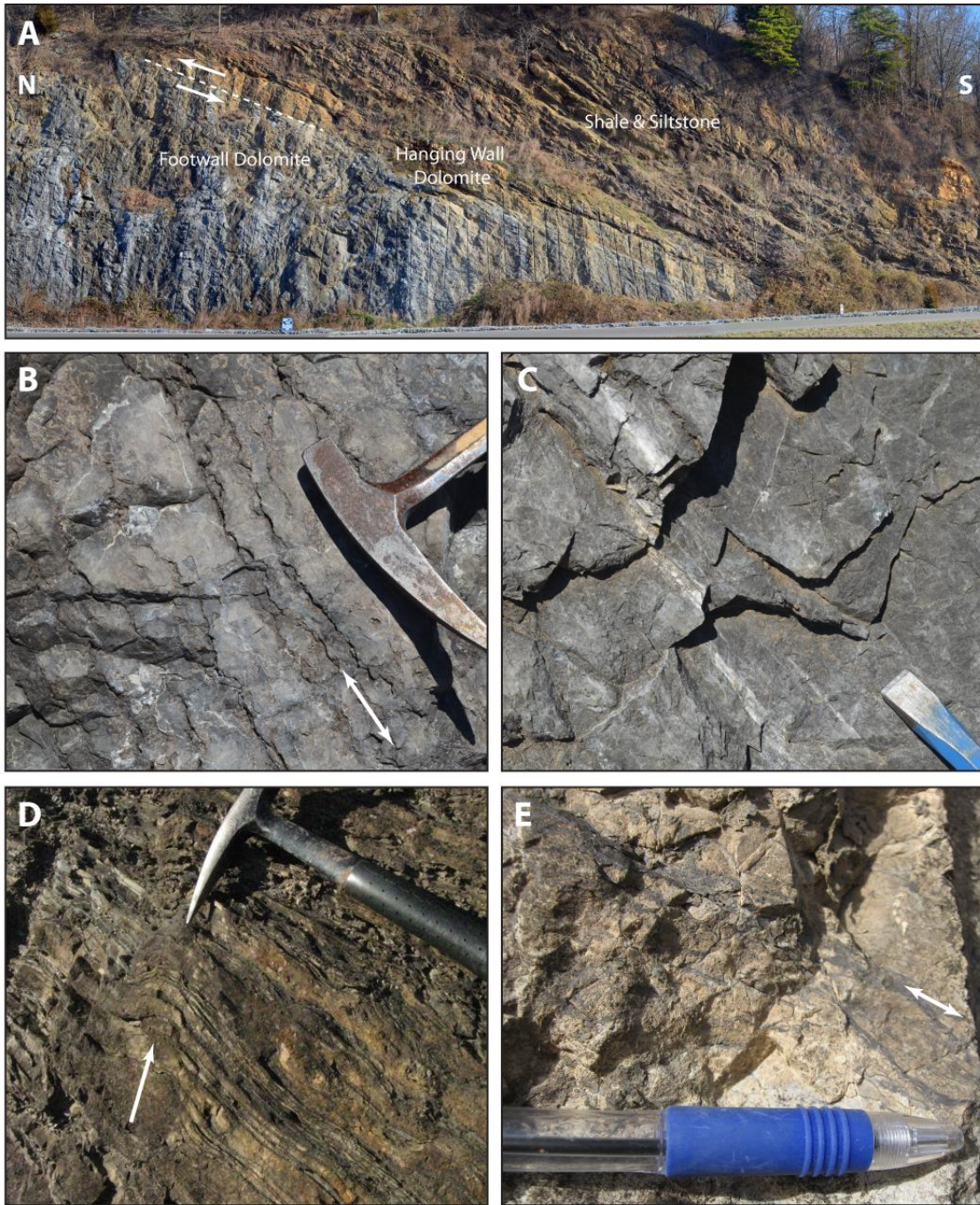


Figure 4.8. Images of the Town Knobs thrust. (A) Localization occurs between dolomite bed in the shale-rich Rome Formation and dolomite units with the Conasauga Group. (B) Bedding parallel stylolites are common (arrow) in the footwall. (C) Veins and ‘vein-like’ structures are observed in the footwall. (D) Folds (arrow) in shale and siltstone units are common in the hanging wall. (E) Stylolites (arrow) occur within the hanging wall dolomite.

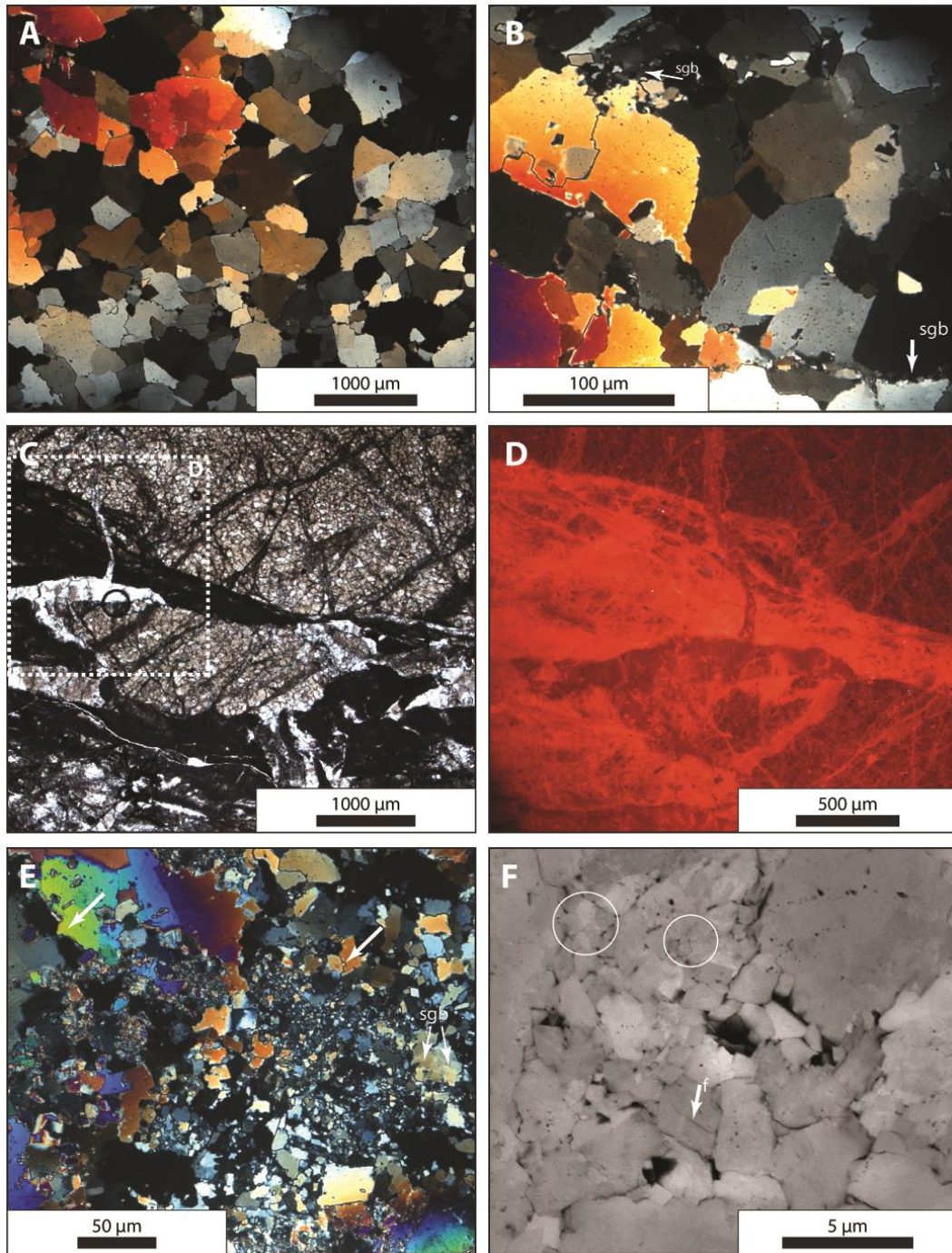


Figure 4.9. Footwall dolomite in the Town Knobs thrust. (A) – (E) Optical photomicrographs. (A) Host dolomite contains serrated grain boundaries. (B) Subgrains (sgb) are common at coarse-grained dolomite boundaries. (C) and (D) show the ‘vein-like’ layer is composed of host dolomite clasts and fine-grained dolomite that luminesce dark red, and coarse-grained vein dolomite that luminesce bright red. CL image. (E) Host dolomite, near the edge of the fine-grained zone, contain lobate grain boundaries (arrows) and subgrains. (F) Within the ‘vein-like’ zone, fine grains have intragranular fractures (f), and four-grain junctions (circle). BSE image.

footwall, are zones composed of intermixed layers of fine-grained dolomite (average grain size of 3 μm) and coarse-grained dolomite veins. The fine-grained dolomite contains interpenetrating grain boundaries (Figure 4.9E), and grains less than 1 μm occasionally form four-grain junctions (Figure 4.9F). Intragranular fractures are also observed in the larger dolomite grains (Figure 4.9F). Porosity within these zones is less than 1%. Coarse-grained dolomite veins (< 700 μm thick) cross-cut the fine-grained dolomite, resulting in angular clasts within the zones (Figure 4.9C-D). We do not observe a noticeable trend in the density of these localized zones towards the shear zone. The coarse-grained dolomite veins contain similar microstructures to those observed in the coarse-grained host dolomite, including patchy extinction, lobate grain boundaries, and subgrains (Figure 4.9E). However, these microstructures are more common in the coarse-grained dolomite veins than in the host dolomite grains (Figure 4.9D-E). Cathodoluminescence indicates slight compositional variations between the host dolomite, dolomite veins, and fine-grained dolomite (Figure 4.9D).

4.4.2.2 Hanging Wall

The hanging wall of the Town Knobs fault is predominantly shale and siltstone within the Rome Formation, except for a thick (4 m) dolomite bed that occurs immediately adjacent to the fault zone (Figure 4.8). Within the shale and siltstone beds, minor faults, with less than 4 m offset, and concentric folds (Figure 4.8D) are common. Siltstone and shale beds contain both planar bedding and cross-bedding with K-feldspar-rich and clay-rich lens (Figure 4.10A). Immediately above the hanging wall dolomite unit, mm-scale sedimentary laminations are observed within a siltstone bed (Figure 4.10B).

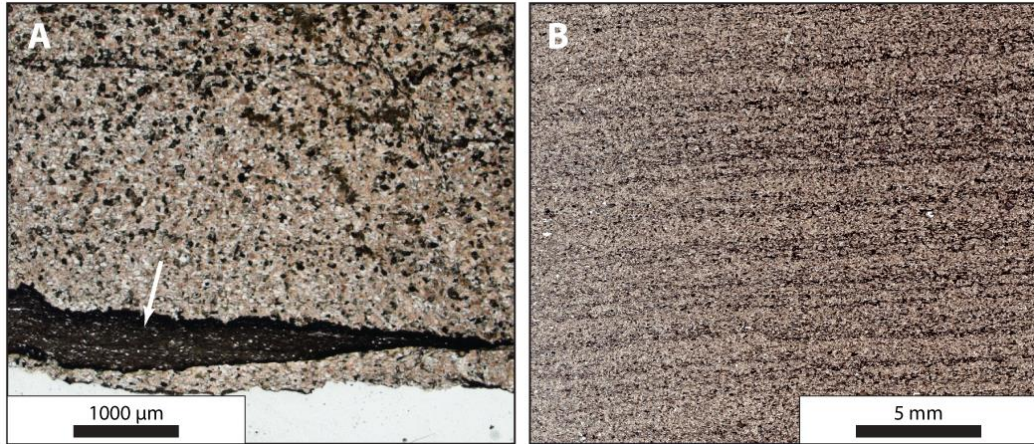


Figure 4.10. Hanging wall siltstone and shale in the Town Knobs thrust. (A) Feldspar-clay lens (arrow) in siltstone bed. (B) Sedimentary laminations in shale-siltstone bed immediately adjacent to the dolomite bed.

The thick dolomite bed adjacent to the fault contains appears to be relatively homogeneous except for bedding parallel stylolites (Figure 4.8A). However, optical microscopy indicates silt-rich areas, cross-cutting calcite veins, and an increase in deformation structures towards the fault zone.

At the top of the dolomite bed, immediately adjacent to a hanging wall shale unit, we observe a silty dolomite with numerous bedding parallel stylolites (Figure 4.11A). average grain size of 20 μm . The fine-grained dolomite does not contain stylolites or other deformation microstructures. Silty sections are composed of dolomite and considerable amounts of K-feldspar, and minor amounts of quartz (Figure 4.11B). Ooids are also observed adjacent to these stylolites in the silty sections. The silt-rich section is adjacent to a fine-grained dolomite with an average grain size of 20 μm . The fine-grained dolomite does not contain stylolites or any other deformation microstructures.

Approximately 50 cm above the fault zone, within the dolomite bed, we observe silt-rich areas within the host dolomite bed, along with localized zones of fine-grained dolomite (3 μm) (Figure 4.12A). Coarse-grained host dolomite contains lobate grain boundaries, undulatory extinction, subgrains, and intergranular fractures (Figure 4.12C). Fine-grained dolomite (< 10 μm) is observed along these fractures. Silt-rich layers contain K-feldspar and dolomite, with minor amounts of quartz and muscovite (Figure 4.12F). Some of the muscovite grains are folded. The localized zones of fine-grained dolomite luminescence differently than the host dolomite (Figure 4.12B), indicating slightly different compositions. Within the localized zones, dolomite grain size ranges from 0.3 -5 μm (Figure 4.12D). Larger grains (> 3 μm) within the zones have lobate grain boundaries, patchy extinction, and

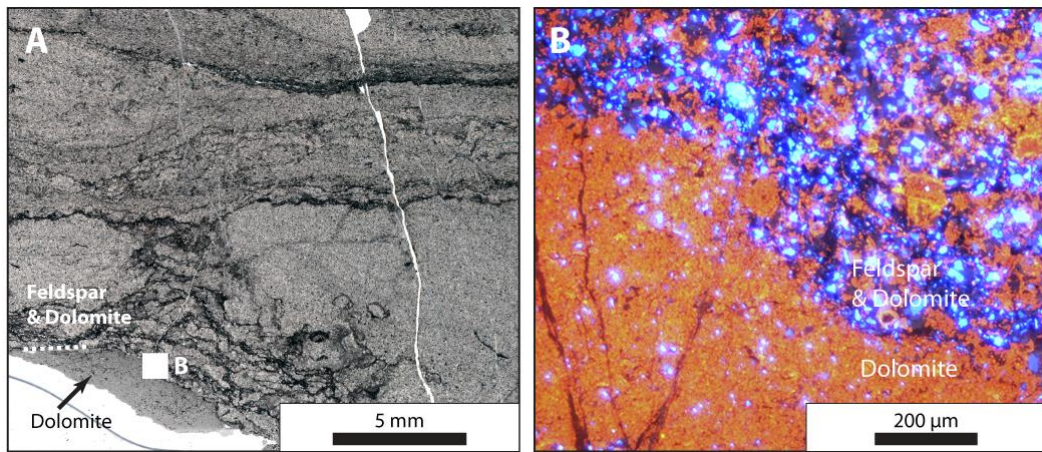


Figure 4.11. Hanging wall dolomite along the Town Knobs thrust. (A) Bedding parallel stylolites adjacent to fine-grained dolomite at top of bed. Optical photomicrograph. (B) Dolomite (orange) and K-feldspar (blue-violet). Silt-rich area has ooids and zoned dolomite. CL image.

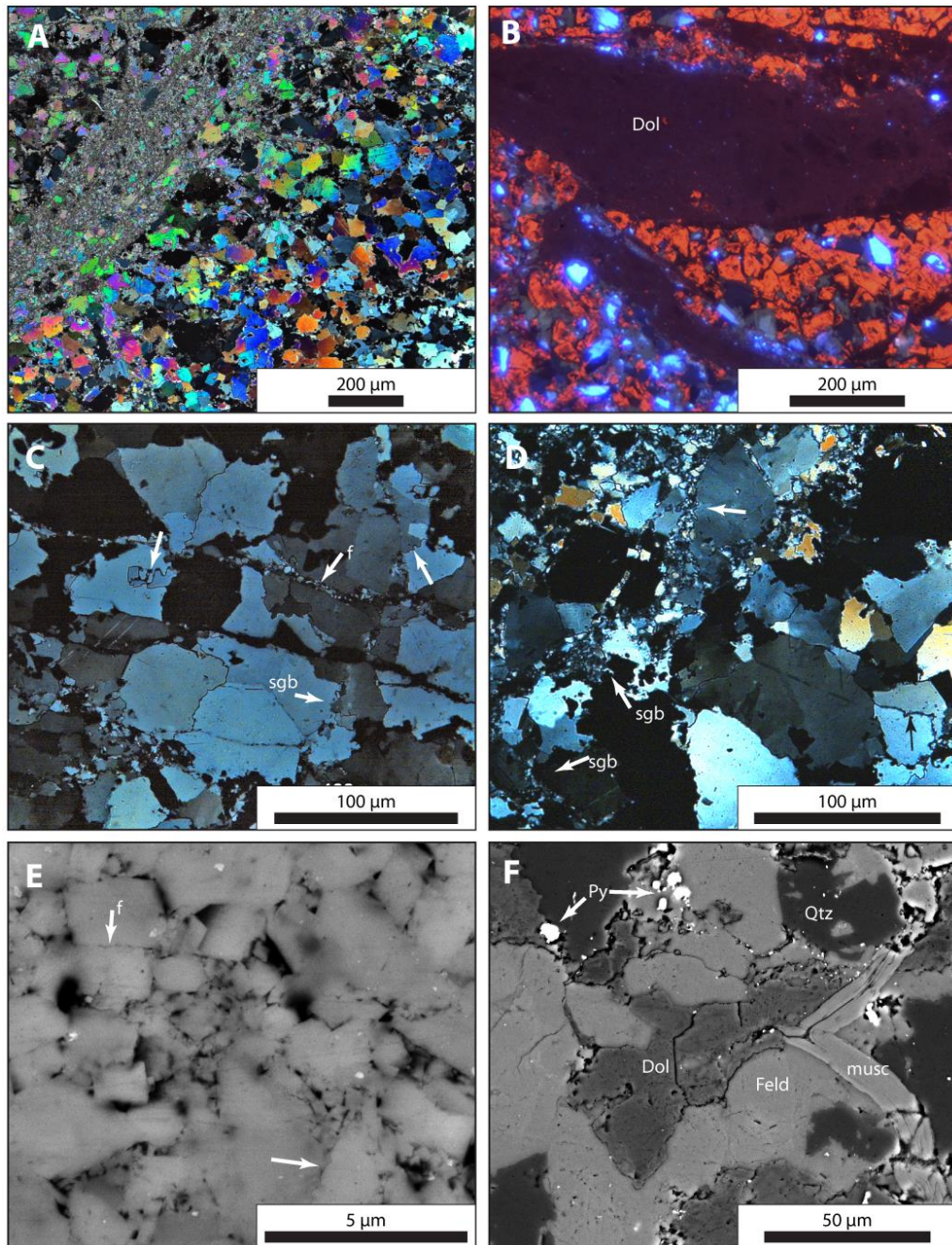


Figure 4.12. Hanging wall dolomite along the Town Knobs thrust continued. (A) – (B) Optical photomicrographs. (A) Localized zones of fine-grained dolomite 51 cm above the shear zone. (B) Localized zones of fine-grained dolomite do not luminesce, unlike the host dolomite (orange) and feldspar (blue). CL image. (C) Coarse-grained dolomite contains lobate grain boundaries (arrow), patchy extinction, subgrains (sgb), and zones of fine-grained dolomite (f). (D) Coarse-grained dolomite adjacent to a larger zone of fine-grained dolomite contain lobate grain boundaries (arrows), undulatory extinction, and subgrains. (E) – (F) BSE images. (E) Fine grains contain intragranular fractures (f) and lobate grain boundaries (arrow). (F) Folded muscovite grains occur in silt-rich section.

subgrains (Figure 4.12D). Finer grains ($< 3 \mu\text{m}$) within the zones are angular, and often contain intragranular fractures and irregular grain boundaries (Figure 4.12E). Porosity within the fine-grained zones is 8%.

Immediately adjacent to the shear zone, we observe dolomite-aggregate clasts, silt-rich aggregate clasts, and zones of fine-grained material (Figure 4.13A). Within the dolomite-aggregate clasts, coarse-grained dolomite and zones of fine-grained dolomite are cross-cut by calcite veins (Figure 4.13B). Veins are rare in the silt-rich aggregate clasts, which is mostly composed of K-feldspar. Most of the calcite veins terminate at the boundary of the silt-aggregate clasts (Figure 4.13B). Coarse-grained dolomite contains similar microstructures to those observed farther from the shear zone within the dolomite bed, including lobate grain boundaries and subgrains. Zones of fine-grained dolomite within the dolomite-aggregate clasts contain irregular grain boundaries and intragranular fractures.

In addition to calcite veins, localized zones of fine-grained material cross-cut dolomite-aggregate and silt-aggregate clasts (Figure 4.13A). A thin ($< 600 \mu\text{m}$) zone of fine-grained calcite and dolomite (grain size $< 50 \mu\text{m}$) cross-cuts dolomite- and silt-aggregate clasts but not the thick ($\sim 5 \text{mm}$) zone of fine-grained material. The shear zone is composed of carbonate-aggregate clasts, silt-aggregate clasts, and grains of various compositions (e.g., dolomite, feldspar, quartz) in a fine-grained matrix (Figure 4.13C). Thin, discontinuous lens of calcite are visible within the fine-grained matrix using CL, which luminesce bright orange (Figure 4.13C). The fine-grained matrix is dominated by K-feldspar, but also contains grains of dolomite and calcite. Porosity within this zone is 5%.

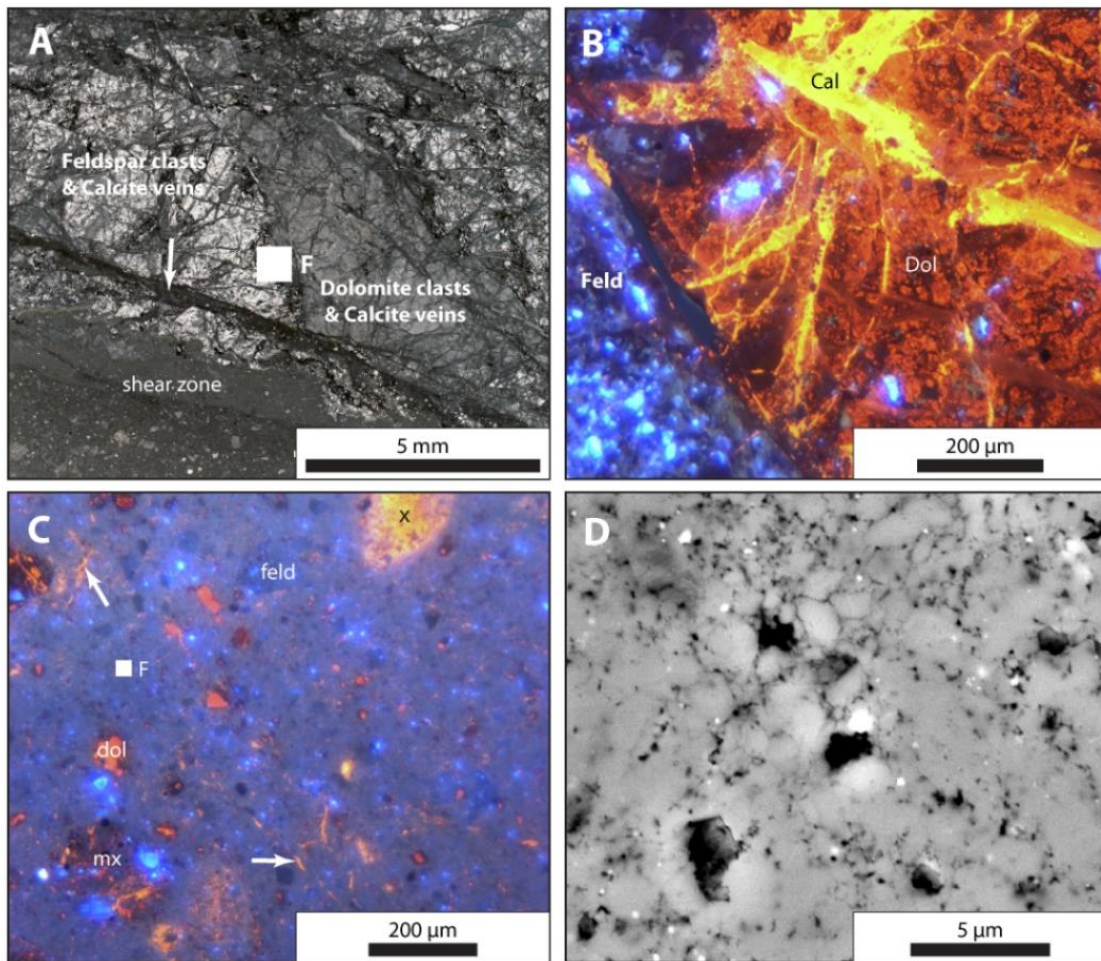


Figure 4.13 Hanging wall dolomite zone along the Town Knobs thrust. (A) Adjacent to the shear zone, dolomite clasts, feldspar clasts, calcite veins, fine-grained matrix, and a localized zone of fine-grained dolomite and calcite (arrow) are observed. Optical photomicrograph. (B) Calcite veins contained within dolomite clast. CL image. (C) The shear zone is composed of feldspar (blue) and dolomite (dark orange) grains, calcite- (x) and mixed-aggregate (mx) clasts, and discontinuous calcite veins (arrows). CL image. (D) The shear zone matrix is composed of angular grains ($< 2 \mu\text{m}$), and porosity is high. BSE image.

4.4.2.3 Fault Zone

The Town Knobs thrust occurs between footwall dolomites of the Conasauga Group and the thick dolomite bed of the shale-rich Rome Formation in the hanging wall. The hanging wall and footwall are separated by a 30 cm thick white fault zone (Figure 4.8A; Figure 4.14). Mesoscopic structures within the shear zone include fault parallel veins and complex, discontinuous layers, defined by differences in composition (i.e., predominantly either carbonate or silt) (Figure 4.14A). The complex layers can be categorized into three basic groups based on composition, including: (1) carbonate-rich layers; (2) silt-rich layers; and (3) a ‘vein-like’ structure. The ‘vein-like’ structure is the most continuous layer and is less than 2 mm across (Figure 4.14), and is composed of a fine-grained matrix of shale and carbonates (Figure 4.14). This structure is narrower than the ‘vein-like’ structures observed in the footwall, which were composed entirely of dolomite. These layers have sharp boundaries and are offset along minor fractures, less than 3 cm in length, that cross-cut other layers.

Carbonate-rich layers are typically composed of coarse-grained host dolomite clasts with zones of fine-grained dolomite and cross-cutting calcite veins (Figure 4.15A). Coarse-grained host dolomite (30-170 μm) contains lobate grain boundaries, patchy undulatory extinctions, and subgrains (Figure 4.15B-C). In localized zones of fine-grained dolomite (average grain size: 0.8 μm), we observe serrated and tapered grain boundaries, which often form four-grain junctions (Figure 4.15D). Porosity is less than 1%. Calcite veins within the carbonate-rich layers range in grain size from 15-150 μm and grains contain irregular-shaped twins and lobate grain boundaries (Figure 4.15E-F). Subgrains (3-15 μm) occur at

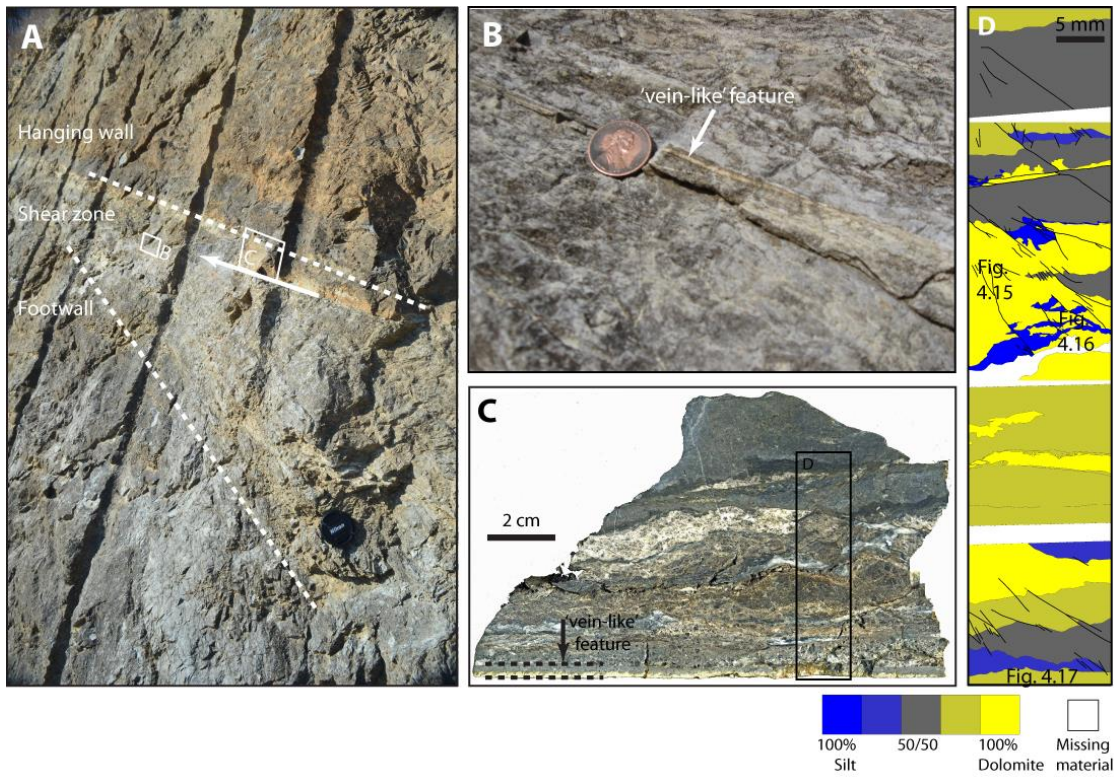


Figure 4.14. Mesoscopic structures along the Town Knobs shear zone. (A) Outcrop of the 30 cm shear zone. (B) ‘Vein-like’ structures are common within the zone. (B) Sample collected from the shear zone contains discontinuous layers with different compositions. The only continuous layer within the zone is a ‘vein-like’ structure. (D) Illustration of shear zone indicates layers that are more silt rich and layers that are more carbonate rich (i.e., predominately dolomite, but also contains calcite veins).

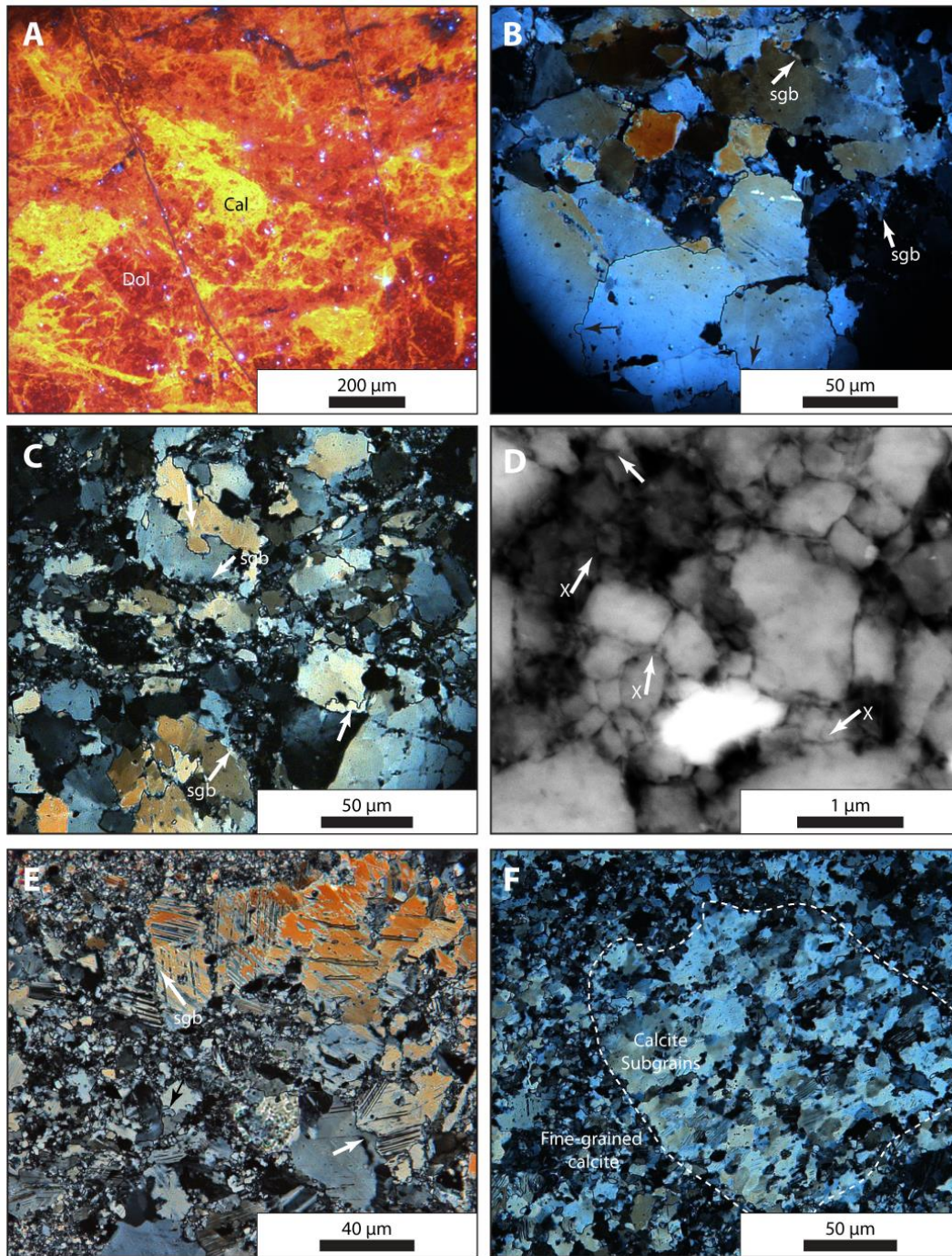


Figure 4.15. Town Knobs shear zone. (A) Carbonate-rich layers contain dolomite clasts (orange), localized zones of fine-grained dolomite (light orange), and calcite veins (yellow). CL image. (B) Lobate grain boundaries (arrow), subgrains (sgb), and patchy extinction are common in coarse-grained dolomite, and in (C) finer-grained dolomite. Optical Photomicrograph. (D) Ultrafine-grained dolomite forms four-grain junctions (X), and tapered boundaries (arrow). BSE image. (E) – (F) Optical photomicrographs. Coarser calcite grains contain irregular twins, lobate grain boundaries (arrows), and subgrains. (F) Subgrains are common in calcite grains.

grain boundaries and along twin boundaries (Figure 4.15F). Some coarser calcite grains are composed entirely of subgrains, which are also twinned (Figure 4.15E).

Silt-rich layers are composed primarily of silt (quartz, K-feldspar, muscovite) with dolomite grains (Figure 4.14D; Figure 4.16). Silt-rich layers are not as common as other compositional layers (Figure 4.16A, 4.16E). Stylolites and microfaults occur in lens composed entirely of K-feldspar (Figure 4.16D-E). Sedimentary bedding occurs in layers farthest from the shear zone center (~5 cm from the “vein-like” structure) (Figure 4.16A). Folded fine-grained muscovite grains also occur along fractures within silt-rich areas (Figure 4.16B-C). Small, discontinuous calcite veins are observed within this bedding (Figure 4.16B), and within the shale-rich layers. While the majority of calcite present within these layers are narrow and discontinuous (Figure 4.16B-C), some larger calcite veins occur within these layers (Figure 4.16E).

The "vein-like" structure is the most continuous structure within the shear zone (Figure 4.17). The structure is composed primarily of a fine-grained, carbonate-rich matrix with no discernible fabric (Figure 4.17A-B). Large aggregate clasts and angular grains are common within the structure, and are composed of dolomite, calcite, K-feldspar, and quartz. The fine-grained matrix is composed of dolomite and calcite grains that are less than 10 μm (Figure 4.17C-D). Some of the larger dolomite grains (~ 20 μm) contain intragranular fractures (Figure 4.17C). Porosity is 10%.

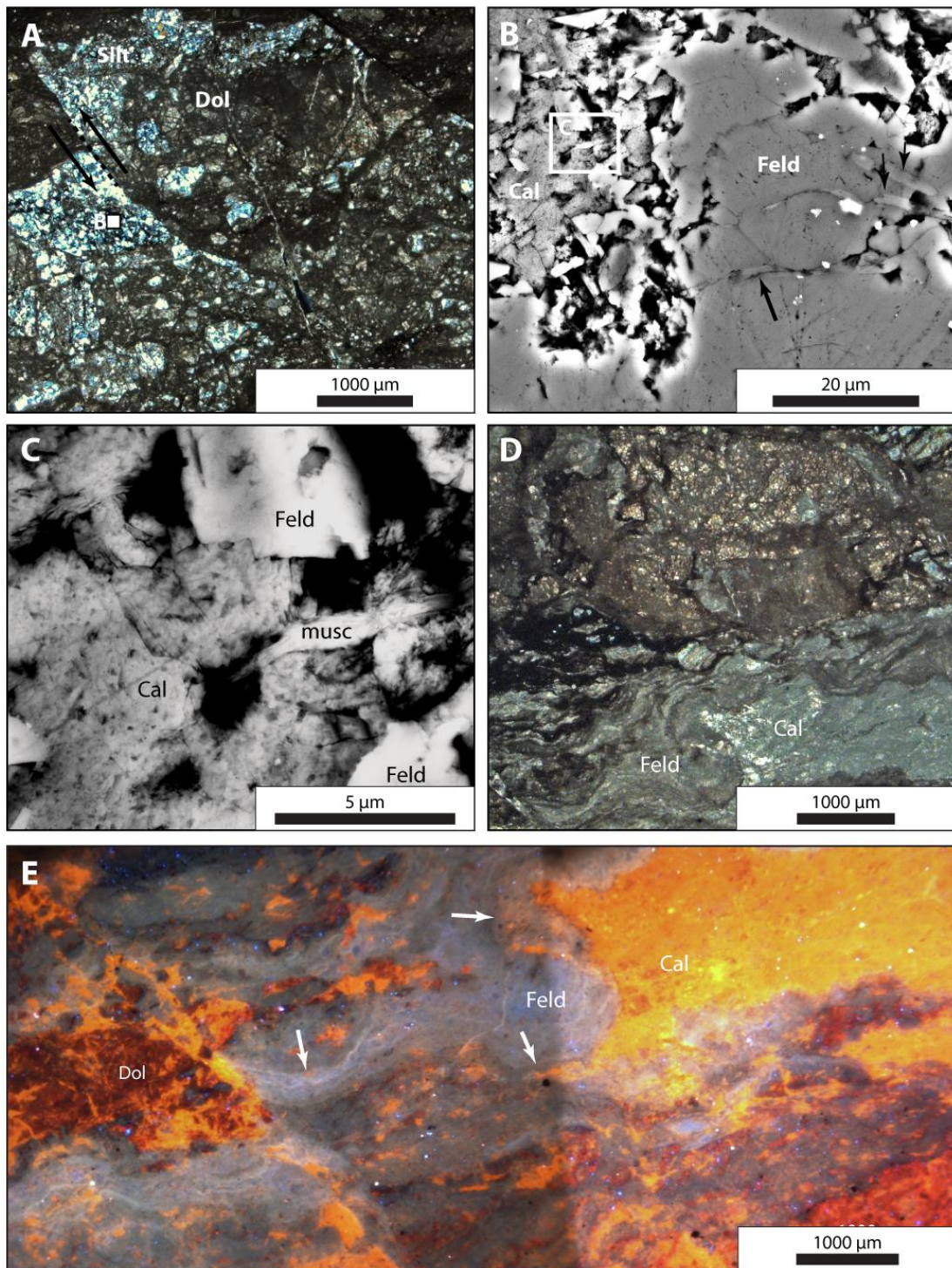


Figure 4.16. Town Knobs shear zone continued. (A) Silt bedding within dolomite, which is offset along a fracture. Optical photomicrograph. (B) and (C) Calcite veins (cal) adjacent to K-feldspar (feld), and folded muscovite (musc) grains (arrows). BSE image. (D) Feldspar-rich area adjacent to calcite-rich area (see Figure 4.12C-D). Optical photomicrograph. (E) Stylolites (white - arrows) are common in silt areas. CL image.

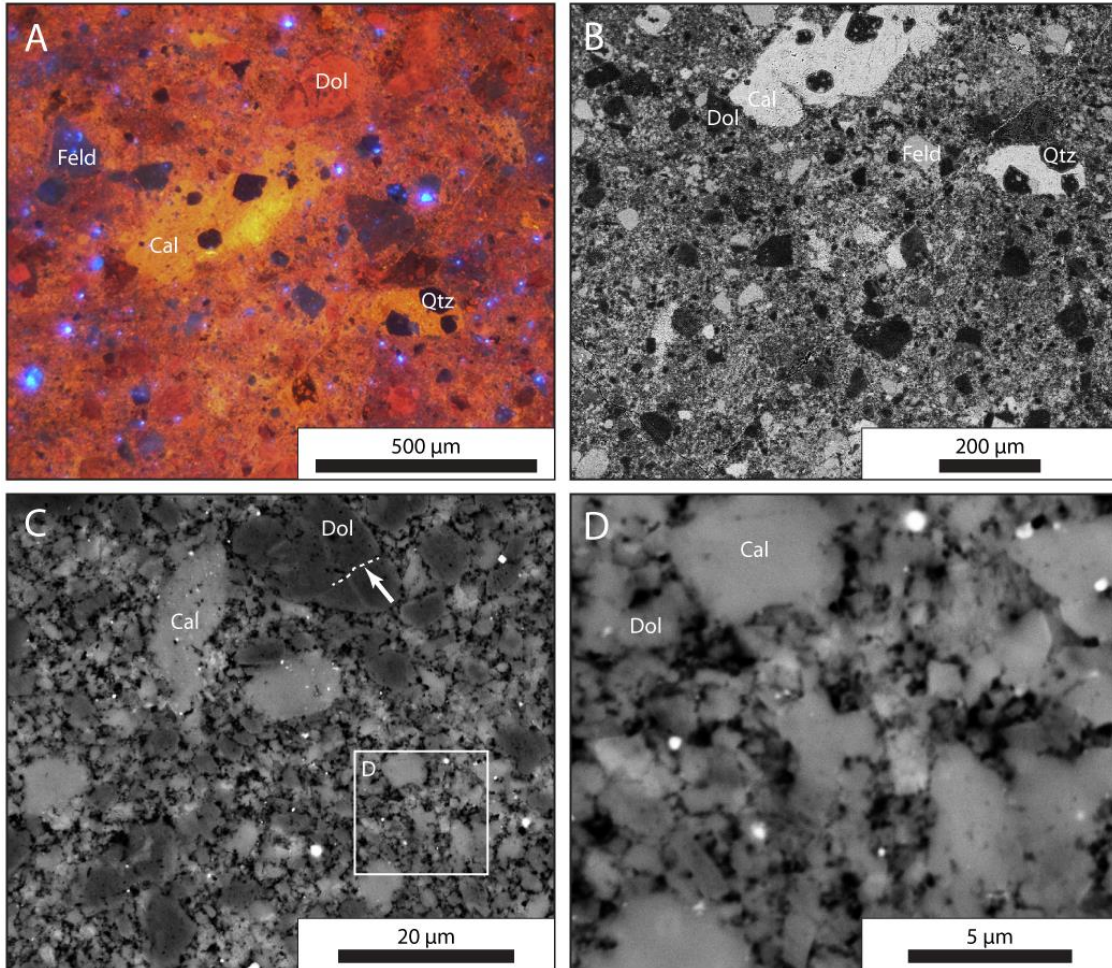


Figure 4.17. 'Vein-like' structure along the Town Knobs shear zone. (A) Clasts and angular grains in a fine-grained matrix composed of carbonate. CL image. (B) – (D) BSE images. (B) There is no discernible fabric within the structure. (C) Matrix is composed of angular, fractured dolomite (arrow) and calcite grains. (D) Intermixed dolomite and calcite grains.

4.5 Fault Zones Evolution

Structures observed along the Copper Creek and Town Knobs thrusts indicate both brittle and ductile deformation processes occurred along each fault zone. While similar lithologies are present along both faults, the fault zone rocks behave differently, experiencing over an order of magnitude difference in displacements. While weakly deforming carbonate vein material is important in localizing deformation along each fault zone, fault structures suggest fault weakening along the Copper Creek thrust and fault strengthening along the Town Knobs thrust. Below, I discuss the deformation processes associated with each lithology within each fault zone.

4.5.1 Deformation along the Copper Creek thrust

Along the Copper Creek thrust, the majority of deformation is located immediately adjacent to, or within the shear zone. No penetrative deformation beyond minor folding in the hanging wall shale is observed in shale and limestone units of the hanging wall and footwall. Within the footwall, we observe sedimentary structures within 35 cm of the shear zone. Within the dolomite unit 4 m above the fault zone, deformation is limited to localized zones of fine-grained dolomite.

Extensive fine-grained dolomite development, fracturing, and veining are largely observed at the base of the dolomite host rock, adjacent to the shear zone. The coarse-grained host dolomite within the hanging wall deformed by brittle and ductile processes. Evidence for brittle processes includes fractures and intragranular fractures within zones of undulatory extinction, indicating brittle behavior associated with slip planes (Barber et al., 1981). The formation of deformation bands, though rare within the dolomite, indicates

dislocation mobility transitioning into subgrain development (Barber et al., 1981). Additional evidence of dislocation creep includes the formation of lobate grain boundaries and subgrains. Lobate grain boundaries are common in the coarse-grained dolomite, and indicates dolomite deformed by bulge recrystallization (Barber et al., 1981; Hirth and Tullis, 1992). The development of subgrains indicates dislocation climb-accommodated subgrain rotation recrystallization, which resulted in the formation of fine-grained dolomite (Barber et al., 1981; Hirth and Tullis, 1992; Leiss and Barber, 1999). Both the brittle and ductile processes result in the formation of fine-grained dolomite, often along localized zones. The development of the fine-grained dolomite increases towards the fault zone, a trend that is also observed along other dolomite-shale thrust faults (Erickson, 1994).

Within these localized zones of fine-grained dolomite, grains deformed primarily by brittle processes. While we observe subgrains and lobate grain boundaries in coarser grains within these zones, the fine-grained matrix is poorly sorted and porosity is high. A poorly sorted matrix is usually associated with brittle fault zones (Higgins, 1971; Sammis et al., 1987; Erickson, 1994). The formation of numerous calcite veins within these zones, particularly closer to the shear zone, also suggest brittle deformation dominated within these zones.

Calcite veins along the Copper Creek fault zone, but not within the main shear zone, also contain evidence for ductile processes (e.g., dynamic recrystallization, diffusion creep-accommodated grain boundary sliding). The development of fine-grains at grain boundaries and along twin boundaries in coarse-grained calcite veins within the hanging wall indicate dynamic recrystallization, which resulted in ultrafine-grains (Schmid et al., 1980; Burkhard,

1993). The ultrafine-grains contain interpenetrating grain boundaries and four-grain junctions, and we observe no evidence of subgrains. These microstructures indicate the ultrafine-grained calcite most likely deformed by diffusion creep-accommodated grain boundary sliding (Schmid, 1977).

Within the shear zone, calcite veins exhibit evidence for both brittle (e.g., plasticity-induced fracturing) and ductile processes (e.g., twinning, diffusion creep-accommodated grain boundary sliding). Coarse-grained vein calcite contains thin twins with voids at twin-twin intersections and along twin boundaries, which suggest plasticity-induced fracturing was responsible for grain size reduction (Rose, 1868; Frederich et al., 1989; Wells et al., 2014). The resulting ultrafine-grained calcite grains contain interpenetrating grain boundaries and four-grain junctions, indicating diffusion creep-accommodated grain boundary sliding control deformation of the fine-grained calcite. Cross-cutting relationships indicate that these veins were repeatedly emplaced within the shear zone as a result of fracturing and fluid flow. These veins also form a stress-supporting network within the shear zone, indicating that calcite, and not the shale, controls the rheology of the fault zone.

4.5.2 Deformation along the Town Knobs Thrust

Along the Town Knobs thrust, shale and siltstone beds above the dolomite bed within the hanging wall preserve sedimentary bedding, indicating no penetrative deformation. While we observe minor faults and localized folds within the shale and siltstone beds, sedimentary structures are preserved throughout these units, including immediately adjacent to the hanging wall dolomite bed. Deformation within the silt and mica rich areas within the heterogeneous dolomite unit is also limited, even though

seritization of the silty-rich matrix often leads to fault weakening (Wintsch et al., 1995). Instead, localization occurs at the base of a large dolomite bed of the shale-rich Rome Formation.

Coarse-grained dolomite within the footwall and hanging wall, and coarse-grained vein dolomite within the footwall deformed primarily by dislocation creep. Lobate grain boundaries and subgrain development indicates grain boundary mobility within coarse-grained dolomite. Grain size reduction by subgrain rotation recrystallization within the coarse-grained dolomite results in grains less than 10 μm (Barber et al., 1981; Hirth and Tullis, 1992; Leiss and Barber, 1999). Within the footwall, fracturing and fluid flow enabled the formation of dolomite veins within these zones of fine-grained dolomite. The coarse-grained vein dolomite deformed by dislocation creep, resulting grain size reduction. However, within the hanging wall dolomite, fracturing along zones of fine-grained dolomite resulted in the formation of coarse-grained calcite veins. Displacement along these localized zones of fine-grained dolomite is minor.

Following grain size reduction, localized zones of fine-grained dolomite within the footwall deformed by diffusion creep or brittle processes, while localized zones of fine-grained dolomite within the hanging wall dolomite bed deformed by either diffusion creep-accommodated grain boundary sliding or by brittle processes. Footwall fine-grained dolomite contains irregular grain boundaries and a weak lattice preferred orientation (Section 3; Figure 3.4D), indicating dislocation creep. The formation of coarse-grained vein dolomite within the footwall zones also suggests brittle deformation also occurred. Ultrafine-grained dolomite within localized zones in the hanging wall dolomite contains

interpenetrating grain boundaries and four-grain junctions. These structures suggest diffusion creep-accommodated grain boundary sliding (Schmid, 1977). The formation of veins within localized zones also indicates brittle deformation; however, fluids were more calcium-rich, resulting in the formation of calcite veins.

While other sections of the fault zone contain evidence for mixed deformation mechanisms, deformation within the “vein-like” structure is dominated by one process. Within the continuous “vein-like” structure in the fault zone, a porous, carbonate-rich matrix consist of poorly sorted fine-grained dolomite, quartz and feldspar silt, and calcite, suggesting cataclasis (Higgins, 1971; Sammis et al., 1987). The carbonate-rich nature of the cataclastic structure is reflective of the carbonate-rich layers within the fault zone that contain the majority of the deformation.

4.5.3 Copper Creek and Town Knobs Thrusts Comparison

Whereas the coarse-grained calcite veins along the Copper Creek thrust deformed by plasticity-induced fracturing, the coarse-grained calcite along the Town Knobs thrust deformed by dynamic recrystallization. Subgrain development in coarse-grained calcite, both at the grain boundaries and along twins, indicates dynamic recrystallization (Burkhard, 1993) resulted in fine-grained calcite (~3 μm). Deformation of the fine-grained calcite outside of the ‘vein-like’ structure indicates deformation by dislocation creep (Kenney and Logan, 1998; Barnhoorn et al., 2004). However, when we examine localized ‘vein-like’ structure within the shear zone, calcite is poorly-mixed with dolomite and porosity is relatively high, suggesting cataclasis (Higgins, 1971; Sammis et al., 1987). While the Copper Creek thrust, which deformed at lower temperatures, contains fine-grained calcite (<

1 μm) that deformed by diffusion-accommodated grain boundary sliding, the Towns Knobs thrust, which deformed at slightly higher temperatures, exhibits evidence for cataclastic deformation. This change from ductile to brittle processes suggest fault strengthening occurred, possibly as a result of changing external conditions (e.g., stress, strain rate) during deformation.

4.5.4 Conditions During Deformation

The Copper Creek thrust and Town Knobs thrust are both low-temperature thrust faults that exhibit evidence for brittle, plastic, and diffusive processes. However, brittle deformation is more prevalent along the Town Knobs fault zone. To explore the fault zone rheologies along the two fault zones, we used experimentally derived flow laws to construct dolomite stress-grain size deformation mechanism maps using dolomite flow laws (Davis et al., 2008; Delle Piane et al., 2008; Holyoke et al., 2013) and calcite flow laws (Herwegh et al., 2003; Walker et al., 1990; de Bresser, 2002) at 180 °C (estimated peak burial depth for the Copper Creek thrust) and at 240 °C (estimated peak burial depth of the Town Knobs thrust) (Figure 4.18).

Along the Copper Creek thrust, the coarse-grained host dolomite contains evidence for dislocation creep (e.g., subgrains), and indicates stresses could have been as high as 400 MPa at extremely slow slip rates (10^{-15} - 10^{-17} s⁻¹) (Figure 4.18). At these conditions, dolomite will deform by either dislocation creep or fracturing rather than by low-temperature plasticity. Similar microstructures are observed in coarse-grained host dolomite along the Town Knobs thrust. Depending on the temperature during deformation, stresses along the Town Knobs thrust could also have occurred at 400-500 MPa and at strain rates of

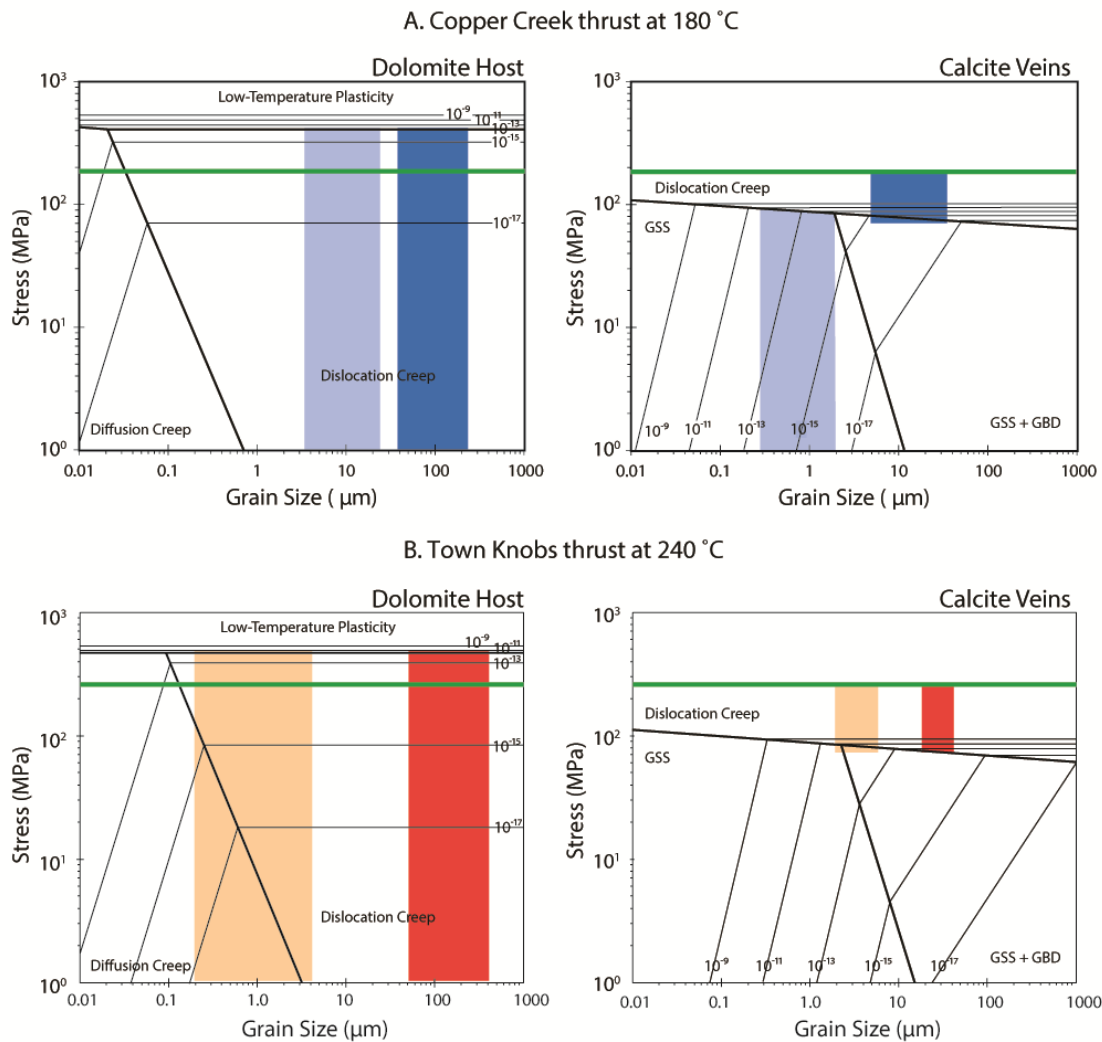


Figure 4.18. Comparison. Estimated conditions for Copper Creek thrust (dark blue - coarse grains; light blue - fine grains) and Town Knobs thrust (dark orange - coarse grains; light orange - fine grains). Calcite deformation mechanism map constructed using flow laws for grain size sensitive creep (GSS) (Herwegh et al., 2003), a mix of GSS and grain size insensitive creep (GSI) (Walker et al., 1990), and dislocation creep (de Bresser, 2002). Dolomite map constructed using flow laws from Davis et al., (2008), Delle Piane et al., (2008), and Holyoke et al., (2013). (A) – (B) Diagrams for dolomite and calcite at 180 °C. Byrelee's Law (green) for 6 km burial depth at saturated conditions is marked in each figure. (C) - (D) Diagrams for dolomite and calcite at 240 °C. Byrelee's Law (green) for 8 km burial depth at saturated conditions is marked in each figure.

10^{-11} - 10^{-17} s⁻¹ (Figure 4.18). At these conditions, dislocation creep results in fine-grained dolomite. Fine-grained dolomite along the Copper Creek thrust exhibits evidence of dislocation creep, indicating dolomite remains within the dislocation creep field. However, fine-grained dolomite along the Town Knobs thrust transitions toward the diffusion creep boundary, as evidenced by the formation of four-grained junctions within the fine-grained localized zones. While the transition from dislocation to diffusion creep indicates changes in either a decrease in stress and/or strain rate, the formation of calcite veins and cataclastic layers within localized zones of fine-grained dolomite and within the Town Knobs fault zone indicates fault strengthening.

Fault localization along the Copper Creek and Town Knobs thrusts occurs along calcite veins and calcite-rich zones. Coarse-grained calcite along the Town Knobs fault zone exhibit evidence of dislocation creep (e.g., subgrains) at slow strain rates (10^{-11} - 10^{-17} s⁻¹) and at stresses as high as 200 MPa (Figure 4.18). However, coarse-grained calcite along the Copper Creek fault zone primarily exhibits evidence of plasticity-induced fracturing, a result of limited dislocation climb. Limited dislocation creep suggests stress and strain rate may have been higher compared to the estimated conditions along the Town Knobs thrust. Following grain size reduction of calcite, fine-grained calcite along the Copper Creek thrust contains evidence for diffusion creep, resulting in fault weakening. While localization occurs along a cataclastic zone of dolomite, silt, and vein calcite in the Town Knobs fault zone, the lack of evidence for diffusion creep within the fine-grained calcite veins and the development of cataclastic zones indicate fault strengthening.

4.6 Controls on Macroscopic Structures

4.6.1 Controls on the Location of Faulting

Earlier studies (Rich, 1934, Wiltschko and Chapple, 1977; Wu, 1993; Thomas, 2001, Ikari et al., 2009, Cobbold et al., 2009) of foreland thrusts propose the locations of thrust faults are determined by a weak shale layer. This hypothesis is supported by numerous analogue (Bonini, 2001; Teixell and Koyi, 2003) and mathematical (Chapple, 1978; Ruh et al., 2012) models that document the tendency for faults to displace along a designated weak layer. Additional studies (Rutter, 1986; Davis and Engelder, 1985; De Paola et al., 2008) have suggested that salt influences the location of thrust faults and other structures (e.g., folds); similar to the shale studies, in that salt is weakly deforming material. However, when we examine the exposure of two foreland thrust faults, both of which occurred within the shale-rich Rome Formation, we document a thick dolomite unit immediately adjacent to the fault zone.

Based observations of along the Copper Creek and Town Knobs thrust, the location of each fault was influenced by a large dolomite bed within the Rome Formation. We suggest the rheological behavior of the dolomite bed (e.g., localization along zones of fine-grained dolomite) coupled with fluid migration along the fine-grained dolomite zones controlled fault propagation past the dolomite unit. Other works have made similar observations in other regions. Contreras and Suter (2015) reported similar structural-stratigraphy relationships along carbonate-shale thrust faults in the Sierra Madre Oriental fold-and-thrust belt (Mexico). The combination of a contact between two materials of different mechanical properties resulted in brittle deformation at the base of a larger, more

competent layer (Wiltschko, 1981; Contreras and Suter, 2015). These models support our observations and offer a mechanical explanation as to why dolomite controls the location of several thrust faults in the Southern Appalachians.

4.6.2 Controls on Fault Displacement

While structures along each fault indicate the location of faulting is determined by the behavior of the overlying dolomite bed, the displacements between these faults are considerably different. The Town Knobs thrust has an estimated displacement of ~275 m while the Copper Creek thrust has a displacement of 15-20 km. Along the Copper Creek thrust, cross-cutting relationships indicate repeated emplacement of weak calcite veins along the fault zone. However, when we examine the Town Knobs fault zone, we observe limited vein emplacement within the fault zone, limited seritization, and the formation of narrow cataclastic zones. If more fluids were migrating along the Town Knobs shear zone, we would have expected more alteration of the feldspar, which is commonly observed along other saturated fault zones (Wintsch et al., 1995; Passchier and Trouw, 1996), and a higher density of veins.

Another factor that may have contributed to the difference in displacement is the strength of the fault zones during deformation. While the temperature estimates for the two thrust zones are similar, each fault zone exhibits evidence for different deformation mechanisms. At slightly lower-temperatures, dolomite along the Copper Creek thrust fault deforms primarily by dislocation creep and brittle failure. Localization instead occurs along coarse-grained vein calcite, which contains evidence for plasticity-induced fracturing, followed by grain size reduction to ultrafine-grain calcite that then deformed by diffusion

creep-accommodated grain boundary sliding. The transition in mechanisms resulted in dramatic weakening along the shear zone and 15-20 km of net slip.

At slightly higher temperatures, dolomite along the Town Knobs thrust deforms by dislocation and diffusion creep, and fracturing. Displacement along localized zones of fine-grained dolomite within the footwall is limited. Along the fault zone, fracturing of the dolomite and silty section resulted in coarse-grained calcite veins that deformed primarily by dislocation creep, resulting calcite grains that are coarser than the fine-grained calcite observed along the Copper Creek thrust. In addition, localized deformation zones composed of fine-grained calcite exhibit evidence for cataclasis within the shear zone, and a lack of evidence for diffusion creep, indicate the calcite veins along the Town Knobs thrust may not have been as weak as those along the Copper Creek thrust (Figure 4.18). The overall formation of cataclastic layers composed of fine-grained dolomite, silt, and calcite suggest fault strengthening along the Town Knobs thrust limited displacement to less than 300 m.

4.7 Conclusions

The location of several foreland thrust faults in the Southern Appalachians is controlled by the brittle behavior of dolomite, and is not dependent on nearby shale horizons. The Copper Creek thrust and the Town Knobs thrust are two low-angle thrust faults within the foreland fold-and-thrust belt that contain a large (3-7 m) dolomite bed adjacent to the faults. Fracturing at the base of this dolomite bed resulted in the formation of calcite veins. Strain localization in both faults occurred predominantly along these calcite veins, which thus controlled the location of these foreland thrusts.

Along the Copper Creek thrust, calcite veins emplaced along the shear zone deformed by plasticity-induced fracturing, resulting in ultrafine-grained calcite that deformed by diffusion-creep accommodated grain boundary sliding. These structures suggest a decrease in stress at constant strain rates, resulting in fault weakening. Along the Town Knobs thrust, calcite veins along the shear zone deformed by recrystallization-accommodated dislocation creep and cataclasis, resulting in grain size reduction and mixing with host dolomite. The transition from recrystallization-accommodated dislocation creep to cataclastic deformation indicates stress likely increased along the fault zone. Displacement along these faults was, thus, likely controlled by the interaction of the rheology of the shear zone material prevailing external conditions during deformation. As stress decreased along calcite-rich shear zones, Copper Creek thrust experienced large displacement (15-20 km), while the increase in stress along the Town Knobs thrust resulted in limited displacement (275 m).

5. SUMMARY

Fault zones commonly occur within and between rocks of different lithologies. Deformation mechanisms within different minerals and rock types are influenced uniquely by external conditions (e.g., stress, strain rate, temperature, and fluids), which, thus, influence the relative strength and behavior of different lithologies deforming concurrently along a fault zone. In this study, we examine three natural fault zones that occur within carbonates and shale, using field and mesoscale observations as well as optical and electron microscopy, in an effort to determine the deformation mechanisms that control the behavior of each mineral, rock type and mixed composition fault rock. We also examine experimentally and naturally deformed dolomites to aid our understanding of the structures observed along localized zones of fine-grained dolomite that are commonly observed in deformed dolomite rocks and often develop weak crystallographic fabric.

Along the Copper Creek thrust, preserved nanograins, vesicular calcite, and coated clasts indicate slip at or near seismic rates. These structures contain cross-cutting relationships with structures that indicate grain-size sensitive diffusion creep in ultrafine-grained calcite. Two populations of nanograins are present: 1) ~7 nm grains adjacent to a slickenside surface along the upper contact of the fault zone; and 2) Clusters of ~30 nm grains with straight grain boundaries and triple junctions, indicating grain growth, within a coarser calcite matrix. Grain growth of the nanograins (7-300 nm) and diffusion creep of the ultrafine-grained calcite (340 nm) increased cohesion of the fault zone during the

interseismic period, resulting in fault strengthening and increased pore fluid pressure, perpetuating the unstable-aseismic cycle.

The formation of a weak c-axis fabric is common within localized deformation zones of fine-grained dolomite, and has been reported from localized zones of experimentally deformed dolomites (900 °C) and naturally deformed localized zones at temperatures as low as ~240 °C. Within the experimentally deformed zones, four-grain junctions, shape preferred orientations, and subgrains, along with an estimated $n=1.3$, suggest that deformation was controlled by a combination of dislocation and diffusion creep processes. Similarly, in naturally deformed dolomite at temperatures of approximately 300 °C (Pioneer Landing thrust), a weak c-axis fabric is observed in zones containing four-grain junctions that suggest diffusion creep and subgrains that indicate dislocation creep. At lower temperatures (~240 °C; Town Knobs thrust), the development of a stronger c-axis fabric in zones that contain subgrains and irregular grain boundaries, suggests dislocation creep resulted in both grain size reduction, and the formation of a crystallographic fabric within these zones. This stronger LPO in dolomite deformed by dislocation creep processes suggests that the weak c-axis LPO observed in experimentally deformed dolomite and along the PL thrust is likely a result of dislocation creep processes concurrent with diffusion creep, occurring at the higher temperatures associated with diffusion creep in dolomite.

While the location of thrust faults is often attributed to the weak behavior of shale beds, the location of many thrust faults in the Southern Appalachians correlates with a thick (3-7 m) dolomite unit within the shale-rich Rome Formation. The Copper Creek thrust and the Town Knobs thrust contain such a dolomite bed in the hanging wall of both fault zones.

Fracturing of the relatively stronger dolomite unit and infiltration of fluids along these fractures resulted in the formation of carbonate veins, and these veins localized fault zone deformation. Along the Copper Creek thrust, deformed at slightly lower temperatures (<180 °C), numerous cross-cutting calcite veins indicate repeated emplacement of calcite veins that deformed by plasticity-induced fracturing, resulting in ultrafine-grained calcite that deformed by diffusion-creep accommodated grain boundary sliding. The transition from plasticity and fracturing to diffusion creep resulted in strain weakening along the narrow zone of calcite veins. Along the Town Knobs thrust, deformed at slightly higher temperatures (< 240 °C), grain size reduction within dolomite veins occurred by fracturing and dislocation creep, while calcite reduced in grain size primarily by recrystallization-accommodated dislocation creep. The resulting fine-grained dolomite deformed by diffusion creep, but is cross-cut by evidence of brittle deformation (i.e., veins). Fine-grained calcite also exhibits evidence (e.g., fractures) of brittle deformation. Mixing of fine-grained dolomite, silt, and calcite within the shear zone occurred primarily by cataclastic flow. Increasing stress, assuming a constant strain rate, may have resulted in a transition from ductilely dominated deformation (dislocation creep) to more brittle-dominant deformation. Within each fault zone, displacement was controlled by the rheology of the vein material and evolving conditions (e.g., stress, strain rate) during deformation. Fault strengthening along the Town Knobs thrust resulted in cataclastic flow, resulting in less displacement (275 m), while fault weakening as a result of weakly deforming calcite veins along the Copper Creek thrust resulted in considerably larger displacement (15-20 km).

REFERENCES

- Barber, D.J., Heard, H.C., and Wenk, H.-R., 1981. Deformation of dolomite single crystal from 20-800 °C: *Physics and Chemistry of Minerals* v. 7, p. 271-286.
- Barnhoorn, A., Bystricky, M., Burlini, L., and Kunze, K., 2005. Post-deformational annealing of calcite rocks: *Tectonophysics*, v. 403, p. 167–191.
- Barnhoorn, A., Bystricky, M., Burlini, L., and Kunze, K., 2004. The role of recrystallisation on the deformation behaviour of calcite rocks: large strain torsion experiments on Carrara marble: *Journal of Structural Geology*, v. 26, p. 885–903.
- Beeler, N.M., Di Toro, G., and Nielsen, S., 2016. Earthquake source properties from pseudotachylite: *Bulletin of the Seismological Society of America* v. 106, p. 1-13.
- Bestmann, M., Kunze, K., and Mathews, A., 2000. Evolution of calcite marble shear zone complex on Thassos Island, Greece: microstructural and textural fabrics and their kinematic significance: *Journal of Structural Geology* v. 22, p. 1789-1807.
- Bestmann, M., and Prior, D.J., 2003. Intragranular dynamic recrystallization in naturally deformed calcite marble: diffusion accommodated grain boundary sliding as a result of subgrain rotation recrystallization: *Journal of Structural Geology* v. 25, p. 1597-1613.
- Bonini, M., 2001. Passive roof thrusting and forelandward fold propagation in scaled brittle-ductile physical models of thrust wedges: *Journal of Geophysical Research* v. 106, p. 2291-2311.

- Boullier, A.M., and Gueguen, Y., 1975. SP-mylonites: Origin of some mylonites by superplastic flow: *Contributions to Mineralogy and Petrology* v. 50, p. 93-104.
- Boullier, A.M., Yeh, E.C., Boutareaud, S., Song, S.R., and Tsai, C.H., 2009. Microscale anatomy of the 1999 Chi-Chi earthquake fault zone: *Geochemistry, Geophysics, Geosystems*, v. 10, p. 1–25.
- Boutareaud, S., Calugaru, D.G., Han, R., Fabbri, O., Mizoguchi, K., Tsutsumi, A., and Shimamoto, T., 2008. Clay-clast aggregates: A new textural evidence for seismic fault sliding?: *Geophysical Research Letters*, v. 35, p. 1–5.
- Burkhard, M., 1993. Calcite twins, their geometry, appearance and significance as stress-strain markers and indicators of tectonic regime: A review: *Journal of Structural Geology* v. 15, p. 351-368.
- Busch, J.P., and van der Pluijm, B.A., 1995. Calcite textures, microstructures and rheological properties of marblemylonites in the Bancroft shear zone, Ontario, Canada: *Journal of Structural Geology* v. 17, p. 677–688.
- Carpenter, B.M., Mollo, S., Viti, C., and Collettini, C., 2015. Influence of calcite decarbonation on the frictional behavior of carbonate-bearing gouge: Implications for the instability of volcanic flanks and fault slip: *Tectonophysics*, v. 658, p. 128–136.
- Chapple, W.M., 1978. Mechanics of thin-skinned of fold-and-thrust belts: *Geological Society of America Bulletin* v. 89, p. 1189-1198.

- Chester, F.M., Evans, J., and Biegel, R.L., 1993. Internal structure and weakening mechanisms of the San Andreas Fault: *Journal of Geophysical Research* v. 98, p. 771-786.
- Cobbold, P.R., Clarke, B.J., and Løseth, H., 2009. Structural consequences of fluid overpressure and seepage forces in the outer thrust belt of the Niger Delta: *Petroleum Geoscience* v. 15, p. 3-15.
- Collettini, C., Viti, C., Tesei, T., and Mollo, S., 2013. Thermal decomposition along natural carbonate faults during earthquakes: *Geology* v. 41, p. 927-930.
- Collettini, C., Carpenter B.M., Viti, C., Cruciani, F., Mollo, S., Tesei, T., Trippetta, F., Valoroso, L., and Chiaraluce, L., 2014. Fault structure and slip localization in carbonate-bearing normal faults: An example from the Northern Apennines of Italy: *Journal of Structural Geology* v. 67, p. 154-166.
- Contreras, J., and Suter, M., 2015. Mechanical stability model of progradational carbonate platform margins under tectonic loads: Deformation of Cretaceous carbonate platforms in the Sierra Madre Oriental fold-thrust belt (east central Mexico): *Journal of Geophysical Research - Solid Earth* v. 120, p. 1-21.
- Davis, D. M., and Engelder, T., 1985. The role of salt in fold-and-thrust belts. *Tectonophysics* v. 119, p. 67-88.
- Davis, N.E., Kronenberg, A.K., and Newman, J., 2008. Plasticity and diffusion creep of dolomite: *Tectonophysics* v. 456, p. 127–146.
- de Bresser, J.H.P., 2002. On the mechanism of dislocation creep of calcite at high temperature: Inferences from experimentally measured pressure sensitivity and

- strain rate sensitivity of flow stress: *Journal of Geophysical Research*, v. 107 (B12), 2337.
- de Bresser, J.H.P., Ter Heege, J.H., and Spiers, C.J., 2001. Grain size reduction by dynamic recrystallization: can it result in major rheological weakening? *International Journal of Earth Sciences* v. 90, p. 28-45.
- de la Chapelle, S., Castelnau, O., Lipenkov, V., and Duval, P., 1998. Dynamic recrystallization and texture development in ice as revealed by the study of deep ice cores in Antarctica and Greenland: *Journal of Geophysical Research* v. 103, p. 5091-5105.
- Delle Piane, C., Burlini, L., Kunze, K., Brack, P., and Pierre Burg, J., 2008. Rheology of dolomite: Large strain torsion experiments and natural examples: *Journal of Structural Geology* v. 30, p. 767-776.
- De Paola, N., Collettini, C., Faulkner, D.R., and Trippetta, F., 2008. Fault zone architecture and deformation processes within evaporitic rocks in the upper crust: *Tectonics* v. 27, p. 1-21.
- De Paola, N., Hirose, T., Mitchell, T., Di Toro, G., Viti, C., and Shimamoto, T., 2011. Fault lubrication and earthquake propagation in thermally unstable rocks: *Geology* v. 39, p. 35-38.
- Di Toro, G., Goldsby, D.L., and Tullis, T.E., 2004. Friction falls towards zero in quartz rock as slip velocity approaches seismic rates: *Nature* v. 427, p. 436-439.
- Dieterich, J.H., 1972. Time-dependent friction in rocks: *Journal of Geophysical Research* v. 77, p. 3690–3697.

- Erickson, S.G., 1994. Deformation of shale and dolomite in the Lewis thrust fault zone, northwest Montana, U.S.A.: *Canadian Journal of Earth Sciences* v. 31, p. 1440-1448.
- Ferri, F., Di Toro, G., Hirose, T., and Shimamoto, T., 2010. Evidence of thermal pressurization in high-velocity friction experiments on smectite-rich gouges: *Terra Nova* v. 22, p. 347–353.
- Fondriest, M., Smith, S.A.F., Di Toro, G., Zampieri, D., and Mittempergher, S., 2012. Fault zone structure and seismic slip localization in dolostones, an example from the Southern Alps, Italy: *Journal of Structural Geology*, v. 45, p. 52–67.
- Fredrick, J.T., Evans, B., and Wong, T.-F., 1989. Micromechanics of brittle to plastic transition in Carrara Marble: *Journal of Geophysical Research*, v. 94, p. 4129-4145.
- Gifkins, R.C., 1976. Grain-boundary sliding and its accommodation during creep and superplasticity: *Metallurgical Transactions* v. 7, p. 1225-1232.
- Goldsby, D.L., and Kohlstedt, D.L., 2001. Superplastic deformation of ice: Experimental observations: *Journal of Geophysical Research* v. 106, p. 11,017-11,030.
- Hadizadeh, J. 1994. Interaction of cataclasis and pressure solution in a low-temperature carbonate shear zone: *Pageoph* v. 143, p. 255-280.
- Hafner, W., 1981. Stress Distributions and faulting: *Bulletin of the Geological Society of America* v. 62, p. 373-398.
- Han, R., and Hirose, T., 2012. Clay-clast aggregates in fault gouge: An unequivocal indicator of seismic faulting at shallow depths?: *Journal of Structural Geology*, v. 43, p. 92–99.

- Han, R., Shimamoto, T., Hirose, T., Ree, J.H., and Ando, J., 2007. Ultralow friction of carbonate faults caused by thermal decomposition: *Science*, v. 316, p. 878–881.
- Handin, J., and Hager, R.V., 1958. Experimental deformation of sedimentary rocks under confining pressure: Test at high temperature: *Bulletin of the American Association of Petroleum Geologist* v. 42, p. 2892-2934.
- Haney, D.C., 1966. Structural geology along a segment of the Saltville fault, Hawkins County Tennessee. Ph.D. thesis, University of Tennessee, Knoxville.
- Hansen, L.N., Zimmerman, M.E., and Kohlstedt, D.L., 2011. Grain boundary sliding in San Carlos olivine: Flow law parameters and crystallographic-preferred orientation: *Journal of Geophysical Research* v. 116, p. 1-16.
- Hansen, L.N., Zimmerman, M.E., and Kohlstedt, D.L., 2012. The influence of microstructure on deformation of olivine in the grain-boundary sliding regime: *Journal of Geophysical Research* v. 116, p. 1-17.
- Harris, L.D., 1976. Thin-skinned tectonics and potential hydrocarbon traps: illustrated by a seismic profile in the Valley and Ridge province of Tennessee: *Journal of Research of the U.S. Geological Survey* v. 4, p. 379-386.
- Harris, L.D., and Milici, R.C., 1977. Characteristics of Thin-skinned Style of Deformation in the Southern Appalachians and Potential Hydrocarbon Traps: *U.S. Geological Survey Professional Paper* v. 1018, p. 1-40.
- Hatcher, R.D., Bream, B.R., and Merschat, A.J., 2007. Tectonic map of the southern and central Appalachians: A tale of three orogens and a complete Wilson cycle, in Hatcher, R.D., Jr., Carlson, M.P., McBride, J.H., and Martínez Catalán, J.R., eds., 4-

- D Framework of Continental Crust: Geological Society of America Memoir v. 200, p. 595-632.
- Heaton, T.H., 1990. Evidence for and implications of self-healing pulses of slip in earthquake rupture: *Physics of the Earth and Planetary Interiors*, v. 64, p. 1-20.
- Heilbronner, R., and Tullis, J., 2002. The effect of static annealing on microstructure and crystallographic preferred orientations of quartzites experimentally deformed in axial compression and shear. *Deformation Mechanisms, Rheology and Tectonics: Current Status and Future Perspectives*, Geological Society London Special Publication v. 200, p. 191– 218.
- Herwegh, M., Xiao, X., and Evans, B., 2003. The effect of dissolved magnesium on diffusion creep in calcite: *Earth and Planetary Science Letters*, v. 212, p. 457–470.
- Hickman, S., Sibson, R., and Bruhn, R., 1995. Introduction to special section: Mechanical involvement of fluids in faulting in faulting: *Journal of Geophysical Research* v. 100, p. 12,831-12,940.
- Higgins, M.W., 1971. Cataclastic rocks. Geological Survey Special Paper v. 687, p. 1-109.
- Hirth, G., and Kohlstedt, D.L., 1995. Experimental constraints on the dynamics of the partially molten upper mantle 2. Deformation in the dislocation creep regime: *Journal of Geophysical Research* v. 100, p. 15,441-15,449.
- Hirth, G., and Tullis, J., 1992. Dislocation creep regimes in quartz aggregates: *Journal of Structural Geology* v. 14, p. 145-159.

- Holyoke, C.W., Kronenberg, A.K., and Newman, J., 2013. Microstructural evolution during strain localization in dolomite aggregates: *Journal of Structural Geology* v. 69, p. 449-464.
- Holyoke, C.W., Kronenberg, A.K., and Newman, J., 2014. Dislocation creep of polycrystalline: *Tectonophysics* v. 590, p. 72-82.
- House, W.M., and Gray, D.R., 1982a. Cataclasites along the Saltville thrust, U.S.A. and their implications for thrust-sheet emplacement. *Journal of Structural Geology* v. 4, p. 257-269.
- House, W.M., and Gray, D.R., 1982b. Displacement transfer at thrust terminations in southern Appalachians – Saltville thrust as example. *The American Association of Petroleum Geologist Bulletin* v. 66, p. 830-842.
- Humphreys, F.J., and Hatherly, M., 1995. *Recrystallization and Related Annealing Phenomena (Second Edition)* Elsevier Science Ltd., Oxford p. 520.
- Ibanez, W.D., and Kronenberg, A.K., 1993. Experimental deformation of shale: mechanical properties and microstructural indicators of mechanisms: *International Journal of Rock Mechanics and Mining Sciences* v. 30, p. 723-734.
- Ikari, M.J., Saffer, D.M., and Marone, C., 2009. Frictional and hydrologic properties of clay-rich fault gouge: *Journal of Geophysical Research* v. 114, p. 1-18.
- Kennedy, L.A., and Logan, J.M., 1997. The role of veining and dissolution in the evolution of fine-grained mylonites: the McConnell thrust, Alberta: *Journal of Structural Geology* v. 19, p. 785-797.

- Kennedy, L.A., and Logan, J.M., 1998. Microstructures of cataclastics in a limestone-on-shale thrust fault: *Tectonophysics* v. 295, p. 167-186.
- King, P.B., and Ferguson, H.W., 1960. Geology of northeastern-most Tennessee: U.S. Geological Survey Professional Paper v. 311, p. 1-190.
- Kirkpatrick, J.D., and Rowe, C.D., 2013. Disappearing ink: How pseudotachylytes are lost from the rock record: *Journal of Structural Geology* 52, p. 183-198.
- Leiss, B., and Barber, B.J., 1999. Mechanisms of dynamic recrystallization in naturally deformed dolomite inferred from EBSD analyses: *Tectonophysics* v. 303, p. 51-69.
- Lemiscki, P.J., and Kohl, M.S., 2006. Geologic excursion across part of the Southern Appalachian foreland fold–thrust belt in northeastern Tennessee: 2006 Southeastern Section meeting, Geological Society of America Field Trip 2, p. 37-64.
- Marone, C., 1998, Laboratory-derived friction laws and their application to seismic faulting: *Annual Review of Earth and Planetary Sciences* v. 26, p. 643-696.
- Michibayashi, K., Suzuki, M., and Komori, N., 2013. Progressive deformation partitioning and recrystallization of olivine in the lithospheric mantle: *Tectonophysics* v. 587, p. 79-88.
- Mitchell, T.M., Smith, S.A.F., Anders, M.H., Di Toro, G., Nielsen, S., Cavallo, A., and Beard, A.D., 2015. Catastrophic emplacement of giant landslides aided by thermal decomposition: Heart Mountain, Wyoming: *Earth and Planetary Science Letters*, v. 411, p. 199–207.
- Miyazaki, T., Sueyoshi, K., and Hiraga, T., 2013. Olivine crystals align during diffusion creep of Earth's upper mantle: *Nature* v. 502, p. 321-326.

- Molli, G., Conti, P., Giorgetti, G., Meccheri, M., and Oesterling, N., 2000. Microfabric study on the deformational and thermal history of the Alpi Apuane marbles (Carrara marbles), Italy: *Journal of Structural Geology* v. 22, p. 1809-1825.
- Molli, G., Cortecchi, G., Vaselli, L., Ottria, G., Cortopassi, A., Dinelli, E., Mussi, M., and Barbieri, M., 2010. Fault zone structure and fluid-rock interaction of high angle normal fault in Carrara marble (NW Tuscany, Italy): *Journal of Structural Geology* v. 32, p. 1334-1348.
- Newman, J., and Mitra, G., 1994. Fluid-influenced deformation and recrystallization of dolomite at low temperatures along a natural fault zone, Mountain City window, Tennessee: *Geological Society of America Bulletin* v. 106, p. 1267-1280.
- Niemeijer, A., Di Toro, G., Griffith, W.A., Bistacchi, A., Smith, S.A.F., and Nielsen, S., 2012. Inferring earthquake physics and chemistry using an integrated field and laboratory approach: *Journal of Structural Geology* v. 39, p. 2-36.
- Noda, H., Dunham, E.M., and Rice, J.R., 2009. Earthquake ruptures with thermal weakening and the operation of major faults at low overall stress levels: *Journal of Geophysical Research* v. 114, p. 1-27.
- Passchier, C.W., Trouw, R.A.J., 2005. *Microtectonics*. Springer-Verlag, Berlin, Germany.
- Pshenichnyuk, A.I., Astanin, V.V., and Kaibyshev, O.A., 1998. The model of grain-boundary sliding stimulated by intragranular slip: *Philosophical Magazine* v. 77, p. 1093-1106.
- Ree, J.-H., and Park, Y., 1997. Static recovery and recrystallization microstructures in sheared octachloropropane: *Journal of Structural Geology* v. 19, p. 1521-1526.

- Ree, J.-H., Ando, J.-I., Han, R., and Shimamoto, T., 2014. Coseismic microstructures of experimental fault zones in Carrara marble: *Journal of Structural Geology*, v. 66, p. 75–83.
- Rempe, M., Smith, S.A.F., Ferri, F., Mitchell, T.M., and Di Toro, G., 2014. Clast-cortex aggregates in experimental and natural calcite-bearing fault zones: *Journal of Structural Geology*, v. 68, p. 142-157.
- Rich, J.L., 1934. Mechanics of low-angle overthrust faulting as illustrated by Cumberland thrust block, Virginia, Kentucky, and Tennessee: *Bulletin of the American Association of Petroleum Geologist* v. 18, p. 1584-1596.
- Rowe, C.D., and Griffith, W.A., 2015. Do faults preserve a record of seismic slip: A second opinion: *Journal of Structural Geology*, v. 78, p. 1–26.
- Rose, G., 1868. Über die im Kalkspath vorkommende hohlen Canfile. *Abh. Konig. Akad. Wiss. Berlin*. v. 23, p. 57-79.
- Rutter, E.H., 1974. The influence of temperature, strain rate and interstitial water in the experimental deformation of calcite rocks: *Tectonophysics* v. 22, p. 311-334.
- Ruh, J.B., Kaus, B.J.P., and Burg, J.-P. 2012. Numerical investigation of deformation mechanics in fold-and-thrust belts: Influence of rheology of single and multiple décollements: *Tectonics* v. 31, p. 1-23.
- Rutter, E. H., 1986. On the nomenclature of mode of failure transitions in rocks: *Tectonophysics* v. 122, p. 381-387.

- Rutter, E.H., Casey, M., and Burlini, L., 1995. Preferred crystallographic orientation development during the plastic and superplastic flow of calcite rocks: *Journal of Structural Geology* v. 16, p. 1431-1446.
- Sammis, C., King, G., and Biegel, R., 1987. The Kinematics of gouge deformation: *Pageoph* v. 125, p. 776-812.
- Schmid, S.M., Boland, J.N., and Paterson, M.S., 1977. Superplastic flow in finegrained limestone: *Tectonophysics* v. 43, p. 257-291.
- Schmid, S.M., Paterson, M.S., and Boland, J.N., 1980. High temperature flow and dynamic recrystallization in Carrara marble: *Tectonophysics* v. 65, p. 245-280.
- Schmid, S.M., Panozzo, R., and Bauer, S. 1987. Simple shear experiments on calcite rocks: rheology and microfabric: *Journal of Structural Geology* v. 9, p. 747-778.
- Scholz, C.H., 1998, 1998. Earthquakes and friction laws: *Nature* v. 391, p. 38-42.
- Scholz, C.H., Wyss, M., and Smith, S.W., 1969. Seismic and aseismic slip on the San Andreas Fault: *Journal of Geophysical Research*, v. 74, p. 2049–2069.
- Sibson, R.H., 1975, Generation of pseudotachylite by ancient seismic faulting: *Geophysical Journal of Research* v. 43, p. 775-794.
- Sibson, R.H., 1977. Fault rocks and fault mechanisms: *Journal of the Geological Society* v. 133, p. 191–213.
- Sibson, R.H., 1992. Implications of fault valve behaviour for rupture nucleation: *Tectonophysics* v. 211, p. 283–293.
- Siman-Tov, S., Aharonov, E., Sagy, A., and Emmanuel, S., 2013. Nanograins form carbonate fault mirrors: *Geology* v. 41, p. 703–706.

- Skrotzki, W., and Welch, P., 1983. Development of texture and microstructure in extruded ionic polycrystalline aggregates: *Tectonophysics* v. 99, p. 47-61.
- Smeraglia, L., Bettucci, A., Billi, A., Carminati, E., Cavallo, A., Di Toro, G., Natali, M., Passeri, D., Rossi, M., and Spagnuolo, E., 2017, Microstructural evidence for seismic and aseismic slips along clay-bearing, carbonate faults: *Journal of Geophysical Research*, v. 122, doi:10.1002/2017JB014042.
- Smith, J.W., 1968. The Saltville fault near Mooresburg, Tennessee: PhD thesis, West Virginia University.
- Smith, S.A.F., Collettini, C., and Holdsworth, R.E., 2008. Recognizing the seismic cycle along ancient faults: CO₂-induced fluidization of breccias in the footwall of a sealing low-angle normal fault: *Journal of Structural Geology* v. 30, p. 1034–1046.
- Smith, S.A.F., Billi, A., di Toro, G., and Spiess, R., 2011, Principal Slip Zones in Limestone: Microstructural Characterization and Implications for the Seismic Cycle (Tre Monti Fault, Central Apennines, Italy): *Pure and Applied Geophysics*, v. 168, p. 2365–2393.
- Spagnuolo, E., Plümper, O., Violay, M., Cavallo, A., and Di Toro, G., 2015. Fast-moving dislocations trigger flash weakening in carbonate-bearing faults during earthquakes: *Scientific Reports* v. 5, p. 1-11.
- Stöckhert, B., and Duyster, J., 1999. Discontinuous grain growth in recrystallized vein quartz - implications for grain boundary structure, grain boundary mobility, crystallographic preferred orientation, and stress history: *Journal of Structural Geology* v. 21, p. 1477-1490.

- Sundberg, M., and Cooper, R.F., 2008. Crystallographic preferred orientation produced by diffusional creep of harzburgite: effects of chemical interactions among phases during plastic flow: *Journal of Geophysical Research* v. 113, p. 1-16.
- Tesei, T., Collettini, C., Carpenter, B.M., Viti, C., and Marone, C., 2012. Frictional strength and healing behavior of phyllosilicate-rich faults: *Journal of Geophysical Research* v. 117, p. 1-13.
- Teixell, A., and Koyi, H.A., 2003. Experimental and field study of the effects of lithological contrasts on thrust-related deformation: *Tectonics* v. 22, p. 1-11.
- Thomas, T., 2001. Mushwad: ductile duplex in the Appalachian thrust belt in Alabama: *AAPG Bulletin* v. 85, p. 1847-1869
- Tommasi, A., Vauchez, A., and Ionov, D.A., 2008. Deformation, static recrystallization, and reactive melt transport in shallow subcontinental mantle xenoliths (Tok Cenozoic volcanic field, SE Siberia): *Earth and Planetary Science Letters* v. 272, p. 65-77.
- Tullis, J., and Yund, R.A., 1982. Grain Growth Kinetics of Quartz and Calcite Aggregates: *The Journal of Geology* v. 90, p. 301–318.
- Turner, F.J., Griggs, D.T., Clark, R.H., and Dixon, R.H., 1956. Deformation of Yule marble. Part VII: Development of oriented fabrics at 300°C-500 °C: *Bulletin of the Geological Society of America* v. 67, p. 1259-1294.
- Violay, M., Nielsen, S., Spagnuolo, E., Cinti, D., Di Toro, G., and Di Stefano, G., 2013. Pore fluid in experimental calcite-bearing faults: Abrupt weakening and

- geochemical signature of co-seismic processes: *Earth and Planetary Science Letters* v. 361, p. 74–84.
- Walker, A.N., Rutter, E.H., and Brodie, K.H., 1990. Experimental study of grain-size sensitive flow of synthetic, hot-pressed calcite rocks: *Deformation Mechanisms, Rheology and Tectonics: Geological Society London Special Publication* v. 54, p. 259-284.
- Wells, R.K., Newman, J., and Wojtal, S. 2014. Microstructures and rheology of a calcite-shale thrust fault: *Journal of Structural Geology* v. 65, p. 69-81.
- Wenk H.-R., and Shore, J., 1975. Preferred orientation in experimentally deformed dolomite: *Contributions to Mineralogy and Petrology* v. 50, p. 115-126.
- Wenk, H.-R., and Christie, J.M., 1991. Comments on the interpretation of deformation textures in rocks: *Journal of Structural Geology* v. 13, p. 1091-1110.
- Wenk, H.-R., Canova, G., Brechet, Y., and Flandin, L., 1997. A deformation-based model for recrystallization of anisotropic materials: *Acta Materialia* v. 45, p. 3283-3296.
- White, J.C., and White, S.H., 1980. High-voltage transmission electron microscopy of naturally deformed polycrystalline dolomite: *Tectonophysics* v. 66, p. 35-54.
- Wiltschko, D.V., 1981. Thrust sheet deformation at a ramp: summary and extensions of an earlier model: *Geological Society of London, Special Publications* v. 9, p. 55-63.
- Wintsch R.P., Christoffersen R., and Kronenberg A.K., 1995. Fluid-rock reaction weakening of fault zones: *Journal of Geophysical Research* v. 100, p. 13,021-13,032.

- Wiltschko, D.V., Chapple, W.M., 1977. Flow of weak rocks in Appalachian Plateau folds: AAPG Bulletin v. 61, p/ 653-670.
- Wojtal, S., and Mitra, G., 1986, Strain hardening and strain softening in fault zones from foreland thrust: Geological Society of America Bulletin, v. 97, p. 674–687.
- Woodward, N.B., 1985. Valley and Ridge thrust belt: balanced structural sections, Pennsylvania to Alabama. University of Tennessee Dept. of Geological Sciences, [Knoxville]
- Woodward, N.B., Wojtal, S., Paul, J.B., and Zadins, Z.Z., 1988. Partitioning of deformation within several external thrust zones of the Appalachian orogen: Journal of Geology v. 96, p. 351-361.
- Violay, M., Nielsen, S., Spagnuolo, E., Cinti, D., Di Toro, G., and Di Stefano, G., 2013. Pore fluid in experimental calcite-bearing faults: Abrupt weakening and geochemical signature of co-seismic processes: Earth and Planetary Science Letters, v. 361, p. 74–84.

APPENDIX A

SUPPLEMENTAL MATERIAL FOR CYCLIC STABLE-UNSTABLE SLIP
PRESERVED ALONG AN APPALACHIAN FAULT

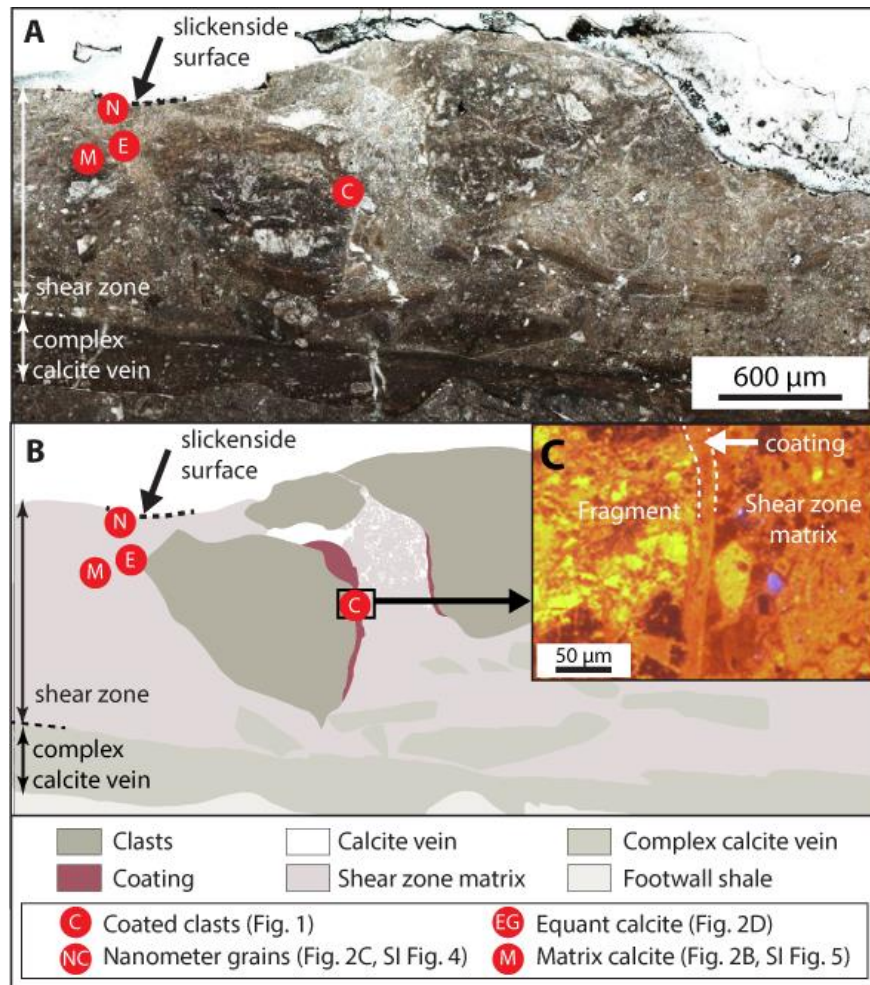


Figure A.1. Copper Creek shear zone schematic. Figure parallel to the slip direction (top to left). (A) Optical photomicrograph of the fault zone and calcite vein layers. (B) Sketch highlights the different layers within the sample and indicates the locations of structures discussed in text. (C) CL image of ultrafine-grained calcite coating.

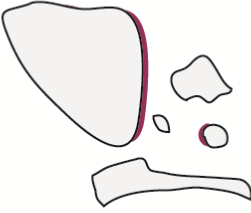
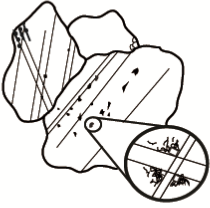




Location	Structure	Description and Deformation Processes	Size range
Throughout shear zone		<p>Aggregate clasts</p> <ul style="list-style-type: none"> - Composed of one or more of the following: <ul style="list-style-type: none"> * Shale and ultrafine-grained calcite matrix * Coarse-grained vein calcite * Complex calcite vein layer - Fine-grained coatings (red) → Proposed evidence of seismic, or near seismic slip → Brittle processes - Additional descriptions in Wells et al., (2014) 	<p>Clasts: 50-1000 μm Grains in clasts: see below</p>
Throughout fault zone		<p>Coarse-grained vein calcite</p> <ul style="list-style-type: none"> - Dislocation tangles at twin-twin intersections - Angular pores at twin-twin intersections - Vesicular textures - Rare subgrains - Weak c-axis LPO → Plasticity-induced fracturing → Limited dislocation climb - Additional descriptions in Wells et al., (2014) 	Grains: 10-1000 μm
Throughout shear zone		<p>Ultrafine-grained calcite</p> <ul style="list-style-type: none"> - Four-grain junctions with irregular grain boundaries - Average grain size of 0.3 μm - Shale present, low porosity - Vesicular texture - No LPO - Forms stress-supporting network around shale (grey) → Diffusion-creep accommodated grain-boundary sliding - Additional descriptions in Wells et al., (2014) 	Grains: 0.2-1 μm
Within 1 mm of slickenside surface		<p>Ultrafine-grained calcite w/ triple junctions</p> <ul style="list-style-type: none"> - Triple junctions - Straight grain boundaries - Dislocation free - Shale absent, no porosity - Adjacent to nanoclusters (grey) → Proposed evidence of grain growth 	Grains: 0.2-0.5 μm
Within 1 mm of slickenside surface		<p>Nanograins in clusters</p> <ul style="list-style-type: none"> - Loosely clustered grains - Average grain size of 30 nm - Straight grain boundaries - Slightly angular → Proposed evidence of grain growth 	<p>Clusters: 0.1-0.4 μm Grains in clusters: 20-50 nm</p>
Within 0.3 mm of slickenside surface		<p>Nanograins in clasts</p> <ul style="list-style-type: none"> - Composed of Ca - Aggregated nanograins - Average grain size of 6.8 nm - Observed in either angular clasts or as matrix → Proposed evidence of thermal decomposition 	<p>Clasts: 0.1-0.3 μm Grains in clasts: 5-10 nm</p>

Figure A.2. Structure and grain size overview.

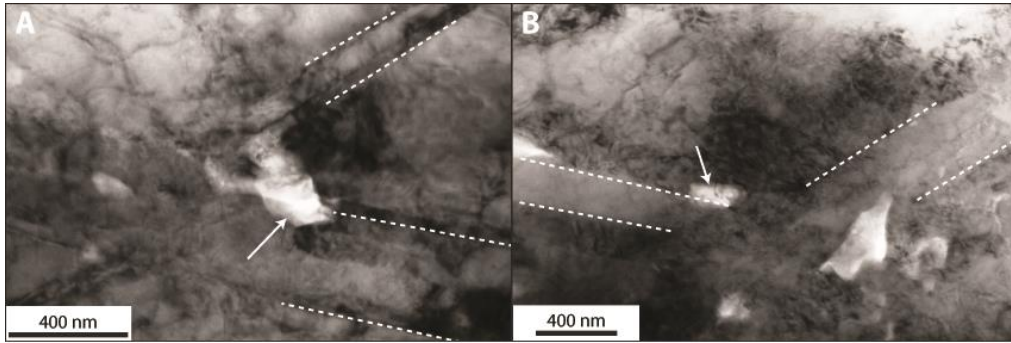


Figure A.3. Twin-Twin intersections. (A) – (B) Twins (dashed lines) are common in coarse-grained vein calcite. Tangled dislocations (dark regions) and angular pores (light areas indicated by arrows) occur at twin-twin intersections. These structures indicate coarse-grained calcite deformed by plasticity-induced fracturing (Fredrich et al., 1989; Wells et al., 2014). TEM images.

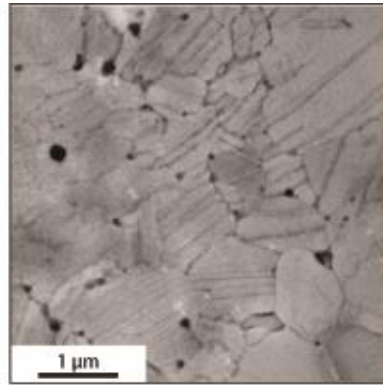


Figure A.4. Vesicular calcite. Vesicular ultra-fine grained calcite within the shear zone.

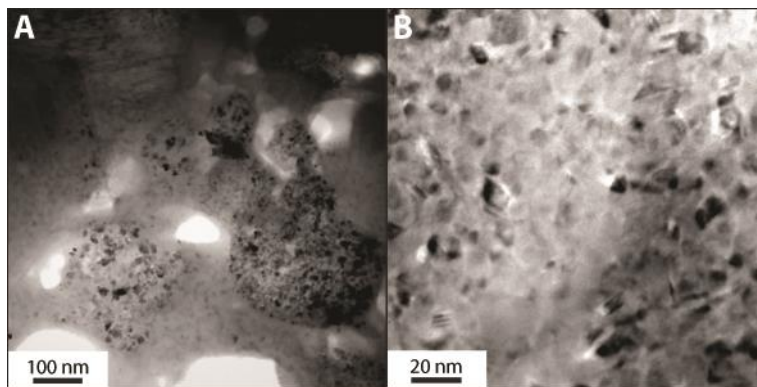


Figure A.5. Shear zone nanograins. (A) – (B) Nanograins (<10 nm) are common only within 1 mm of the slickenside surface in the Copper Creek shear zone.

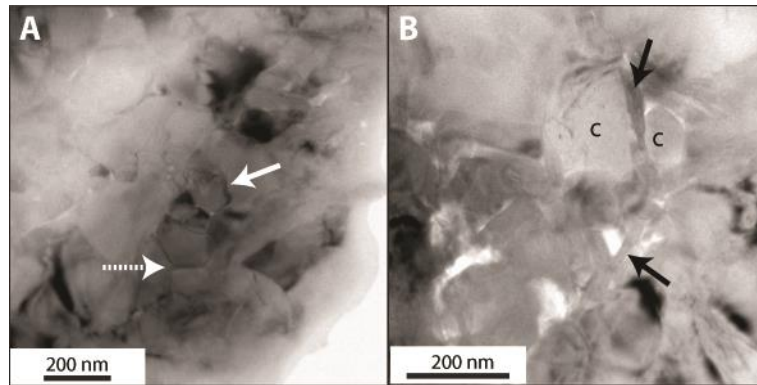


Figure A.6. Ultrafine-grained calcite in shear zone matrix. Ultrafine-grained calcite forms a stress-supporting network in the Copper Creek fault zone (Wells et al., 2014). (A) In areas where calcite is dominant, interpenetrating grain boundaries are common, while triple junctions (arrows) are rare. (B) Ultrafine-grained calcite (c) and clay particles (arrows) documented in Wells et al., 2014. TEM images.